AN INVESTIGATION INTO SOME PROPERTIES

OF THIN AND ULTRA THIN

NIOBIUM FILMS.

A THESIS SUBMITTED FOR THE DEGREE OF

DOCTOR OF PHILOSOPHY

IN THE UNIVERSITY OF ASTON IN BIRMINGHAM

Ian William Salter, B.Sc.

Physics Department
April. 1973.

<u>ABSTRACT</u>

Thin films of niobium were prepared by the thermal evaporation of 99.99% pure niobium. The electrical properties of the films were measured before the films were removed from the deposition chamber. The effects on the electrical properties of the various deposition parameters of vacuum, substrate temperature and deposition rate were noted.

A series of films, ranging in thickness from 80 $\overset{o}{A}$ to 5475 $\overset{o}{A}$, was prepared by depositing niobium in a vacuum of 5×10^{-8} torr at rates of about 250 $\overset{o}{A}$ min^{-1} onto substrates held at 500°K. After removal from the vacuum the superconducting current densities, the transition temperature and the normal resistivity of each film was determined.

An optical technique is described for the determination of the oxide thickness grown on the film after exposure to an atmospheric environment. Film thickness was measured by an electrical method and by means of an interferometer. Good agreement was obtained between both methods providing a correction was made for the oxide layer.

The resistivity of the films increased as the thickness decreased, with the resistivity ratio ρ_{300}/ρ_{10} varying from 1.16 for a film 45 $\overset{o}{A}$ thick to 5.75 for a film 5440 $\overset{o}{A}$ thick. The transition temperature decreased from the bulk value 9.22°K to a minimum of 3.0°K for a film 45 $\overset{o}{A}$ thick.

These results can be explained by assuming that modifications to the phonon spectrum in these films are responsible for the observed decrease in the transition temperatures. By applying the McMillan equation, with the suggested modifications to the phonon spectrum, to the films prepared in this work, values are derived for transition temperature and grain size which are in close agreement with the experimental results.

INDEX

Preface

Prior to the work outlined in this thesis several researchers had reported on the preparation of niobium thin films, by thermal evaporation, section 1.7.2, and by sputtering, section 1.7.3. The properties of these films are summarised in section 1.8.

The principal finding of previous workers had been the sensitivity of the transition temperature of these films to small amounts of gaseous impurities. The transition temperature was found to decrease as the concentration of gaseous impurities, principally oxygen, increased. However, Asada and Nose[19] reported transition temperatures which were too low to be solely accounted for by interstitial oxygen. It was suggested that the discrepancy could be due to the decrease in grain size of very thin films, although there was no confirmatory evidence to this effect.

In another context McMillan[44] had derived an expression for the transition temperature of a superconductor in terms of the Debye temperature, the electron-phonon coupling parameter λ and the Coulomb coupling constant μ^*. Leger and Klein[85] suggested that the enhanced transition temperature observed in thin aluminium films was due to a modification of the phonon spectrum which in turn affects the electron-phonon coupling parameter. From tunnelling character-istics of thin aluminium films the appearance of a low frequency tail to the phonon spectrum was observed. When the average phonon frequency as determined from the experiments was substituted into the McMillan equation, the calculated transition temperature was found to be in good agreement with that observed experimentally. The effect of small grain size on the phonon spectrum had been studied

by Theil[87] who suggested that quantization of the phonon wave vector within a small sample could result in a low frequency phonon cut off.

It was the intention in the early stages of the present investigation to examine both the optical and electrical properties of thin niobium films prepared and measured in an ultra high vacuum environment. The objective was to decrease the probability of oxygen contamination and to determine transition temperatures for films over a wide range of thickness. Preliminary examination of the McMillan equation suggested the possibility of a decrease in the electron-phonon coupling parameter λ with a decrease in transition temperature. In oxygen free films such a decrease might be attributable to a decrease in particle size.

A modification to the phonon spectrum would affect the optical constants of the material and permit the evaluation of λ through equations given by Hopfield[96] and relating particularly to studies of transition metals in the wavelength region of 2μ. This would provide an alternative method of measuring λ and the optical measurements could be carried out at room temperature.

An apparatus was designed and built for the preparation and examination of thin niobium films. An ultra high vacuum system and technique were employed to prepare pure films without interstitial impurities. In this way, any observed decrease in the transition temperature could be wholly attributable to the thickness of the film and the influence if any, of the grain size on the phonon spectrum.

A helium cryostat was attached to the vacuum chamber so that the normal electrical and superconducting properties of the films could be examined 'in situ'. The vacuum chamber was fitted with windows to facilitate the optical study of the films by means of an

ellipsometer. In this way the electrical and optical properties of pure niobium films could be examined simultaneously over the temperature range 2°K to 300°K. At a later stage a modified helium cryostat containing a superconducting solenoid was to be used to determine the critical fields and the variation of critical current density with magnetic field of the 'in situ' films. Because of problems arising with equipment this part of the programme was never realised and although critical current densities were measured it was not possible to evaluate the corresponding critical fields at the surfaces of the films.

Due to the development of a leak in the cryostat it was not possible to prepare and examine pure films 'in situ'. The cryostat was removed from the vacuum system and the alternative approach of depositing the films in one system and examining them in a separate system had to be employed. Exposing the films to an atmospheric environment resulted in the growth of an oxide layer on the films, this required that the oxide thickness should be determined. This was achieved by ellipsometry and by comparing the measured thickness of the film to the thickness determined from the electrical measurements.

The initial objective of determining the electron-phonon coupling constant by ellipsometry and relating the transition temperature to the grain size was not realised. However, by assuming a decrease in the value of the coupling constant the measured values of transition temperature and grain size were found to be in good agreement with the values deduced from the McMillan equation.

CHAPTER I

THEORETICAL AND EXPERIMENTAL FOUNDATIONS

1.1. Introduction

A description of the normal electrical resistivity of metals and the introduction of Matthiessen's Rule leads to an outline of metallic film resistivity and the determination of film thickness from electrical measurements.

A review of the phenomenological theories of superconductivity is presented and followed by a review of the preparation, structure and electrical properties of niobium thin films.

1.2. Normal Electrical Conductivity

A theory of metallic electrical conductivity based on the average velocities of conduction electrons was developed by Drude[1]. This theory was modified by Lorentz[2] using the Boltzman transport equation and a simplified model for the collisions between the electrons and the atoms in the lattice. Subsequently Sommerfeld[3] recalculated the conductivities along the lines of Lorentz' theory but replaced classical statistics by Fermi-Dirac statistics.

Electrical conductivity of a metal in the free-electron gas theory of Drude-Lorentz-Sommerfeld was given by

$$\sigma = \frac{ne^2 \tau}{m} \tag{1.1}$$

where n is the number of free electrons per unit volume

e is the electronic charge

m is the effective mass of the electron

τ is the relaxation time of electron-phonon interaction

If the electron velocity is v_F then

$$\tau = \frac{\ell}{v_F} \qquad (1.2)$$

where ℓ is the mean distance travelled between scattering collisions and is known as the mean free path.

Rewriting equation (1.1) to include the mean free path the resistivity is given by

$$\rho = \frac{m\, v_F}{n\, e^2 \ell} \qquad (1.3)$$

This simple relation was only correct for an isotropic, monovalent metal with a single conduction band. The generalised resistivity expression deduced from the free-electron model in the Quantum Mechanical Theory consisted of ideal and residual resistivity terms. The ideal resistance term was obtained from equation (1.3) and was found to be proportional to temperature ($T^{\circ}K$) at high temperatures and T^5 at low temperatures.

The principally temperature dependent parameter in equation (1.3) is ℓ , the mean free path. At high temperatures ℓ is limited by lattice vibrations and therefore ℓ increases with decreasing temperature until close to the absolute zero of temperature it reaches an upper limit determined by impurities or specimen dimensions. This limiting value of the mean free path corresponds to the residual resistivity, ρ_r. The dependence of the resistivity on the variation of temperature can therefore be explained in terms of the affect of temperature on the mean free path. The mean free path is also affected by impurities and the dimensions of the specimen.

1.3. Matthiessen's Rule

This stated that the contributions to the metallic resistivity due to different scattering mechanisms add approximately linearly, assuming that the mean free paths due to the scattering mechanisms are completely independent.

Consider the mean frequency f between scattering collisions where

$$f = \frac{1}{\tau} \tag{1.4}$$

By assuming that f_t was the temperature dependent scattering frequency and f_i was the scattering frequency associated with impurity or imperfection scattering then the total scattering frequency f was given by

$$f = f_t + f_i \tag{1.5}$$

Hence from equations (1.3) and (1.4)

$$\rho_t = \frac{m}{ne^2} \cdot f_t \tag{1.6}$$

$$\rho_i = \frac{m}{ne^2} \cdot f_i \tag{1.7}$$

$$\rho = \frac{m}{ne^2} \cdot f \tag{1.8}$$

Rewriting equation (1.5) leads to

$$\rho = \rho_t + \rho_i \tag{1.9}$$

Since ρ_t varies with temperature whereas ρ_i is independent

of temperature the resistivity will be equal to ρ_i close to the absolute zero of temperature. This is called the residual resistivity, ρ_r and its magnitude is a measure of the strains and impurities present in the conductor. Hence equation (1.9) may be written

$$\rho = \rho(T) + \rho_r \qquad (1.10)$$

1.4. Film Resistivity

Most metal surfaces appear to scatter conduction electrons diffusely. As the thickness of such a metal film is reduced to a length comparable to the mean free path in the bulk material, the effective resistivity of the film as determined from the measured resistance and specimen dimensions increases. This effect can be taken into account by replacing the bulk value of mean free path, ℓ_∞ by an effective mean free path calculated from the specimen dimensions.

The dependence of mean free path on film thickness has been derived by Fuchs[4] and is shown in Figure 1. in terms of the reduced resistivity ρ/ρ_∞ and reduced film thickness $k = t/\ell_\infty$

Limiting forms of ρ/ρ_∞ for very thick and very thin films are given by

$$k \gg 1 \quad \frac{\rho}{\rho_\infty} = 1 + \frac{3}{8k} \qquad (1.11)$$

$$k \ll 1 \quad \frac{\rho}{\rho_\infty} \quad \frac{4}{3k \left(\ln \frac{1}{k} + 0.4228 \right)} \qquad (1.12)$$

1.5. Determination of Film Thickness

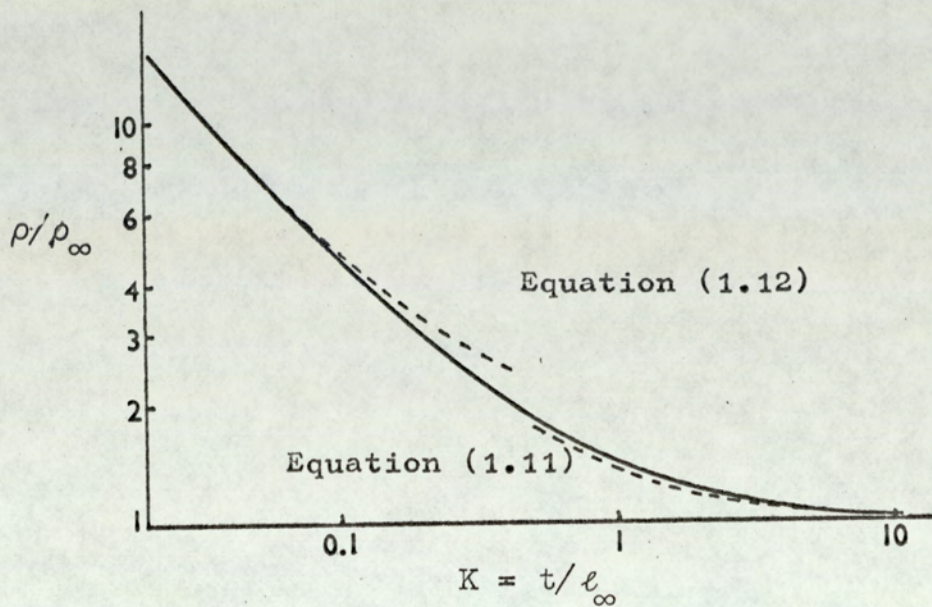The expression for the resistivity of thick films, equation

Figure 1. Reduced resistivity as a function
of reduced thickness, for a metal
film. After Mayer[5]. Solid line
represents exact equation.[4]

(1.11) may be rewritten as

$$\rho = \rho_{\infty} + \frac{3\rho_{\infty}\ell_{\infty}}{8t} \qquad (1.13)$$

If v_F is assumed to be temperature independent it follows from equation (1.3) that the term $\ell_{\infty}\rho_{\infty}$ is also independent of temperature, hence differentiating equation (1.13) with respect to temperature leads to

$$\frac{d\rho}{dT} = \frac{d\rho_{\infty}(T)}{dT} \qquad (1.14)$$

which is independent of film thickness. Hence for a film of resistance R

$$\frac{dR}{dT} = \frac{d\rho_{\infty}}{dT} \cdot \frac{film\ length}{width \times thickness} \qquad (1.15)$$

Since $d\rho_{\infty}/dT$ is a constant of the material the film thickness can be estimated from measured values of dR/dT if the width and length are known.

1.6. Superconductivity

The disappearance of the electrical resistance of mercury at liquid helium temperature was first observed by Onnes[6] in 1911, he called this phenomenon 'superconductivity'. An early step towards a phenomenological theory of superconductivity was made by Gorter and Casimir[7] who showed that the thermodynamic properties of super-conductors could be accounted for by assuming that their conduction electrons were divided into two 'fluids' or phases. The electrons in one phase were considered to retain their normal properties (n_n), but a proportion $(n_s/n_s + n_n)$ was assumed to be condensed into a lower free energy phase in which it could carry current without Joule dissipation of heat. This proportion

$(n_s/n_s + n_n)$ was assumed to be unity at the absolute zero of
temperature and zero at the critical temperature (T_c).

An analysis of the electrodynamic properties of a zero
resistance material showed that under the influence of an electric
field E the conduction electrons of mass m and charge e would be
accelerated indefinitely according to

$$m \dot{v} = E e \tag{1.16}$$

with a resultant current

$$J = n v e \tag{1.17}$$

this leads to

$$\frac{n e^2}{m c} \dot{H} + \text{curl } \dot{J} = 0 \tag{1.18}$$

F. and H. London incorporated this perfect conductivity and
the perfect diamagnetic characteristics by replacing equation
(1.18) with

$$\frac{n_s e^2}{m c} H + \text{curl } J_s = 0 \tag{1.19}$$

where n_s and J_s are respectively the volume density and current
density of the superconducting portion of the conduction electrons.
The spatial penetration of an external magnetic field H_o into a
superconductor was given by combining Maxwell's equations with
equation (1.19) and led to

$$H = H_o \exp(-x/\lambda_L) \tag{1.20}$$

where $\lambda_L^2 = \dfrac{mc^2}{4\,\Pi\,ne^2}$ (1.21)

The London penetration depth, λ_L calculated from free electron values, was found to be about 10^{-6} cm. Observed values for the penetration depth are generally about 5×10^{-6} cm.

Ginzburg and Landau[9] (GL) introduced an effective wave function or superconducting order parameter ψ . This wave function satisfied the normalised condition.

$$\left|\psi\right|^2 = n_s \qquad (1.22)$$

where n_s was the density of super electrons. They predicted a positive interphase boundary energy when

$$K > 1/\sqrt{2} \qquad (1.23)$$

where K was the low field (London) limit and was given by

$$K = \dfrac{\sqrt{2}.\ \overset{*}{e}.\ H_c.\ \lambda^2}{\hbar\,c} \qquad 1.24$$

here $\overset{*}{e}$ was the charge of the superelectron. The GL theory predicted that a superconductor with a positive interphase boundary would remain superconducting up to a magnetic field

$$H_{c2} = \sqrt{2}.\ K.\ H_c \qquad (1.25)$$

without exhibiting the Meissner effect. Abrikosov[10] called this Type II or hard superconductivity, Figure 2. The state below H_{c2} but above H_{c1} was called the mixed state. Superconductors which satisfy

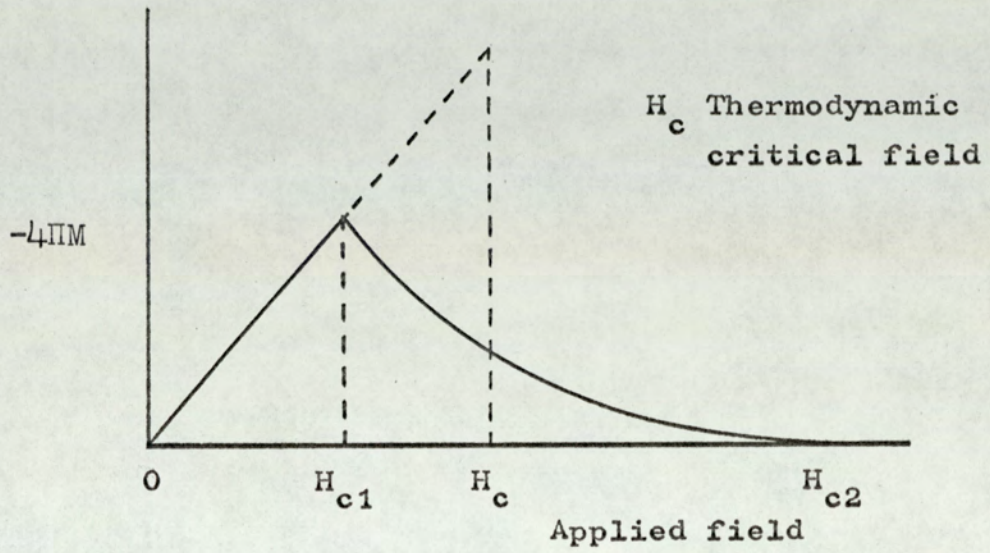$$K < 1/\sqrt{2} \qquad (1.26)$$

Figure 2. Behaviour of Type II superconductor
in an external magnetic field.
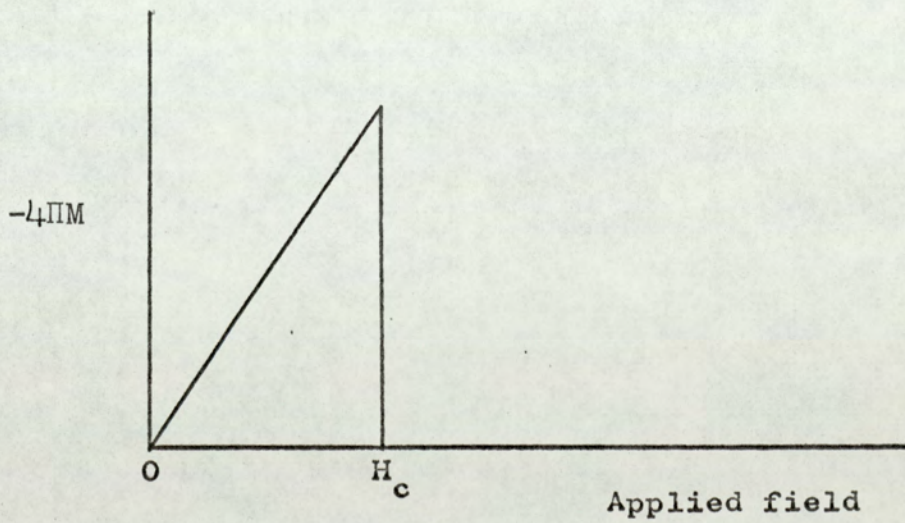
Figure 3. Behaviour of Type I superconductor
in an external magnetic field.

were termed Type I or soft superconductors, Figure 3.

Pippard[11] suggested that the superconducting state could be characterised by a finite range of momentum coherence such that the order parameter gradually changed over a distance ξ , the 'coherence length'. The coherence length may be estimated from the Uncertainty Principle as

$$\xi \; \simeq \; \frac{\hbar}{\triangle p} \; \simeq \; \frac{h.v_F}{k.Tc} \qquad (1.27)$$

Pippard estimated the value of ξ to be 10^{-4} cm from the available data on the field dependence of the penetration depth.

The microscopic theory of superconductivity was proposed by Bardeen, Cooper and Schrieffer[12] (BCS). This theory was based on the condensation into a lower energy phase of pairs of electrons with equal and opposite momentum, due to an attractive electron-phonon interaction. The low energy state was separated from the normal state by an energy gap of $2\triangle$ electron volts, which decreases from 3.52 kT_c electron volts ($\sim 10^{-4}$ electron volts) at 0°K to zero at $T_c^{\;\circ}$K.

The size of the Cooper pair or the correlation distance of the BCS theory corresponded to Pippard's coherence length and was given by

$$\xi_o \; = \; 0.18 \; \frac{h\,v_F}{k.T_c} \qquad (1.28)$$

Gorkov[13] showed that the GL theory may be derived from the BCS theory provided that

$$\overset{*}{e} = 2e \qquad (1.29)$$

such that the superelectron was a Cooper pair and for a pure
superconductor very close to the transition temperature, (T_c).

$$K \simeq 0.96 \frac{\lambda}{\xi_o} \qquad (1.30)$$

Abrikosov's analysis of Type II superconductivity based on
the GL theory predicted flux penetration in filaments parallel
to the external field and arranged in a regular pattern. These
filaments were believed to consist of individual quanta of flux.
The GL theory as applied to Type II superconductivity in
conjunction with the modifications submitted by later workers is
usually denoted as the Ginzburg-Landau-Abrikosov-Gorkov (GLAG)
theory.

Saint-James and de Gennes[14] have shown that even above H_{c2}
and up to

$$H_{c3} = 1.7 \, H_{c2} \qquad (1.31)$$

a superconducting 'sheath' persisted on surfaces parallel to the
applied field. This phenomenon was called 'surface superconductivity'.

1.7 Preparation of Niobium Thin Films

1.7.1. Introduction

Some difficulties arise in the preparation of films of high
melting point materials such as niobium. Thermal evaporation
techniques require heating the sample to temperatures of the order
of $3000^{\circ}K$ to achieve satisfactory evaporation rates. Such high
temperatures in the evaporation chamber lead to increased outgassing

rates and to a subsequent deterioration of the vacuum. The gettering action of freshly deposited niobium makes it important that the evaporation pressure, and particularly the partial pressure of oxygen in the evaporation chamber should be as low as possible.

An alternative method would be the use of sputtering techniques. However although this method does not involve very high temperatures in the evaporation chamber, it does require a high pressure for the plasma which does involve the need for special sputtering techniques in order to preclude gaseous impurities from the films.

In the following sections various methods are described which have been employed for the preparation of niobium films of high purity by thermal evaporation and sputtering techniques.

1.7.2. Thermal Evaporation of Niobium

The method most commonly employed consisted of heating the niobium sample by means of electron beam bombardment. In an alternative suggested by London and Clarke[15], niobium wire was heated directly by the passage of a heavy current. Since the wire could not be heated to the melting point the deposition rate was necessarily low; about 18 $\overset{o}{A}$ min.$^{-1}$. However the pressure in the evaporation chamber could be maintained at 1×10^{-10} torr during the evaporation. The films were deposited onto substrates held at $220^{o}K$ and the electrical properties of the films were determined before and after removal from the vacuum chamber.

Using a 13 kW electron beam Fowler[16] achieved deposition rates of 400 to 1200 $\overset{o}{A}$ sec.$^{-1}$. The films were deposited onto

polished quartz or copper substrates held at 500°K in a vacuum of 1×10^{-5} torr. The films so produced were shiny, metallic and adhered strongly to the substrates. After removal from the vacuum the dependence of the critical current upon the applied external field was determined.

Neugebauer and Ekvall[17] suggested a method for preparing pure films that did not necessitate such high deposition rates. It was argued that due to the strong gettering action for oxygen and gases containing oxygen displayed by niobium, an extensive evaporation of niobium onto the surfaces of the vacuum chamber prior to the deposition of the films, would reduce the partial pressures of these gases sufficiently to enable pure thin films to be prepared even at a pressure of 1×10^{-5} torr. With a deposition rate of 80 Å min.$^{-1}$ films were deposited onto substrates held at 220°K, 300°K and 800°K. After removal from the vacuum chamber the critical temperatures and the structure of the films were determined.

Using this method, Neugebauer and Rairden[18] deposited films at a rate of 2000 Å min.$^{-1}$ with a 6 kW electron beam in a vacuum of 1×10^{-5} torr. The effect of substrate temperature on the resistance ratios, lattice parameters and critical temperatures was determined for the films after removal from the vacuum chamber.

Asada and Nosé[19] prepared niobium films at a pressure of 5×10^{-8} torr achieving deposition rates of 100 to 300 Å min.$^{-1}$ onto substrates held at 550°K. Film structure was examined by

transmission electron microscopy. The transition temperatures

and the variation of transition temperature with film thickness

and residual resistivity was determined.

Hutchinson[20], Olsen[21] and Conella[22] have made extensive

studies of the structure of niobium films prepared in a vacuum

of 10^{-7} to 10^{-5} torr at rates varying from 2 $\overset{o}{A}$ min^{-1} to 800 $\overset{o}{A}$ min^{-1}

onto substrates held at $300^{o}K$ to $1000^{o}K$.

Gerstenberg and Hall[23] deposited films at a rate of 1800 $\overset{o}{A}$ min^{-1}

onto polished quartz substrates held at $700^{o}K$ in a vacuum of

2×10^{-6} torr. The resistivity of the films was determined at

$300^{o}K$ and $10^{o}K$ and the transition temperature was determined as a

function of the resistance ratio.

1.7.3. Sputtering of Niobium

Sputtering techniques offer an alternative method for the

deposition of films of high melting point materials without the

need for very high temperatures within the vacuum chamber.

Frerichs[24] observed that during the sputtering of niobium,

the substrate and the surfaces of the vacuum chamber were covered

by a dark brown-black film which contained the impurities gettered

during the deposition. However, the cathode itself stayed bright

and clean due to the constant bombardment by argon ions which

drove out the impurities. It was concluded that pure films could

be obtained if the substrates were subjected to a similar bombardment

by the argon ions during the deposition process.

To achieve this, sputtering was done using an asymmetric

alternating current. In the forward direction (substrate positive)

the cathode was sputtered with a current density of 0.5 mA cm^{-2}, on the reverse phase the electrode carrying the substrate was sputtered with a current density of 0.1 mA cm^{-2}. Using an argon pressure of 0.1 to 0.2 torr, bright shiny films were produced which were perfectly superconducting at 4.2°K.

Using this method Frerichs and Kircher[25] deposited films at rates of 70 to 200 Å min^{-1} onto substrates held at 77°K, 370°K and 800°K in order to investigate the effect of substrate temperature on film purity and the dependence of the transition temperature on film purity. It was also found that the optimum ratio of the sputtering to reverse sputtering current densities was 4 : 1.

Hauser and Theuerer[26] introduced the method of getter sputtering for niobium and similar metals. The essential feature of this method was that it utilised the gettering action of the sputtering material to purify the argon before it reached the part of the system where film deposition was taking place. Films were deposited at rates of 150 to 440 Å min^{-1} onto substrates held at 600 to 800°K. Later work[27] performed on films prepared in this way was an investigation into size effects of thin films.

Edgecumbe et al[28] deposited films in a low pressure hot cathode discharge tube. Deposition rates of 40 to 400 Å min^{-1} were obtained in an argon pressure of 0.6 to 2 x 10^{-3} torr onto substrates held at 700°K. Transition temperatures and resistivity ratios were determined.

Sosniak and Hull[29] prepared films using direct current diode

sputtering. The effects of different presputter periods and different substrate temperatures on the purity of the films was investigated. Film thicknesses ranged from 1500 to 2000 $\overset{o}{A}$ with deposition rates of 90 $\overset{o}{A}$ min^{-1}.

Later work by Sosniak[30] compared the properties of films prepared by direct current diode sputtering and substrate bias sputtering. Electrical resistivities of the films were invest-igated as a function of substrate temperature and residual vacuum. Crystal structure was investigated by X-ray diffraction for a number of films.

Ogawa et al[31] prepared films by tetrode sputtering, the argon gas used in the sputtering procedure was purified by using the getter action of a titanium sublimation pump. Films 2500 to 3500 $\overset{o}{A}$ thick were deposited at a rate of 150 $\overset{o}{A}$ min^{-1} onto substrates held at 600°K. The electrical properties of the films were determined as a function of substrate temperature, presputter period and purity of the argon gas.

1.8. Review of the Properties of Niobium Films

1.8.1. Structure

The effects of adsorbed gas, deposition rate and substrate temperature on the structure and grain size of niobium films has been investigated by several workers.

Neugebauer and Ekvall found that films deposited onto substrates held at 800°K had the body centred cubic (bcc) niobium structure only, with the pure niobium lattice parameter a_{o} = 3.300 $\overset{o}{A}$ $\pm$ 0.001 $\overset{o}{A}$. However it was found that the body

Table 1   Comparison of d values obtained from a niobium film to d values obtained from Nb_6O [17]

hkl	Nb film ($a_o = 3.39$) $d\ \overset{o}{A}$	Nb_6O ($a_o = 3.39$) $d\ \overset{o}{A}$
110	2.40	2.39
200	1.70	1.69
211	1.39	1.37
220	1.20	1.20
310	1.07	1.07

Table 2   Effect of substrate temperature on lattice parameter [18]

Thickness $\overset{o}{A}$	$a_o (T_s = 500^{\circ}K)$	$a_o (T_s = 700^{\circ}K)$
5000	3.313	3.303
10000	3.313	3.307
20000	3.303	3.300

T_s - Temperature of substrate

centred cube was distorted and the lattice parameter inflated by
3% to 60% for films deposited onto substrates at 300°K or less.
A comparison is shown in Table I of the d values obtained from a
film of a_{o} = 3.390 Å to the d values obtained by Brauer et al[32]
for a suboxide of niobium that led to the belief that the films
were partially composed of Nb_6O.

Rairden and Neugebauer deposited equal thickness films
simultaneously onto substrates held at 500°K and 700°K. A
comparison of the lattice parameters is shown in Table 2. As can
be seen the lattice parameters for the films deposited at the higher
temperature are closer to that of pure niobium than the corresponding
films deposited at the lower temperature. Grain sizes were estimated
to be greater than 100 Å and usually several thousand Angstroms.

Investigations into the structure of niobium films deposited
onto polished magnesium oxide crystals showed that the most
favourable conditions for bcc niobium structures were deposition
rates of 120 to 240 Å min^{-1} and substrate temperatures of 300 to
800°K[20,22]. At higher temperatures, 800 to 1100°K, a thin initial
layer of fcc niobium or niobium oxide or both may precede the normal
bcc growth structure[21,22].

Deposition rates of 100 to 200 Å min^{-1} onto magnesium oxide
substrates held at about 500°K produced films with grain sizes of
a few hundred Angstroms. Films deposited under similar conditions
on glass substrates were observed to have a bcc structure without
oxide and to be polycrystalline with grain sizes of 100 to 200 Å [19].

For films 2500 to 3500 Å thick Ogawa et al identified the

crystal structure as bcc niobium in all cases. Films having resistivities below $35\mu\Omega$-cm could be characterised by the single lattice parameter a_o = 3.300 Å which was in good agreement with that of pure niobium.

Hauser and Theuerer showed a dependence of grain size on film thickness. A film of thickness quoted as 37000 Å was found to have a grain size of slightly larger than 100 Å but this was reduced to about 30 Å for a film 120 Å thick.

1.8.2. Resistivity

In common with most metallic films the resistivity of niobium films was found to increase as the thickness of the film decreased. Since the temperature dependent portion of the resistivity increased with decreasing thickness, the resistivity ratio ρ_{300}/ρ_{10}, or resistance ratio R_{300}/R_{10} was found to decrease with decreasing thickness.

The relationship between the thickness of the film and the resistivity was complicated by the ready adsorption of oxygen into the films. Experiments performed by DeSorbo[33] on bulk niobium demonstrated that the residual resistivity was increased by $5.2\mu\Omega$-cm/ atomic % of oxygen. Rairden and Neugebauer extended these results to niobium films, two equal thickness films were simultaneously deposited onto substrates held at 500°K and 700°K. It would be expected that the film deposited onto the higher temperature substrate would have a lower concentration of gaseous impurities. The results are summarised in Table 3 and as can be seen a considerable improvement of the purity, as determined by the

Table 3   Effect of substrate temperature on the resistance
ratio and the transition temperature [12]

Thickness Å	Substrate 500°K		Substrate 700°K	
	R_{300}/R_{10}	T_c	R_{300}/R_{10}	T_c
5000	1.86	7.95	4.17	9.18
10000	4.30	9.18	5.40	9.35
20000	5.00	9.25	13.0	9.46

Table 4   Effect of deposition rate on the resistivity
ratio of similar thickness films [22]

Thickness Å	Rate Å min^{-1}	ρ_{300}/ρ_{10}
46800	780	28.4
42000	470	15.3
3560	15	3.14
3560	120	8.10

resistance ratios was observed for films deposited at the higher temperature.

Conella demonstrated a similar improvement of resistivity ratio by depositing similar thickness films onto substrates held at the same temperature but with different deposition rates, the results are shown in Table 4.

Providing that a series of films of different thickness are deposited under the same conditions, so as to maintain a constant concentration of gaseous impurities or no impurities at all, then the resistivity or the resistivity ratio will increase as the film thickness decreases. The results of Gerstenberg and Hall, Table 5, and Asada and Nosé, Table 6, demonstrate the dependence of resistivity upon the thickness.

1.8.3. Transition Temperature

The transition temperature of niobium films has been found to depend upon the degree of gaseous impurity in the film and the thickness of the film. Many workers have based their interpretation of film properties on the work of DeSorbo on the effect of dissolved oxygen in bulk niobium.

DeSorbo determined that for bulk niobium the transition temperature was decreased by 0.93°K/atomic % of oxygen. At an oxygen concentration of 3.83 atomic % the transition temperature had a minimum value of 5.84°K. Increasing the concentration beyond this value resulted in an increase of the transition temperature from the minimum value until at a concentration of 6.43 atomic % the transition temperature reached a value of 9.02°K. At higher concentrations it was found that oxygen precipitated yielding various oxides[34-36]. No results were quoted of bulk inclusion

Table 5 The effect of decreasing film thickness on the room temperature resistivity and the transition temperature [23]

ρ_{300} $\mu\Omega$ -cm	Thickness Å	T_c °K
14.6	∞	9.46
16.9	6000	9.11
21.6	2050	8.81
25.4	420	8.12

Table 6 The effect of decreasing film thickness on the residual resistivity and the transition temperature [19]

ρ_{10} $\mu\Omega$ -cm	Thickness Å	T_c °K
0.164	∞	9.28
7.0	7500	9.00
13.0	4500	8.95
54	1050	8.50
71	500	7.00
88	400	6.40

of oxygen producing a non-superconducting condition.

According to DeSorbo the critical temperature of niobium
varies with oxygen concentration as

$$T_c = 9.46 - C \rho_{10} \tag{1.32}$$

where $C = 0.177$ deg/$\mu\Omega$-cm. This formula holds only down to the
minimum transition temperature $T_c = 5.84^{\circ}$K.

Gerstenberg and Hall applied this formula to niobium films.
As can be seen from Figure 4 the agreement between evaporated films
and bulk niobium with interstitial oxygen was found to be very good.
Rairden and Neugebauer modified equation (1.32) by assuming that
the increase in the room temperature resistivity was entirely due
to the increase in the residual resistivity i.e. Matthiessen's
Rule was obeyed and $\rho_{300} - \rho_{10} =$ constant. Therefore the
inverse resistance ratio also varies linearly with oxygen concentration,
hence

$$\frac{R_{10}}{R_{300} - R_{10}} = \frac{\rho_{10}}{\rho_{300} - \rho_{10}} = \text{(constant)} \times \text{(oxygen concentration)} \tag{1.33}$$

the resulting equation from combining (1.32) and (1.33)

$$T_c = 9.46 - 2.48 \frac{R_{10}}{R_{300} - R_{10}} \tag{1.34}$$

A plot of equation (1.34) and the experimental results are
shown in Figure 5.

The dependence of the critical temperature upon film thickness
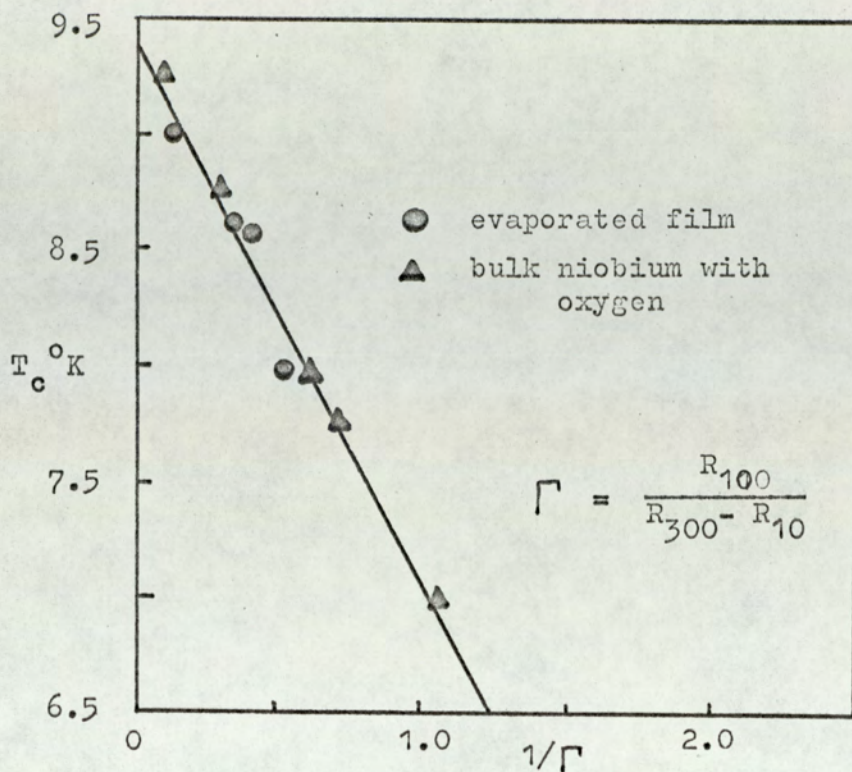and residual resistivity obtained from the results of Asada and

Figure 4. Critical temperature of niobium films as
a function of the inverse resistance ratio
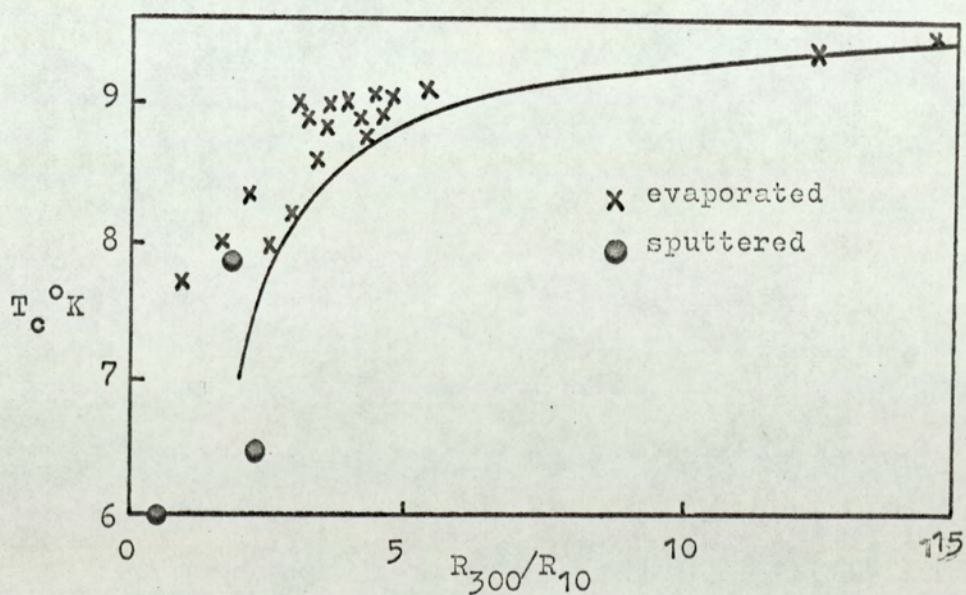compared to bulk niobium with interstitial
oxygen.[23]

$$\Gamma = \frac{R_{100}}{R_{300} - R_{10}}$$

Figure 5. Critical temperatures of niobium films as
a function of the resistance ratio compared
to the predicted modified DeSorbo relationship.[18]

Nosé are shown in Figures 6 and 7. However, these workers noted that a film of 490 $\overset{o}{A}$ which had a predicted transition temperature of 8.63^{o}K had an observed value of 7.90^{o}K. Since the film was prepared under conditions in which it was estimated that the oxygen contamination should not be more that 0.7 atomic % it was suggested that the decrease in the transition temperature depended not only on the amount of interstitial impurities but also upon another factor, possibly grain size.

As can be seen it is not easy to discriminate between variations in the transition temperature introduced by oxygen content and by reducing film thickness or particle size.

1.8.4. Critical Current Density

These are reported variations of the values for critical current density. This may be due to the variation in methods employed, for example, pulsed current techniques or direct current measurements and the type of substrate used, copper, quartz or glass. Fowler found that heating of films occurred on quartz substrates for currents greater than 10 amp, but no heating effects were observed for currents of up to 50 amp for similar films deposited on copper substrates.

Some results are shown in Figures 8-10, in the examples shown the films were deposited on quartz substrates and direct current measurements were made. Edgecumbe et al determined current densities of 1×10^{6} A cm^{-2} for a 500 $\overset{o}{A}$ film increasing to 4×10^{6} A cm^{-2} for a 1500 $\overset{o}{A}$ film both being held at 4.2^{o}K. Using pulsed current techniques Frerichs and Kircher obtained 1×10^{4}A cm^{-2} for a film deposited on Vycor tubing.
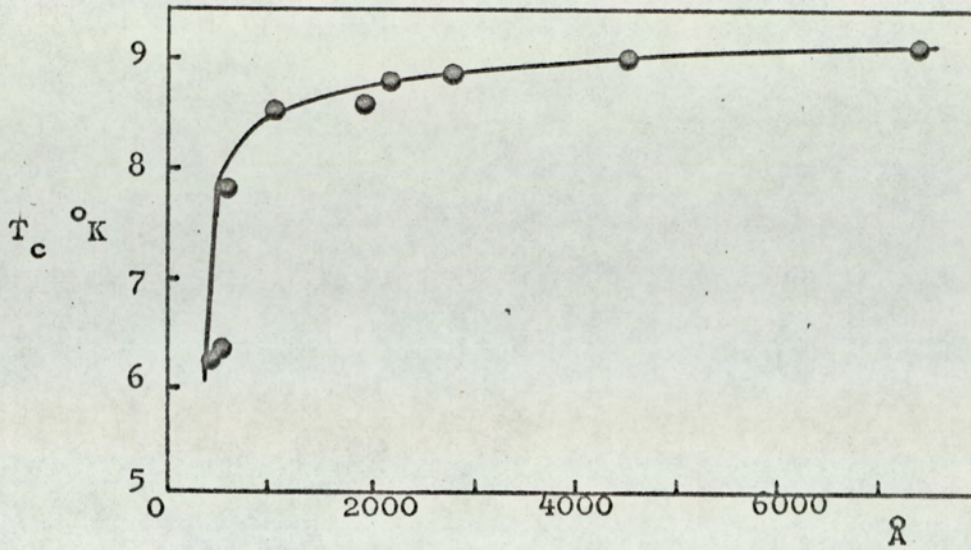
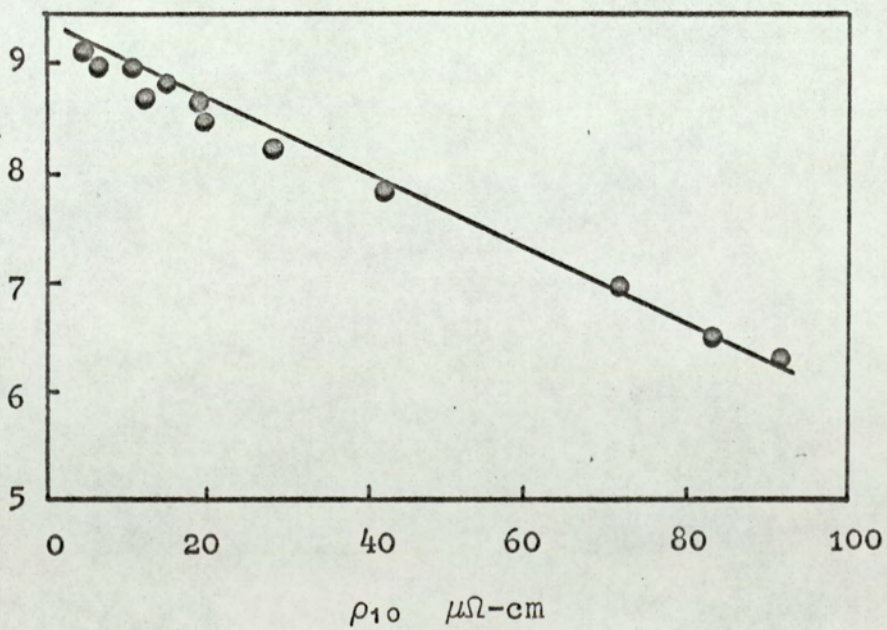Figure 6. Variation of transition temperature
with film thickness.[19]

Figure 7. Variation of transition temperature
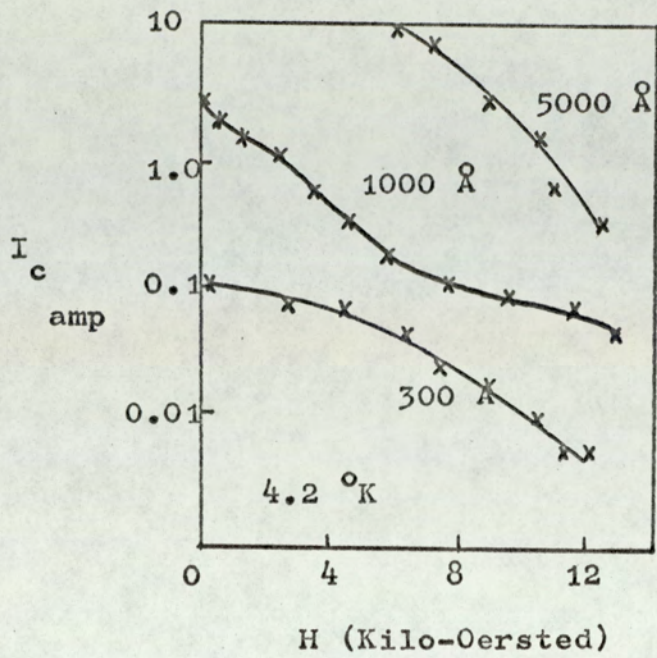with residual resistivity.[19]

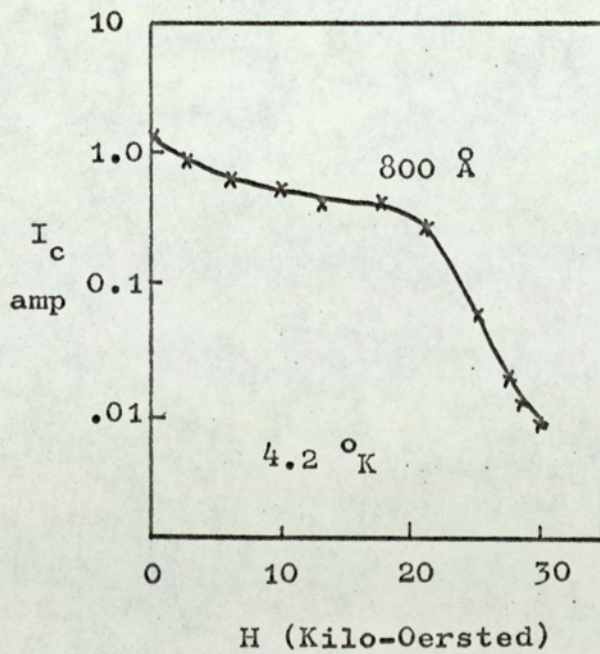Figure 8. Critical current vs transverse field.
(Fowler)[16]

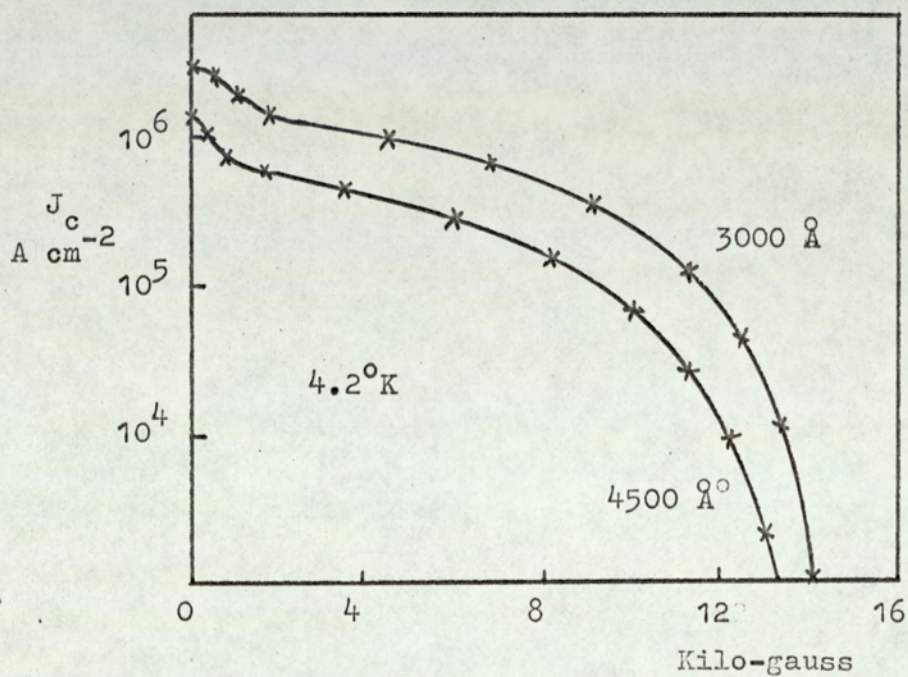Figure 9. Critical current vs longitudinal field.
(Fowler)[16]

Figure 10. Critical current density versus
longitudinal magnetic field.
(Neugebauer and Ekvall)[17]

CHAPTER 2

ESSENTIAL THEORY

2.1. Introduction

Until recently, the only method displaying any success for predicting whether a material would superconduct and at what temperature, was based on the empirical rules of Matthias[37]. Using these rules and with some experience and knowledge of transition temperatures for a variety of superconducting elements, compounds and alloys a better than order-of-magnitude estimate of transition temperature for a new material could be determined. However, this method gives no indication of the mechanisms responsible for super-conductivity whereas by a detailed study of the interactions it should be possible to predict the value of the transition temperature with some degree of accuracy.

The BCS[12] theory of superconductivity suggested that the electron-phonon interaction was the dominant mechanism. According to the BCS theory there is a relationship between the transition temperature Tc, a typical phonon energy $<\omega>$ and the interaction strength $N(O)V$

$$Tc = 1.14 \ <\omega> \ exp \left[-1/N(O)V \right] \qquad (2.1)$$

where $N(O)$ is the electronic density of states at the Fermi surface.

V is the pairing potential arising from the electron-phonon interaction.

A better understanding of the electron-phonon and electron-electron interactions followed from the BCS theory, and it has been shown by Schrieffer[38] that the current theory as summarized by the gap equation of Eliashberg[39] is accurate to a few per cent. Hence,

if all the required normal state parameters of a metal are known, the transition temperature can be calculated to this accuracy.

Such calculations have been performed by Ambergoakar and Tewordt[40], Scalapino et al[41], Carbotte and Dynes[42], and Allen and Cohen[43]. In general it is a tedious operation and usually it is easier to actually measure the transition temperature. McMillan[44] developed a simpler expression, to determine the transition temperature, which only contained parameters which were either known or easily calculable.

2.2. The McMillan Equation

McMillan derived an expression for determining the transition temperature of a superconductor using the so called "strong coupled" theory, as a function of the coupling constants for the electron-phonon and Coulomb interactions. It was assumed that the BCS theory of superconductivity was applicable and that given certain properties of the normal state of a metal it was possible to calculate the transition temperature.

Since the necessary properties were not sufficiently well known the problem was approached from the reverse direction. For a large number of metals and alloys the transition temperature Tc, the Debye temperature Θ and the electronic specific heat γ were well known and also for a few metals there were values of the phonon energies and the isotope shift of the transition temperature.

By making use of the theoretical formula for the transition temperature in conjunction with the known experimental data, empirical values for the electron-phonon coupling constant λ , and the phonon enhancement of cyclotron mass and specific heat can be

found.   The measured isotope shifts can be used to find empirical values for the Coulomb coupling constant μ^*.

Solutions of the integral equations given by Ambegoakar and Tewordt and Scalapino et al for the normal and pairing self energies at the transition temperature were computed by McMillan following the procedure of Morel and Anderson[45].

This led to the definition of a dimensionless electron-phonon coupling constant λ,

$$\lambda \; \equiv 2 \int_{0}^{\omega_o} \alpha^2(\omega) \, F(\omega) \, \frac{d\omega}{\omega} \qquad (2.2)$$

where ω_o is the maximum phonon frequency

$\alpha^2(\omega)$ is an average of the electron-phonon interaction

$F(\omega)$ is the phonon density of states

The strong coupling expression analogous to equation (2.1) was found and given by McMillan:-

$$\frac{T_c}{\omega_o} = \exp\left[\frac{-(1+\lambda)}{\lambda - \mu^* - (\langle\omega\rangle/\omega_o)\lambda\mu^*} \right] \qquad (2.3)$$

$\langle\omega\rangle$ is the average phonon frequency

μ^* is the Coulomb coupling constant of Morel and Anderson, given by

$$\mu* = \frac{N(0)V_c}{1 + N(0)V_c \, Ln(E_B/\omega_o)} \qquad (2.4)$$

V_c is the matrix element of the screened Coulomb interaction averaged over the Fermi surface.

E_B is the electronic bandwidth.

Using the available data for niobium the final formula for
the transition temperature as determined by McMillan was given by

$$Tc = \frac{\Theta}{1.45} \exp \left[\frac{-1.04(1 + \lambda)}{\lambda - \mu^* (1 + 0.62 \lambda)} \right] \qquad (2.5)$$

Although McMillan used the Debye temperature Θ for the
characteristic phonon frequency, the maximum phonon frequency
ω_o, or the average phonon frequency $<\omega>$ could just as well have
been used.

In weak coupled superconductors equation (2.3) reduces to the
BCS result with $\lambda - \mu^*$ playing the role of N(O)V. In strong
coupling the Coulomb interaction modifies the gap function in such
a way that the phonon contribution is reduced from λ to
$\lambda [1 - (<\omega> / \omega_o) \mu^*]$.

2.3. Generalised McMillan Equation

The use of some algebraic relation such as the McMillan equation
was found to be necessary for detailed interpretation of the variation
of Tc with pressure p, isotopic mass M, electron-phonon coupling
constant λ , crystal structure or lattice disorder. The McMillan
equation was adequate for calculating $\partial Tc / \partial p$ or $\partial Tc / \partial M$, but it
has been shown by Chen et al[46] to be in error for predicting maximum
transition temperatures for very strongly coupled ($\lambda > 1$) superconductors.
Strongin et al[47] and Garland et al[48] have shown that it has only
limited application in relating the transition temperature to the
electron density of states which result from lattice disorder.

McMillan had found that the transition temperature could be
given by an equation of the form

$$Tc = <\omega> \exp \left[\frac{-(1+\lambda)}{A\lambda - B\mu^* - C(<\omega>/\omega_o)\lambda\mu^*} \right] \quad (2.6)$$

where McMillan determined the values of the constants as
$A = B = 0.96$, $C = 1.03$ and $<\omega>/\omega_o = 0.58$.

In order to generalise the McMillan equation Garland and
Allen[49] replaced $<\omega>/\omega_o$ and A in equation (2.6) by monotonic
increasing functions

$$x = <\omega^2/\omega_o^2> = \frac{\int_0^\infty \alpha^2(\omega)F(\omega)(\omega/\omega_o)d\omega}{\int_0^\infty \alpha^2(\omega)F(\omega)(\omega/\omega_o)^{-1}d\omega} \quad (2.7)$$

Best fits were made from available electron tunnelling data
on lead, mercury, bismuth and gallium to yield the generalised
McMillan equation

$$Tc = (0.25 + 0.67x)\omega_o$$

$$x \exp \left[\frac{-(1+\lambda)}{(0.53 + 0.62x^{\frac{1}{2}})\lambda - \mu^* - (0.25 + 0.67x)\lambda\mu^*} \right] \quad (2.8)$$

This equation was estimated to be accurate to approximately
10% for calculations of λ from Tc. The greatest error was due to
uncertainties in x. When x was known from tunnelling data,
equation (2.8) was easy to use and in most cases more accurate than
the McMillan equation. However, since McMillan used the data for
niobium to determine the relationship, it was found that both
equations were in very good agreement for niobium. Since this was

the case the McMillan equation was used in the present analysis
for the investigation of the possible dependence of the transition
temperature on the phonon frequency. This analysis will be
examined later in the discussion.

2.4. Critical Current Densities in Superconducting Thin Films

2.4.1. Introduction

If the current carried by a superconductor exceeds a certain
critical value, a transition to the normal state is induced. The-
oretically the critical current could be determined conveniently
only for film geometries in which the current distribution was
uniform over the whole film so that edge effects were negligible.
Two film geometries were found that could satisfy this condition.
Feigin and Shal'nikov[50] and Ginzburg[51] showed that one geometry
was that of a film deposited on an insulating cylinder much
longer than its radius, which itself was much larger than the
film thickness. Newhouse et al[52] and Edwards and Newhouse[53]
showed that an alternative arrangement was of a flat film deposited
adjacent to and parallel to a much larger superconducting plane
of higher critical temperature.

For a thick cylindrical film, (thickness $>>$ empirical penetration
depth), the current was found to flow in an outer region to an
approximate depth of three penetration depths ($3\lambda_E \simeq 1500$ Å). The
critical current in this case was given by Silsbee's rule, that is
the current which produced a surface field equal to the film critical
field H_{CF}, at the surface of the cylinder. However, if the film was
thin, (thickness $<<$ empirical penetration depth) the current was
distributed approximately uniformly throughout the film thickness

and the surface field corresponding to the critical current was found to be smaller than H_{CF}.

For a cylindrical film or a flat film deposited on a shield plane the critical surface field H_I is given by Newhouse et al as

$$H_I = \frac{4 \Pi J_c t}{c} \qquad (2.17)$$

where J_c is the critical current density

t is the film thickness

c is the velocity of light

The field produced by a uniform current density was found to be uniform over the film surface and parallel to it.

2.4.2. Non-uniform Current Distribution

In the case of the commonly used geometry of a flat unshielded film, the surface field and the current density vary from point to point of the surface. The measured critical current density of a flat film must be less than that calculated by assuming a uniform current density, since the requirement that the surface field generated by the current be parallel to the film surface leads to the very uneven current distribution. As can be seen from figure 11 the current density approaches infinity at the film edges. If the film was thin ($t < <\lambda_E$) then magnetic fields normal to the film surface can be present.

Broom and Rhoderick[54] made an experimental study of the perpendicular component of the magnetic field produced by the current in a superconducting lead film 2000 Å thick and 0.15 cm wide. Rhoderick and Wilson[55] compared the results obtained with
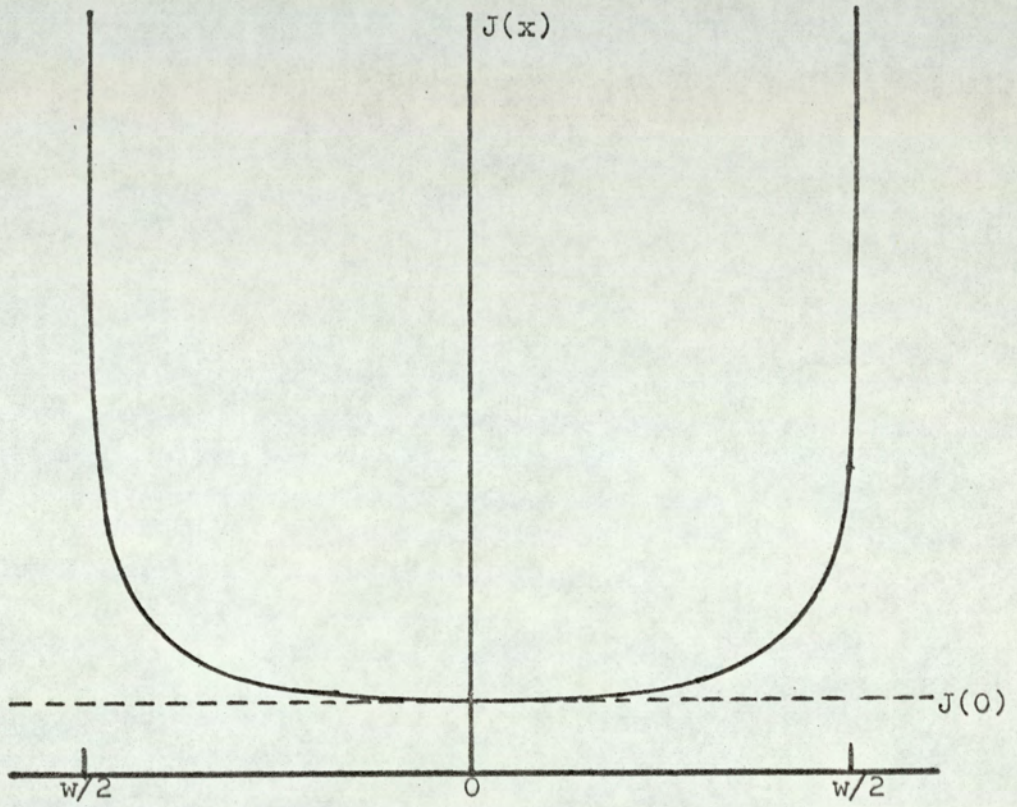
Figure 11. Current distribution across the width of a
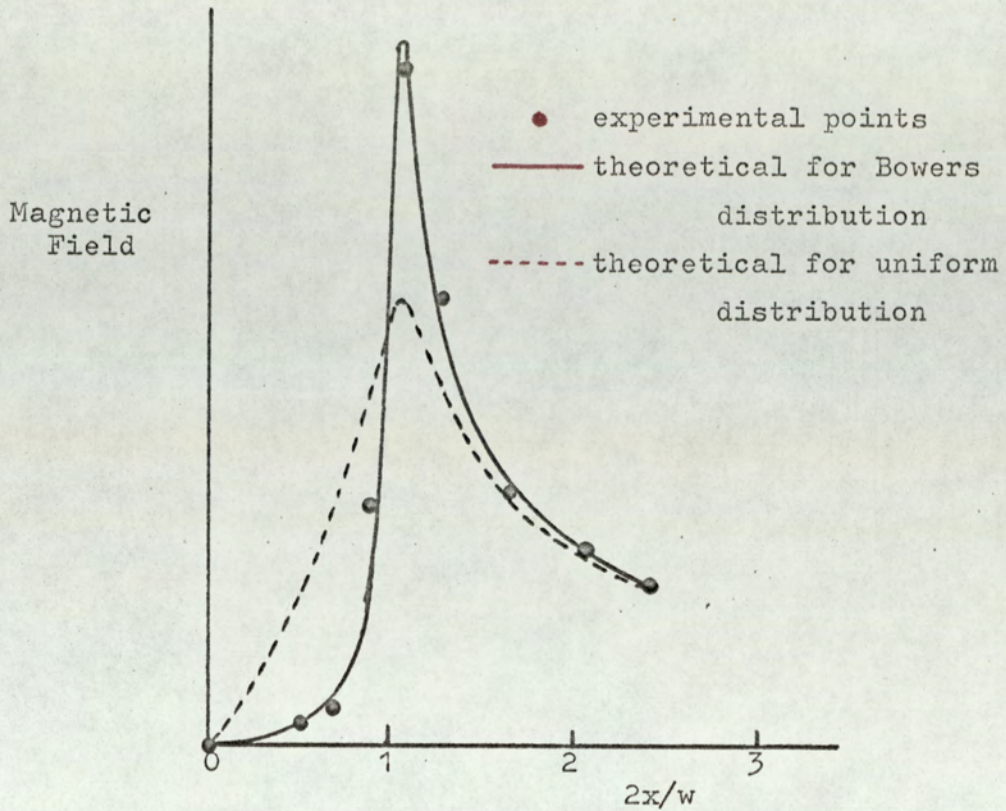flat, unshielded superconducting film.

Figure 12. Comparison of the perpendicular component
of the magnetic field due to a current
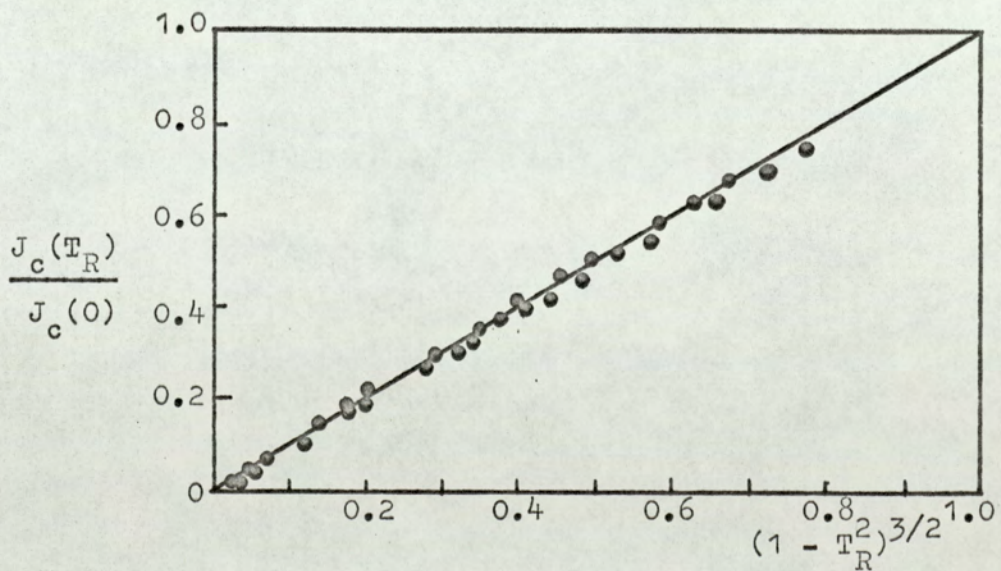through a superconducting film with that
to be expected theoretically.[55]

Figure 13. Normalised critical current densities
as a function of $(1 - T_R^2)^{3/2}$.[57]

the magnetic field distribution to be expected from Bowers'[56]
expression for the current density. The comparision is illustrated
graphically in figure 12.

Bowers' equations were for the current distribution in a
flat rectangular film subject to the London equations (1.20) and
(1.21). It was assumed that the current density was constant
through the film thickness t where $t < \lambda_E$ and that for a film of
width w, $wt > \lambda_E^2$.

The current density, in all but the extreme edge regions,
at a distance X from the centre of the film was given by Bowers
as

$$J(x) = J(0) \left[1 - \left(\frac{2x}{w} \right)^2 \right]^{-\frac{1}{2}} \qquad (2.18)$$

this solution was the same as the charge distribution on the
surface of a thin conducting strip in the analogous electrostatic
problem.

For the edge regions Bowers predicted that the current density
was of the form

$$J(x) = J\left(\frac{w}{2}\right) \exp - \left[t \left(\frac{w}{2} - x \right)/b \, \lambda_E^2 \right] \qquad (2.19)$$

where b is a constant of the order of unity.

The two solutions can be matched at a point $b \, \lambda_E^2/2t$ from
the edge of the film since there can be no discontinuity in $J(x)$,
so that the slopes and magnitudes are equal. At this point

$$J\left(\frac{w}{2}\right) = \left[\frac{2.718 \, wt}{2b} \right]^{\frac{1}{2}} \frac{J(0)}{\lambda_E} \qquad (2.20)$$

By integrating over the total width of the film Glover and Coffey[57] determined the total current to be

$$I = \Pi wt \frac{1}{2} J(0) \qquad (2.21)$$

As shown in figure 11 the maximum current density occurs at the edges of the film and the minimum at the centre of the film. Since λ_E is temperature dependent the peaking of the current at the edges will change with temperature, becoming more pronounced as the temperature is lowered.

Assuming the temperature dependence of the penetration depth to be of the form given by the Gorter and Casimir[7] two fluid model of a superconductor

$$\lambda_E(T_R) = \frac{\lambda_E(0)}{(1 - T_R^4)^{\frac{1}{2}}} \qquad (2.22)$$

where $\lambda_E(0)$ is the empirical penetration depth at $T_R = 0$

T_R is the reduced temperature $= T/T_c$

Glover and Coffey eliminated $J(0)$ from equations (2.20) and (2.21) to determine the current density at the edge of the film.

When the total current is the critical current I_c, (the measured quantity) the current density at the edge is the critical current density given by

$$J_c(T) = \left[\frac{2 \times 2.718}{bwt}\right]^{\frac{1}{2}} \frac{I_c(T)(1 - T_R^4)^{\frac{1}{2}}}{\Pi \lambda_E(0)} \qquad (2.23)$$

It was found more convenient to examine the temperature dependence of the critical current density by normalizing equation

(2.23)

$$\frac{J_c(T)}{J_c(0)} = \frac{I_c(T)}{I_c(0)\,(1 - T_R^4)^{\frac{1}{2}}} \qquad (2.24)$$

where $J_c(0)$ is the critical current density at $T = 0^\circ K$

$I_c(0)$ is the critical current at $T = 0^\circ K$

Bardeen[58] had established an expression for the critical current density for the case where the electron mean free path was very much less than the coherence length.

$$\frac{\ell}{\xi_0} \ll 1 \qquad (2.25)$$

The expression was obtained from the equations giving the temperature dependence of the critical field and of the penetration depth.

$$H_c(T_R) = H_c(0)\,(1 - T_R^2) \qquad (2.26)$$

$$\lambda_E(T_R) = \frac{\lambda_E(0)}{(1 - T_R^4)^{\frac{1}{2}}} \qquad (2.27)$$

so that $\dfrac{H_c(T_R)}{\lambda_E(T_R)} = \dfrac{H_c(0)}{\lambda_E(0)}\,(1 - T_R^2)^{3/2}\,(1 + T_R^2)^{\frac{1}{2}} \qquad (2.28)$

To obtain a useful approximation valid for all temperatures, the resistivity ρ, can be expressed in terms of the conductivity of the normal state.

$$\frac{1}{\rho} = \sigma = \frac{ne^2\ell}{mv_F} \qquad (2.29)$$

for $\ell \ll \xi_o$, the usual situation for thin films,

$$J_c(T_R) \simeq \frac{2}{3} H_c(0) \left(\frac{\sigma}{\xi_o} \right)^{\frac{1}{2}} (1 - T_R^2)^{3/2} \qquad (2.30)$$

$$= \frac{1}{2} H_c(0) \left[\frac{\Delta(0) \sigma}{\hbar} \right]^{\frac{1}{2}} (1 - T_R^2)^{3/2} \qquad (2.31)$$

where $\Delta(0)$ is half the energy gap at $0^\circ K$

σ is the residual normal state conductivity

Since $H_c(0)$ is proportional to $\Delta(0)$ and ξ_o proportional to $\Delta(0)$, the current density varies as $T_c^{3/2}$. An approximate formula based on the free electron model is given by

$$J_c(T_R) \simeq 3 \left(\frac{\ell}{\xi_o} \right)^{\frac{1}{2}} T_c (1 - T_R^2)^{3/2} \times 10^6 \text{ A cm}^{-2} \qquad (2.32)$$

Glover and Coffey obtained values of normalized critical current density from measurements of critical current I_c, and transition temperature T_c. Their results are shown in figure 13, where the normalized critical current density is plotted as a function of $(1 - T_R^2)^{3/2}$. The constant $I_c(0)$ (estimated critical current at $0^\circ K$) was picked for each film so as to put the measured points on the line in the vicinity of $T_R = 0.6$. As can be seen, all the points were found to be on the straight line of slope equal to unity.

Hence the critical current density as determined from equation (2.24) is given by

$$J_c(T_R) = J_c(0) (1 - T_R^2)^{3/2} \qquad (2.33)$$

By setting $T = 0$ in equation (2.23) the critical current
density at $0^\circ K$ can be expressed as

$$J_c(0) = \left[\frac{2 \times 2.718}{bwt} \right]^{\frac{1}{2}} \frac{I_c(0)}{\Pi \lambda_E(0)} \qquad (2.34)$$

A combination of equations (2.24) and (2.33) leads to

$$I_c(T_R) = I_c(0) \frac{(1 - T_R^2)}{(1 + T_R^2)^{\frac{1}{2}}} \qquad (2.35)$$

by extrapolation to $0^\circ K$ this expression can be used to obtain a
value for the critical current density at $0^\circ K$.

2.5. Determination of Oxide Thickness by Ellipsometry

Ellipsometry is a technique well suited for the examination
of thin films of materials and surface layers. Essentially, the
technique involves the determination of the optical properties of
a reflecting surface or film and which in turn enables the thickness
of film on substrates to be measured. This was achieved by
determining the ellipticity, after reflection from a surface, of
light which was initially plane polarized. For absorbing materials
the limit of the depth from which information is available
obviously depends on the penetration of the electromagnetic radiation.

The Fresnel reflection coefficients for non absorbing media
are given by

$$R_{olp} = \frac{n_o \cos \phi_1 - n_1 \cos \phi_o}{n_o \cos \phi_1 + n_1 \cos \phi_o} \qquad (2.36)$$

$$R_{ols} = \frac{n_o \cos \phi_o - n_1 \cos \phi_1}{n_o \cos \phi_o + n_1 \cos \phi_1} \qquad (2.37)$$

for light travelling from medium 0 to 1, having angles of incidence and refraction ϕ_o and ϕ_1 respectively, with the non absorbing media having refractive indices n_o and n_1 respectively. Suffices p and s refer to the electric vector parallel and perpendicular to the plane of incidence respectively.

The basic equation of ellipsometry is

$$\frac{R_p}{R_s} = \tan \psi \; e^{i\Delta} \qquad (2.38)$$

The angles ψ and Δ are determined by polariser and analyser readings of the instrument.

For a non absorbing surface film of refractive index n_1 on a substrate of refractive index n_2, the Fresnel reflection coefficients are written as

$$R_p = \frac{R_{olp} + R_{12p} \; \exp D}{1 + R_{olp} R_{12p} \; \exp D} \qquad (2.39)$$

with a similar expression for R_s.

where $D = 4 \Pi n_2 \cos \phi \; t / \lambda$

    t is the film thickness

    λ is the wavelength of light used

For an absorbing media a complex refractive index $N = n - ik$ replaces the refractive index n so that the Fresnel coefficients also become complex as does the value of D.

$$D = 4 \Pi i N_2 \cos \phi_1 \; t_2 / \lambda \qquad (2.40)$$

For an opaque, clean film surface, n and k are related to the instrument readings ψ and Δ through equations (2.36), (2.37) and (2.38) and are given in a form suitable for computation by Ditchburn[59] as

$$n^2 - k^2 = \frac{\sin^2 \phi_o \tan^2 \phi_o (\cos^2 2\psi - \sin^2 2\psi \sin^2 \Delta) + \sin^2 \phi_o}{(1 + \sin 2\psi \cos \Delta)^2}$$

(2.41)

$$2nk = \frac{\sin^2 \phi_o \tan^2 \phi_o \sin 4\psi \sin \Delta}{(1 + \sin 2\psi \cos \Delta)^2}$$

(2.42)

For an oxidized surface, the angles ψ and Δ are changed from the values for a clean surface. Providing that the optical constants of the oxide free surface are known then any subsequent changes of the instrument angles ψ and Δ can be used to determine the thickness of the oxide film formed if k is zero for such a film. For an absorbing film the thickness can be computed if the refractive index is known. Alternatively the refractive index can be determined experimentally by various methods, (Neal and Fane)[60].

CHAPTER 3

EXPERIMENTAL DETAILS

3.1. Evaporation Unit

3.1.1. Introduction

In order to obtain niobium films of sufficiently high purity
to demonstrate reproducible superconducting characteristics, the
amount of gas, particularly oxygen, present in the films must be
kept to a minimum. This condition may be satisfied in three ways:

1. The vacuum system must be capable of producing a base
vacuum better than 10^{-8} torr in the evaporation chamber.

2. The rate of deposition of the films must be high in order
to minimise the time for gaseous contamination.

3. The maintenance of the substrate at an elevated temperature
to reduce the sticking coefficient of gas molecules that do impinge
on the film during deposition.

By incorporating all three conditions in the evaporation
unit it was found possible to deposit niobium films of the required
characteristics given above.

3.1.2. Vacuum System

The arrangement of the vacuum system can be seen in Figures
14 and 15. The ultra high vacuum (U.H.V.) was obtained by means
of a 200 lit. $\sec^{-1}$ Ultek Sputter Ion Pump attached directly to the
vacuum chamber. The rough vacuum elements were connected to a
2.5 cm diameter manifold which could be isolated from the vacuum
chamber by a bakable U.H.V. valve.

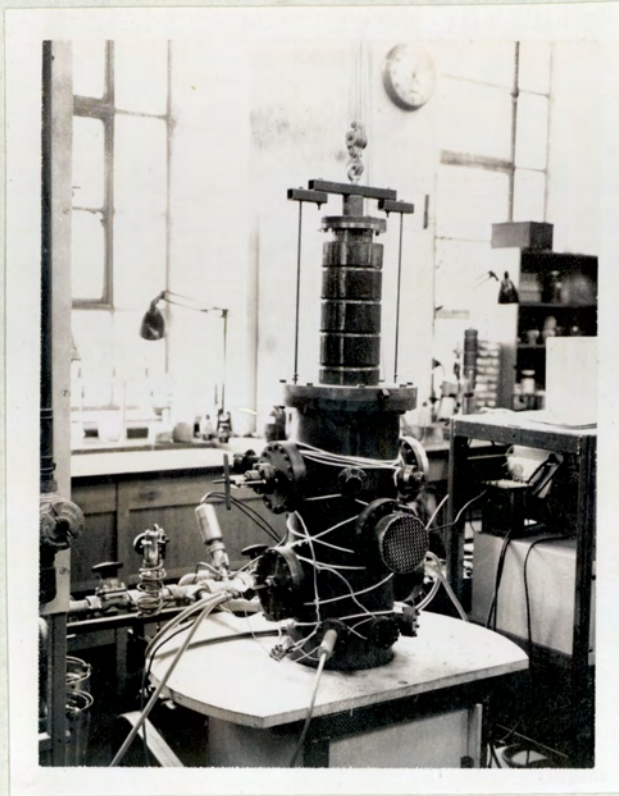The initial rough pumping of the vacuum chamber was by means

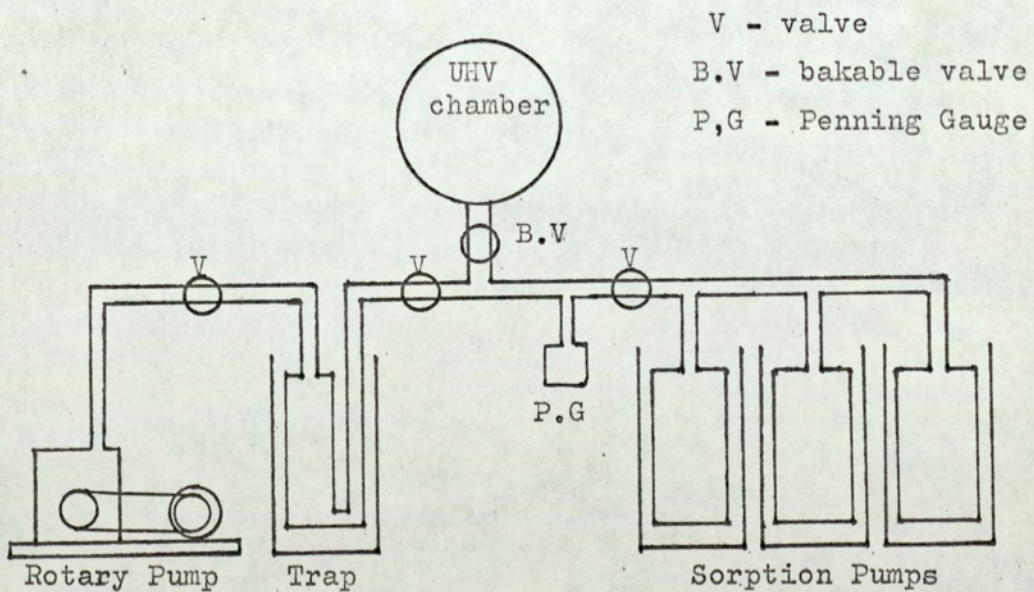Figure 14. General view of vacuum chamber and cryostat.

Figure 15. Arrangement of rough pumping elements.

of a 250 lit. sec^{-1} Edwards single stage rotary pump, followed by
sorption pumping. A liquid nitrogen trap was interposed between
the pump and the manifold to prevent backstreaming of rotary pump
oil into the vacuum system. This trap was of the glass disc type
and has been fully described elsewhere[61]. The rotary pump was also
employed to evacuate the sorption pumps prior to cooling the pumps
with liquid nitrogen.

The three sorption pumps used were constructed of stainless
steel and perforated copper sheet. The body of each pump was a
stainless steel cylinder, 10 cm diameter and 30 cm long, inside
each cylinder were six perforated copper sheets brazed to the wall
of the cylinder to act as heat exchangers. Each cylinder was
sealed by a stainless steel plate at top and bottom, the upper
plate being fitted with a 2.5 cm diameter stainless steel tube
that connected to the manifold. Each pump was filled with zeolite
and mounted in a dewar.

The ion pump was surrounded by an oven containing two 500 watt
heater elements controlled by a Variac, this enabled the pump to be
baked and maintained at a temperature of 400°K while in operation.
Similarly controlled heater tapes positioned around the vacuum
chamber would raise the temperature of the chamber to 420°K.

3.1.3. Vacuum Chamber

The stainless steel vacuum chamber was constructed by Ferranti Ltd.
The chamber consisted of a cylinder, 25 cm in diameter and 60 cm long,
fitted with a number of flanges. The five 6.5 inch diameter
flanges were sealed by means of aluminium wire seals[62]. The

remaining flanges were standard 2.75 inch diameter copper gasket flanges. The cryostat assembly and the ion pump were mounted directly onto the vacuum chamber and sealed by means of aluminium wire.

Observation ports were fitted to three flanges so as to be able to view the substrate, the shutter assembly and the niobium sample in the crucible of the electron beam evaporator. The latter was viewed indirectly via a stainless steel mirror positioned inside the vacuum chamber.

Other ports were utilised to carry electrical lead throughs for supplying power to the electron beam evaporator and the substrate heaters, and one eight-way lead through that carried all the connections and thermocouple wires concerned directly with measurements on the films.

One port carried the electron beam evaporator in conjunction with cooling water for the crucible. In preliminary tests on the vacuum system it was found that radiation from the electron beam evaporator produced unacceptably high temperatures on the walls of the vacuum chamber. To overcome this a water cooled stainless steel shield was designed and fitted around the evaporator, Figure 16. The shield reduced the amount of radiant heat from the molten niobium sample to the walls of the vacuum chamber and it also provided a cooled surface for the deposition of niobium for gettering purposes.

One port was used for mounting a bellows type linear motion drive, which was designed to operate the shutter mechanism. The
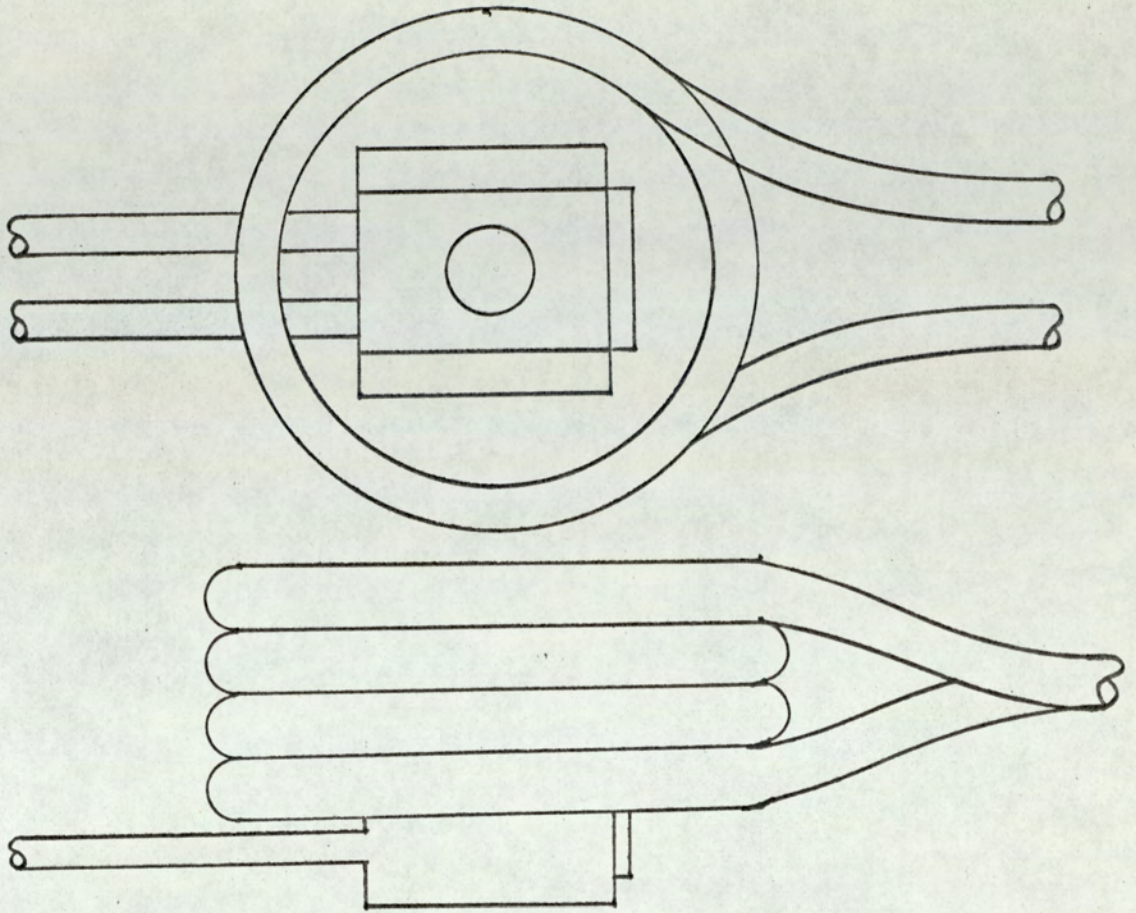
Figure 16. Positioning of the water cooled shield around
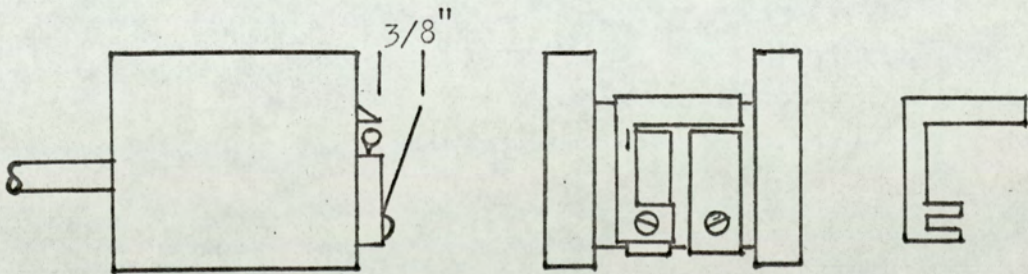the e-gun evaporator.

Figure 17. Position of the 'overspray' shield as fitted
to the e-gun evaporator.

remaining ports were used for auxiliary electrical lead throughs
for extra thermocouples, an ion gauge for pressure measurement and
a mass spectrometer head for partial pressure measurement.

3.1.4. Electron Beam Evaporator

Niobium has a melting point of about $3000^{\circ}K$ and in order to
obtain a reasonable evaporation rate, temperatures of the order of
$3800^{\circ}K$ are required. The electron beam evaporator can not only
provide these sort of temperatures but also has the advantage of
not contaminating the sample which is held in a water cooled copper
crucible.

A Varian No. 980-0001 electron beam evaporator was mounted in
the chamber so that the niobium sample in the crucible was 20 cm
from the substrate position. The evaporator was supported by the
stainless steel tubes which carried the cooling water for the
crucible. Electrical connections between the evaporator and the
lead throughs were made by uninsulated 12 SWG copper wire.

The electron beam current could be varied continuously from
0 to 500 mA, giving up to 2000 watt beam power. The initial low
rates of evaporation were considerably improved by the fitting of
an 'overspray' shield fixed to the evaporator. This was a modification
introduced by Varian on later models of the electron beam evaporator
and was reported to increase the percentage of the electron beam
striking the sample from 97% to 99%. The shield was cut from
0.05 cm thick molybdenum sheet and affixed to the evaporator as
shown in Figure 17.

3.1.5. Substrate Holder for Transfer Experiments

The substrate mounting for films that were to be examined after
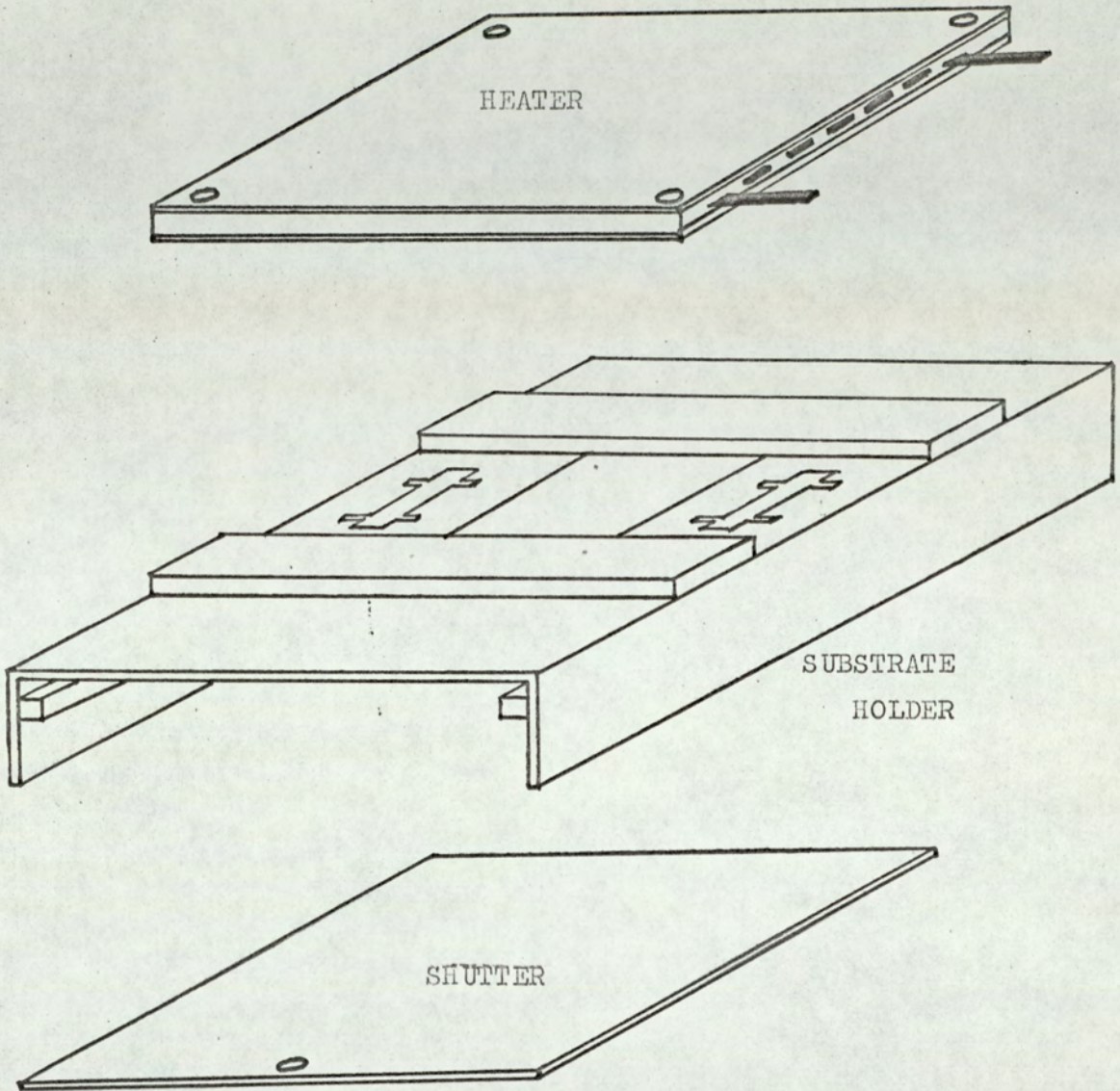
HEATER

SUBSTRATE
HOLDER

SHUTTER

Figure 18. Substrate holder for transfer experiments.

removal from the vacuum chamber was designed with the minimum of complications. The body of the holder was made of 0.10 cm thick stainless steel sheet as shown in Figure 18a, and had provision for depositing films on three substrates simultaneously.

A shutter was built into the holder, Figure 18b, and also a 120 watt nichrome heater which was capable of maintaining the substrates at temperatures up to 500°K during the deposition of films. The temperature of the substrates was determined by a copper/constantan thermocouple which was clamped onto one substrate.

The substrate holder was designed so that the freshly deposited films could be removed and clean substrates inserted without the necessity of removing the holder from the vacuum chamber. Once the heater assembly was moved to one side the substrates were exposed and could easily be replaced.

3.2. Cryostat and Substrate Holder for 'in situ' Measurements

3.2.1. Introduction

Films which were to be examined 'in situ' required a rather more sophisticated substrate holder. Since the superconducting properties of the films were to be investigated a helium cryostat was required to maintain the necessary low temperatures for an extended period of time. The substrate holder had to be attached to the cryostat so that good thermal contact existed between the liquid helium and the substrate which had to be shielded against heat radiation from the surrounding chamber. There had to be provision for an aperture in the shielding so that the deposition of a film could take place and the substrate holder had to be capable of being heated to 500°K. Finally, electrical contact to

the film had to be made and the electrical leads thermally 'grounded'
to prevent heat leaks to the film when at low temperatures.

3.2.2. Cryostat

The cryostat assembly was an integral part of the vacuum
chamber, Figure 19. The cryostat was manufactured by the Oxford
Instrument Co. and completely constructed of stainless steel. A
subsequent modification in order to improve the thermal conductivity
from the liquid helium to the substrate was the insertion of a
1.25 cm diameter copper plug brazed into the base of the helium
cryostat. The substrate holder was secured to this copper plug
thus providing an uninterrupted path of high thermal conductivity
material from the liquid helium to the substrate.

The liquid nitrogen jacket had a volume of 2 litres and the
liquid helium chamber a usable volume of 1 to 1.5 litres. When
fully operational the heat input to the helium chamber was <0.1 watt.
Thus the substrate could be maintained at near liquid helium temper-
ature for 10 to 15 hours.

A 250 lit sec^{-1} rotary pump was linked to the helium chamber
for reducing the pressure over the liquid helium, in this way it
was possible to cool the liquid helium to a temperature of about
2.1°K, giving a film temperature of about 4.0°K. A 60 watt
nichrome heater was positioned in the helium chamber so that the
heater was in partial contact with the copper plug in the base of
the cryostat. This heater could maintain the substrate at
temperatures up to 500°K. The heater was mounted on a stainless
steel tube, Figure 20, which was used to remove the liquid nitrogen
introduced to precool the helium chamber prior to the transfer of
liquid helium.

To rotary pump

Nitrogen space

Helium space

Heater
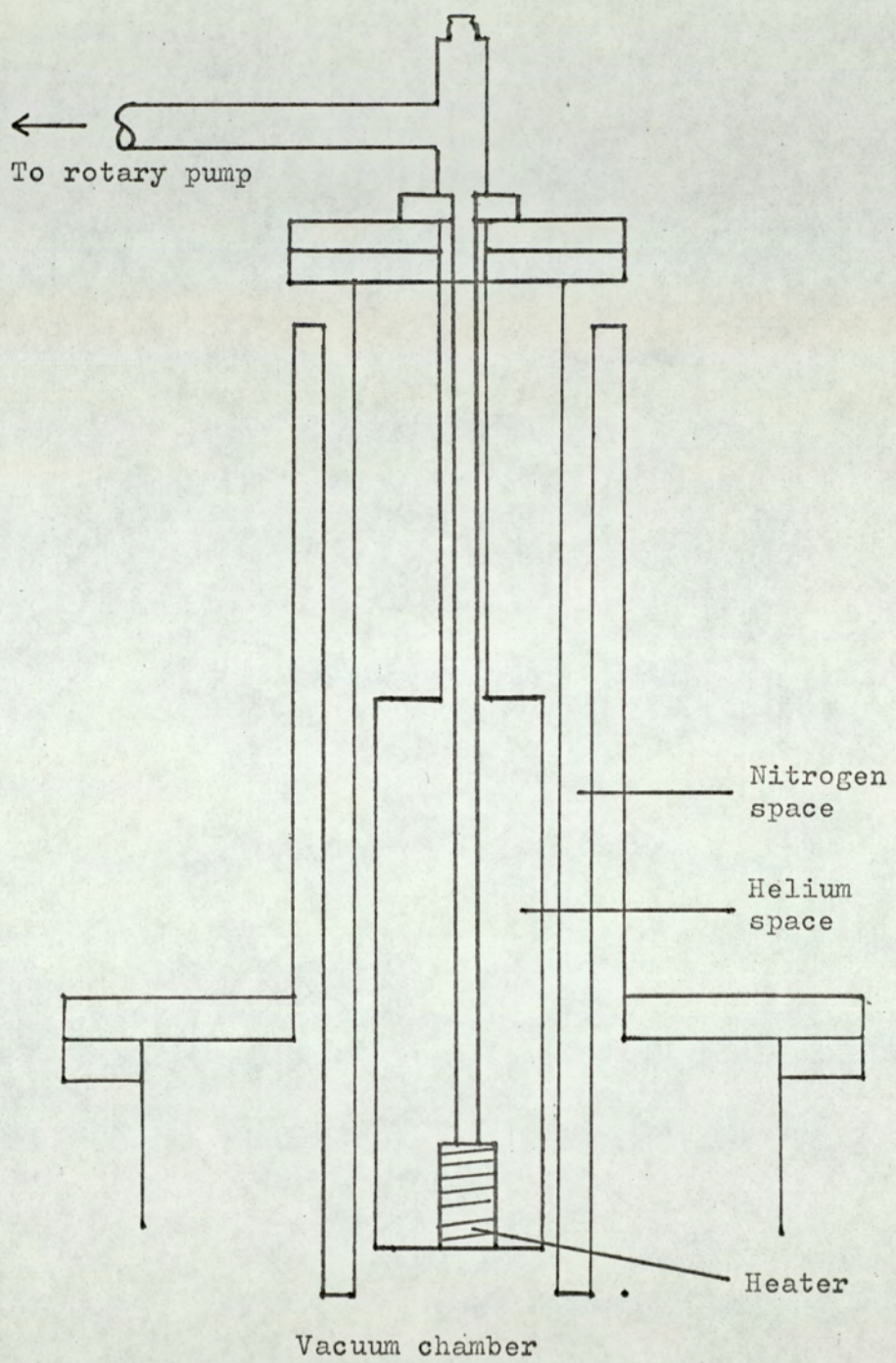
Vacuum chamber

Figures 19 and 20. Showing the heater assembly mounted
in the helium cryostat, the complete cryostat
was mounted on the vacuum chamber.

The thermal shielding for the substrate and holder was provided by two Oxygen Free High Conductivity (OFHC) copper shields, 0.1 cm thick, one of which was clamped to the helium chamber and the other to the nitrogen jacket, Figure 21. The base of the helium shield was also constructed of 0.1 cm thick copper and was fitted with a shutter which exposed an aperture 2 cm x 1.5 cm when open. The base of the nitrogen shield was constructed of 0.3 cm thick copper and was similarly fitted with a shutter. Both shutters were linked by a length of stainless steel cryogenic tubing 0.15 cm diameter so that both shutters operated simultaneously.

All the electrical leads and thermocouple wires that had to be connected to the substrate holder were anchored to the nitrogen shielding for a length of 45 cm and then to the helium shielding for a further 30 cm before reaching the substrate holder. This was in order to minimise the heat input to the substrate and the thermocouple junctions. During normal low temperature operation it was found that the shutters were the hottest parts of the shielding, having temperatures of about $11^{o}K$ and about $100^{o}K$ for helium and nitrogen shielding respectively.

3.2.3. Substrate Holder

The substrate holder was constructed from OFHC copper and was made in two parts, Figure 22a. The base component was fastened to the copper plug in the base of the helium chamber and the substrate was mounted on this component. The second part was a 'picture frame' which carried the mask, electrical contacts and thermocouple leads. Clamping the 'frame' to the base component secured the substrate and made electrical contact to the film.
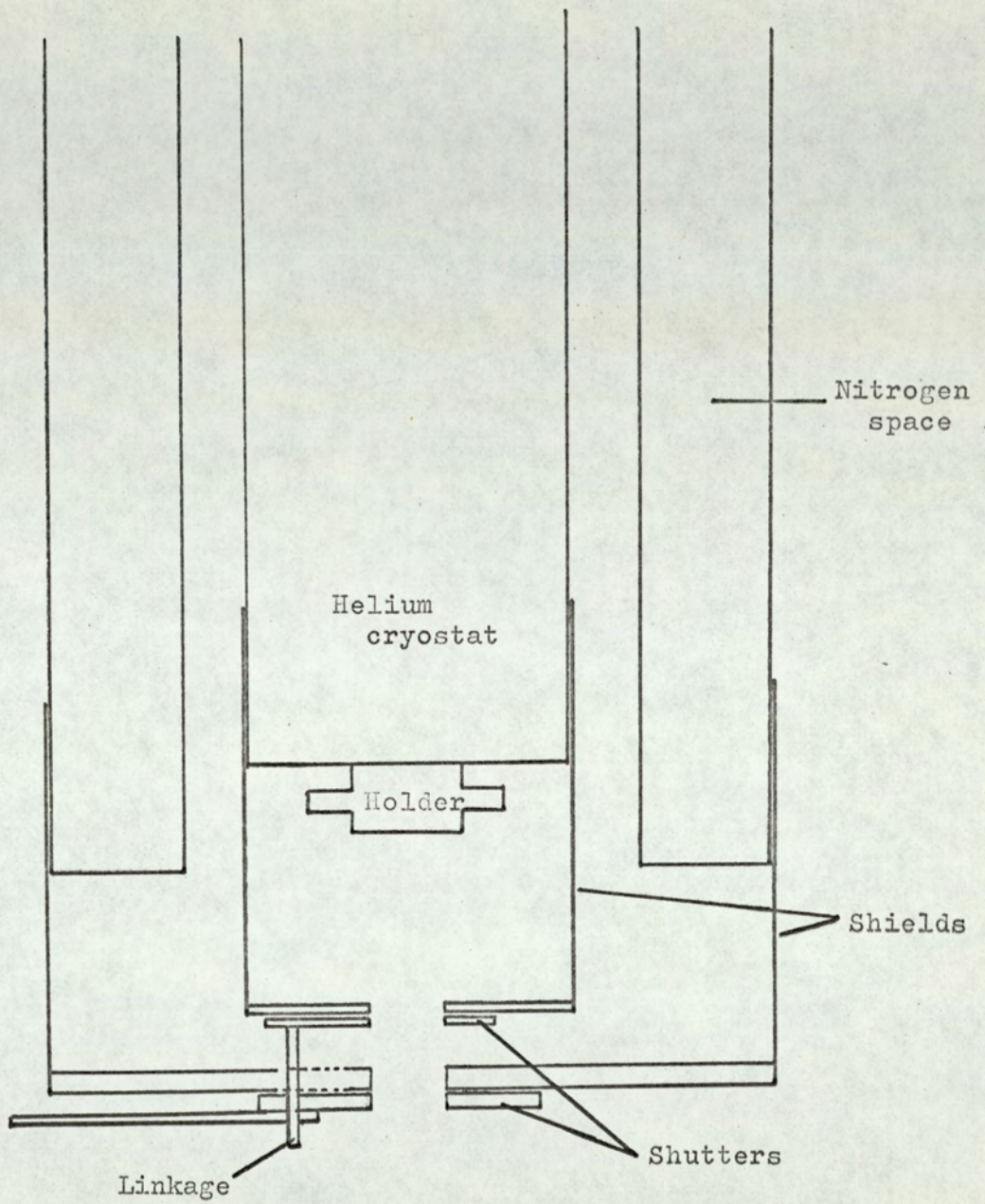
Figure 21. Arrangement of shutters and shielding for
'in situ' substrate holder

MASK

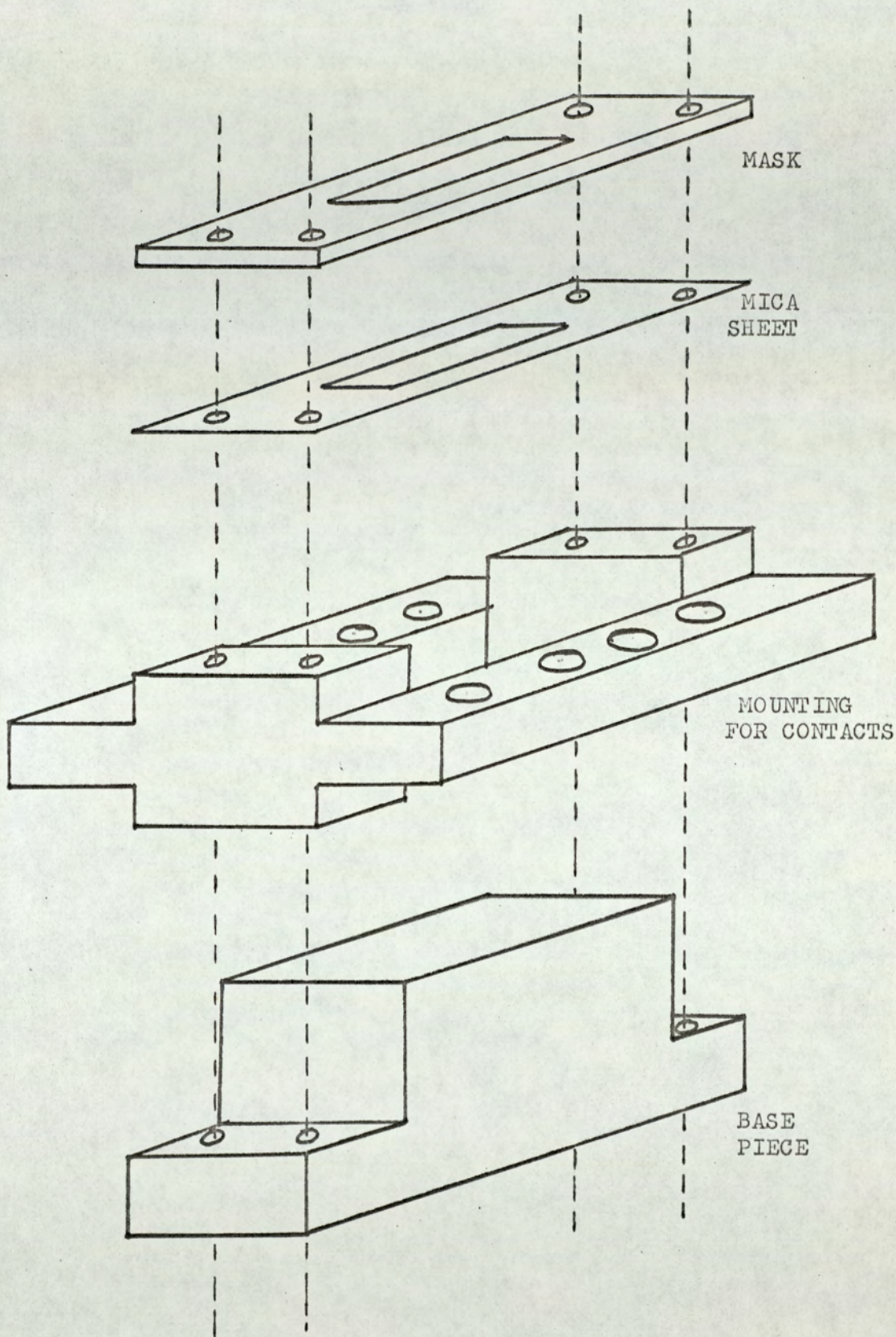MICA
SHEET

MOUNTING
FOR CONTACTS

BASE
PIECE

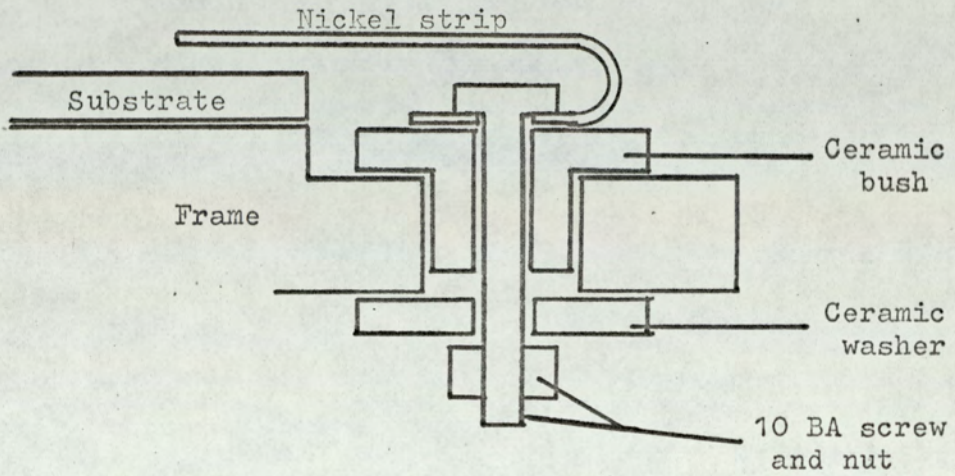Figure 22a. 'In situ' substrate holder.

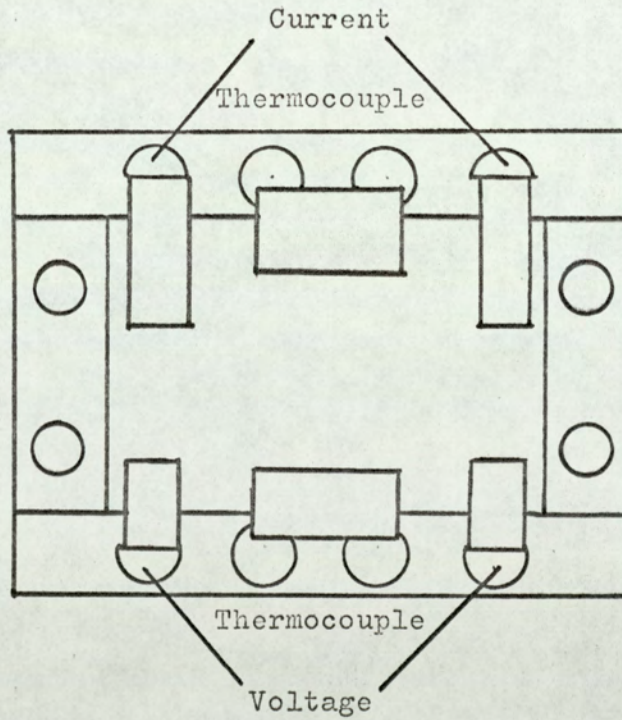Figure 22b. Detail of fixing electrical contacts to frame.

Figure 22c. Arrangement of contacts and thermocouples
on frame.

The base was machined to take a 5 watt constantan heater used for varying the temperature of the substrate over a limited range, 4 to 15°K.

Electrical contact to the film was by means of four pieces of nickel cut from a sheet 0.025 cm thick. Each piece was cut to form a narrow strip 0.2 cm wide by 1.0 cm long which widened at the base and was drilled to accommodate a 10 BA stainless steel screw. The base of the strip was doubled over to provide some springyness for the contacts. The 10 BA screws passed through ceramic bushes fitted along both longer sides of the 'frame' using nuts and ceramic washers, Figure 22b.

Voltage leads were of 40 SWG nylon covered constantan wire and current leads of 40 SWG nylon covered copper wires, all leads were spot welded to their respective nickel contacts.

Two thermocouples were used to monitor the temperature of the substrate, a copper/constantan thermocouple calibrated over the range 30°K to 500°K and a gold-iron/chromel thermocouple calibrated over the range 2°K to 80°K, and at spot temperatures up to 400°K to provide a check on the other thermocouple.

Both thermocouples were secured to the substrate in the same way. A nickel pad 0.5 cm x 0.5 cm was fashioned from 0.025 cm sheet, one end of the pad was bent over to form a 'U' channel into which was inserted the thermocouple junction. The channel was then crimped so as to hold the wires firmly in place. Each wire was then sandwiched between a ceramic bush and the securing screw so as to position the nickel pad in its correct position on the substrate, Figure 22c.

With a suitably prepared substrate in position on the base part the complete frame was clamped over it. The action of clamping the frame, pushed the nickel contacts into position onto the nichrome contact areas previously deposited on the substrate.

3.2.4. Auxiliary Cryostat and Substrate Mounting used in Transfer Experiments

The cryostat used for this part of the investigation was a standard helium cryostat manufactured by the Oxford Instrument Co. The assembly containing the substrate mounting was positioned in this cryostat by suspending it from a 1.2 cm diameter stainless steel tube which also served for evacuating the assembly.

The body of the assembly was a copper tube 15 cm long and 5 cm in diameter. The base was a 0.3 cm thick detachable brass flange sealed by means of an indium wire ring. The other end of the assembly was sealed by a fixed brass flange which also served as a mounting for the 1.2 cm stainless steel tube, Figure 23.

The substrate mounting is shown in Figures 24a and 24b, it consisted of a 1.2 cm diameter brass rod 10 cm long soldered to the base flange. Around this rod was wound a 20 watt constantan heater to raise the film temperature from $2^{\circ}K$ to $300^{\circ}K$. At the other end of the rod a 0.3 cm thick copper plate was attached to serve as a base for the substrate.

Electrical contact to the films was made in a similar manner as described in section 3.2.3. However in this case the contacts were cut from 0.012 cm thick copper foil as were the pads for the thermocouples. The copper contacts were soldered to insulated supports mounted on the copper base piece, and the contacts and pads

To rotary pump

Vacuum leadthrough for electrical connections
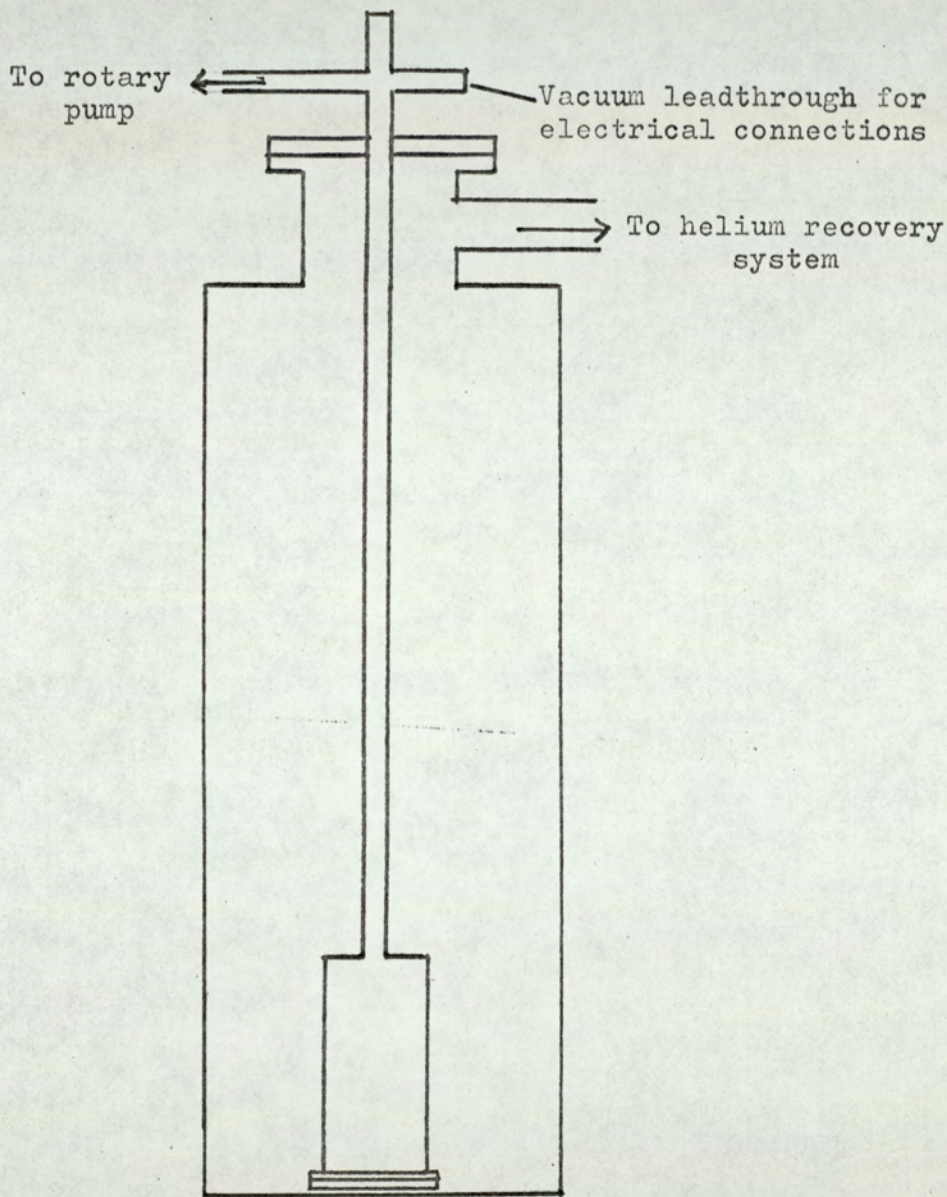
To helium recovery system

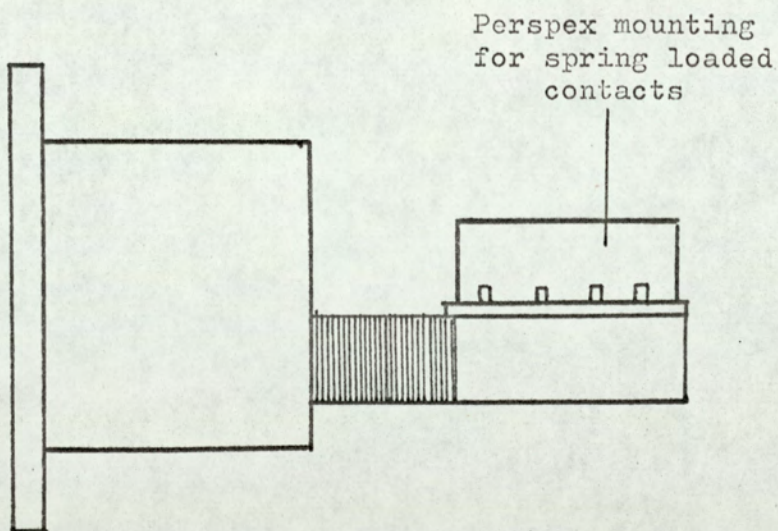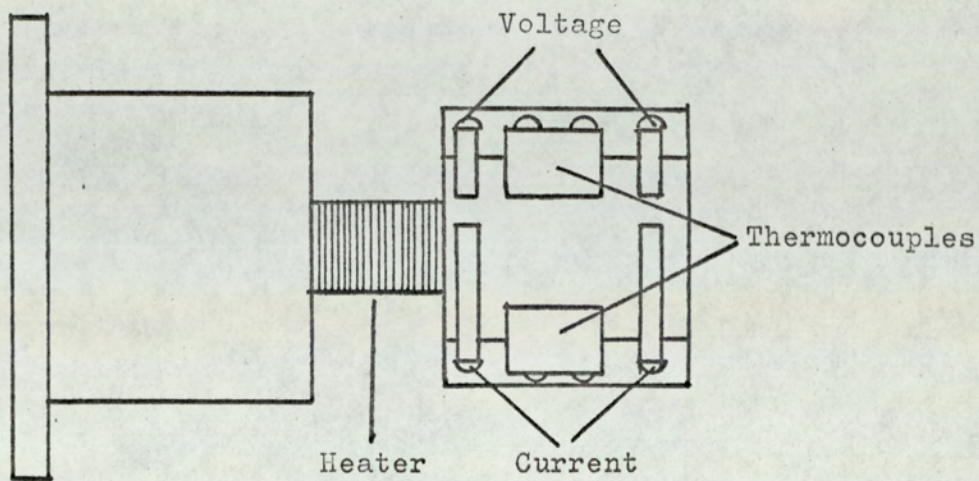Figure 23. Cryostat and assembly for transfer experiments.

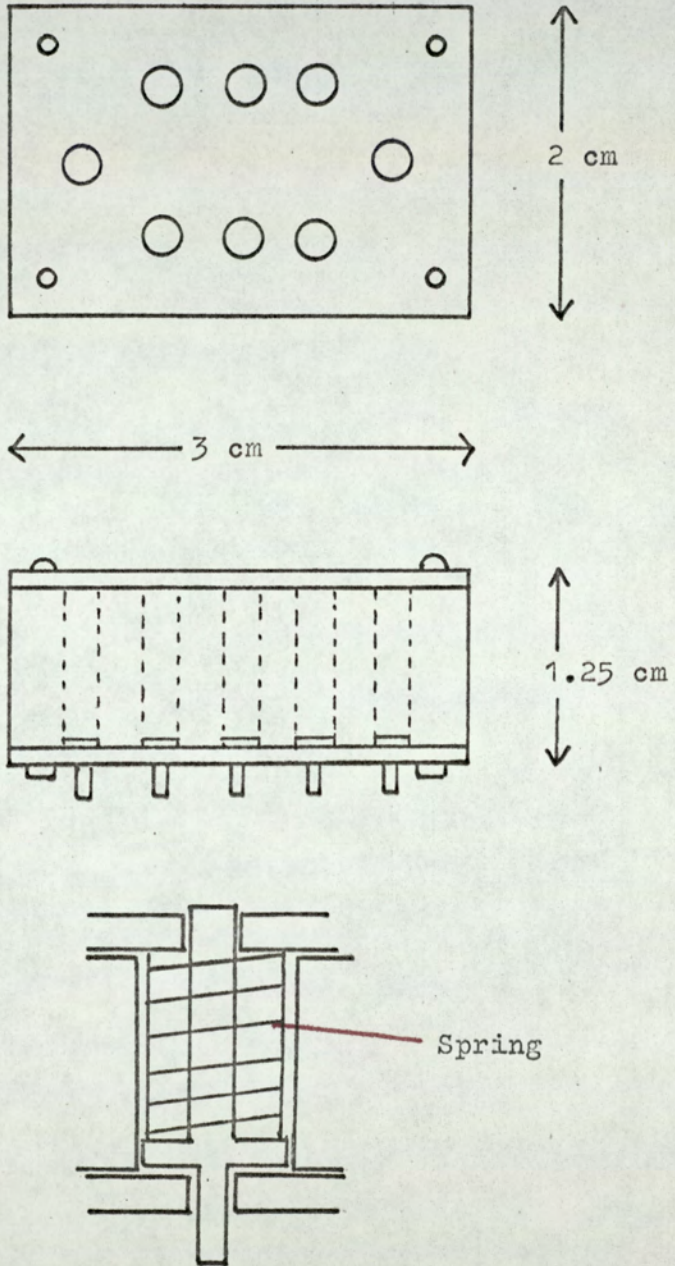Figure 24. Substrate mounting assembly for
transfer experiments.

Figure 25. Details of spring loaded contact
system.

were held down on the substrate by spring loaded rods. These rods were held in a perspex mounting that could be clamped over the substrate, Figure 25. As the mounting was tightened down the spring loaded rods pushed the copper contacts firmly onto the film. Since each rod was individually sprung even very rapid cooling of the assembly did not result in the loss of contact with the film.

The thermocouple and electrical leads were anchored for a length of 30 cm to a copper tube soldered to the brass base flange. This was to minimise the thermal input to the film. The leads then passed along the supporting tube and were brought out to the measuring circuits via a vacuum leadthrough.

A 250 lit sec^{-1} rotary pump was connected to evacuate the assembly prior to cooling, normally once the pressure in the assembly had fallen to 0.03 torr the assembly was isolated and the pump was then free to be used for reducing the pressure over the liquid helium in the cryostat. A minimum temperature of about 2.1°K could be achieved in this way.

3.2.5. Measuring Circuits

The arrangement of the electrical circuits for the investigation of the electrical properties of the films is shown in Figure 26. The current through the films was measured on a Cambridge unipivot microammeter. The current supply was a 2 volt accumulator, the output of which was controlled by suitable variable potentiometers and could be varied between 1μA and 500 mA. A reversing switch in the circuit enabled any standing voltages to be eliminated from the results. The potential developed across the film and the
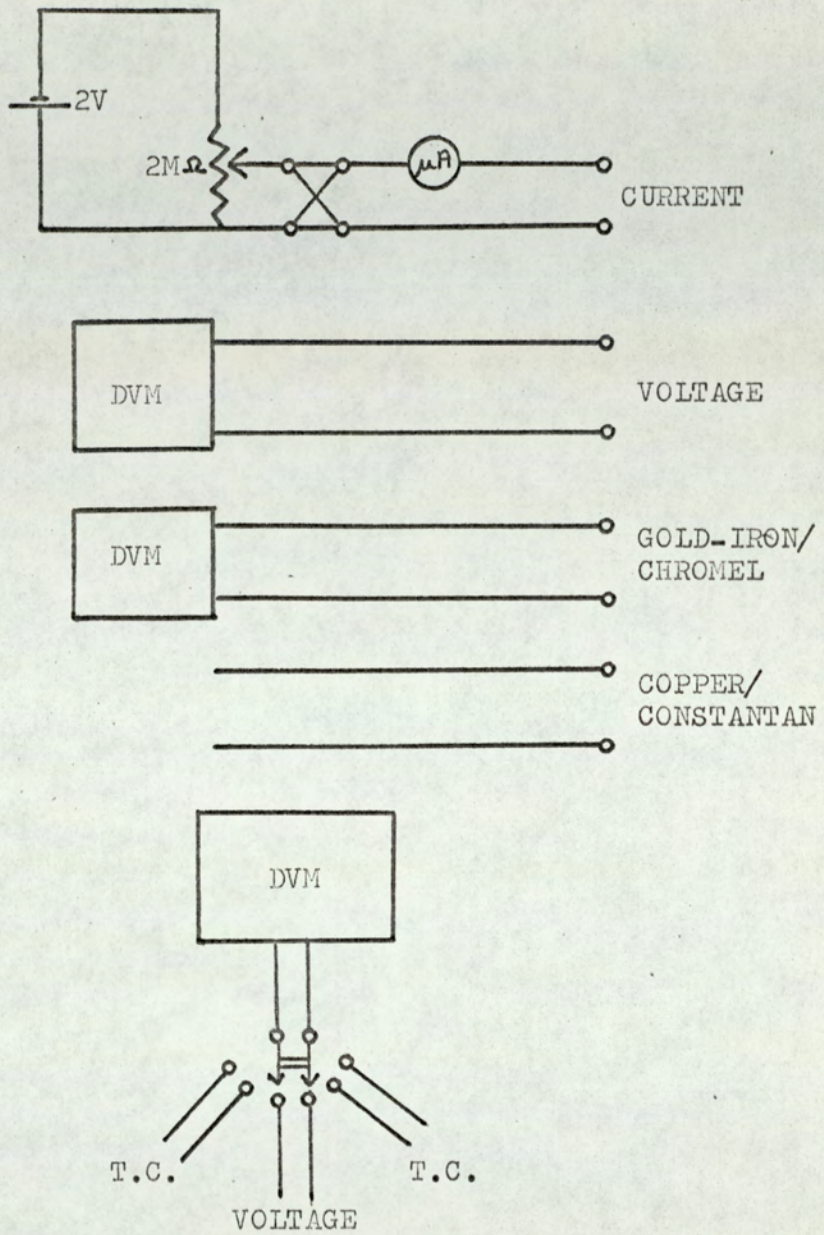
When examining the normal resistivity
only one DVM was employed.

Figure 26. Circuits used to investigate the
electrical properties of films.

outputs of the two thermocouples were taken through a selector switch to a Solartron Digital Voltmeter, Type LM 1604 DC. The selector switch was a Muirhead Rotary Stud switch having silver plated contacts for noise free operation.

When investigating the superconducting properties of the films it was found convenient to display the potential developed across the film on a separate digital voltmeter, Solartron DVM LM 1450. This was because as the film returned to normal resistance Joule heating raised the temperature of the film by several degrees very quickly. In order to obtain accurate transition temperatures it was necessary to display the thermocouple output and the film potential simultaneously.

3.3. Ellipsometer

An existing ellipsometer was used as means of investigating oxide growth on the niobium films after removal from the vacuum chamber. The ellipsometer components were mounted on two triangular section optical benches mounted at an angle of about 128 degrees, as shown in Figure 27. The light source was a 24 volt, 150 watt tungsten filament projector lamp operated from a 13 volt transformer controlled by a Variac.

A condenser lens L_1, focussed the light on a pin-hole A_1 which was arranged to be at the focus of the lens L_2. The wavelength of the resultant parallel beam of light was chosen by means of a Balzer interference filter F, having a pass-band of about 20 $\overset{o}{A}$. Three wavelengths were used 4960 $\overset{o}{A}$, 5470 $\overset{o}{A}$ and 5760 $\overset{o}{A}$. The aperture A_2 restricted the beam so that the divergence was less than 0.005 radian before passing through the polariser. After
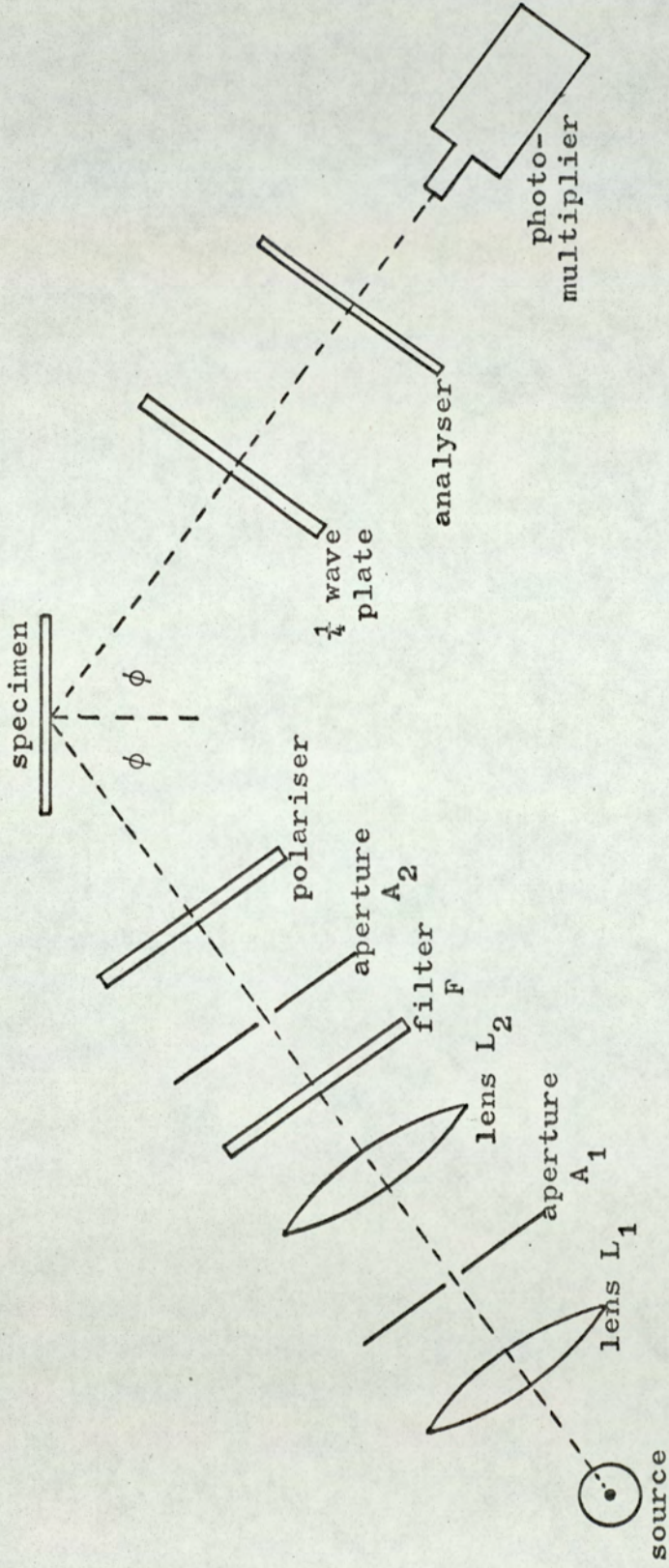
Figure 27. Arrangement of the ellipsometer components.

falling on the specimen film the beam of light passed through
the quarter wave plate and analyser before reaching the detector.

The polariser and analyser consisted of HN 22 polaroid mounted
in graduated circular vernier scales accurate to with $\pm$ 2 minutes
of angle. The quarter wave plate was made of mica sheet also mounted
in a circular scale. The error imparted to the analyser setting
if a non-exact quarter wave plate was used has been discussed by
Seward[63]. Calculations by O'Shea[64] showed that the quarter wave
plate used was acceptable over the range 4800 Å to 5800 Å.

The detector used was a type 6094B photomultiplier tube
supplied by E.M.I. Electronics Ltd. and was used in conjuction
with a stabilised power supply type 532/D from Isotope Developments
Ltd. and a Pye Scalamp Galvanometer having a sensitivity of
0.0113μ A mm^{-1}.

3.4. Experimental Procedure

3.4.1. Preparation of Substrates

The substrates for the films were cut from Corning 0211 glass
slides. Two substrates each 2 cm x 1.5 cm x 0.05 cm were formed
by cutting in half the standard slide. The substrates were cleaned
using the following procedure prior to mounting in the evaporation
unit.

The substrates were washed in a 5% detergent solution in an
ultrasonic cleaner for 10 to 15 minutes, rinsed twice with distilled
water then cleaned ultrasonically in distilled water. The substrates
were then immersed in boiling iso-propyl alcohol for a few minutes.
As the substrates were removed they were held in the vapour of the

boiling alcohol for a few seconds.

A subsidiary evaporation unit was used for the deposition of nichrome contact areas on the substrate. The substrate was mounted with a suitably shaped mask, Figure 28, in the evaporation unit and nichrome contact areas were deposited on the substrate from a heated tungsten wire helix at a pressure of $<5 \times 10^{-6}$ torr.

Originally, lead contact areas had been used to take advantage of the superconducting nature of lead below $7^{\circ}K$. However, it was found that the movement of the nickel contact strips either during assembly of the substrate mounting or subsequent cooling of the substrate tended to remove some of the lead resulting in loss of contact to the film. No such damage to the nichrome contact areas was experienced.

As a final precaution, after the evaporation of the contact areas, the substrates were again cleaned in the vapour of boiling iso-propyl alcohol before being mounted in the main deposition chamber.

3.4.2. Establishment of Vacuum

Initial rough pumping of the vacuum chamber and the sorption pumps was carried out by means of the rotary pump which reduced the pressure from 760 torr to 0.1 torr. The rotary pump was then isolated and the sorption pumps cooled with liquid nitrogen. This resulted in the pressure in the vacuum chamber falling from 10^{-1} torr to 10^{-4} torr, at this pressure the ion pump could be switched on and the rough vacuum elements isolated from the chamber. The ion pump was capable of producing a vacuum in the chamber of $<1 \times 10^{-7}$ torr.
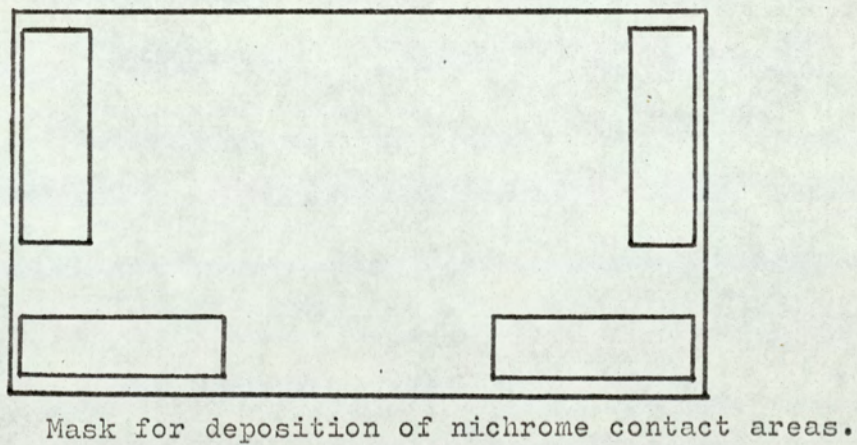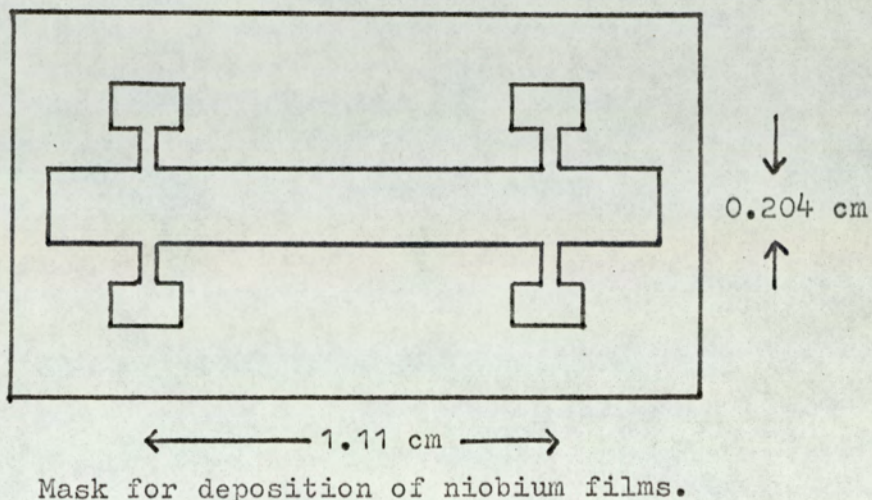
0.204 cm

←——— 1.11 cm ———→

Mask for deposition of niobium films.

Mask for deposition of nichrome contact areas.

Figure 28. Masks used in the preparation of
niobium films.

After baking the chamber at $420^{\circ}K$ for eight hours and allowing to cool the pressure would fall to $< 1 \times 10^{-8}$ torr. A further reduction in the pressure could be achieved by outgassing the niobium sample and ulitising the gettering action of freshly deposited niobium to produce a vacuum of $<1 \times 10^{-9}$ torr.

3.4.3. Evaporation of Niobium

High purity niobium, 99.99%, was obtained from Johnson Matthey Metals Ltd. The niobium was received as a rod 0.6 cm diameter and 10 cm long. The rod was cut into pieces about 0.5 cm long and the crucible of the electron beam evaporator was charged with about 10 gm of niobium. After melting, the niobium assumed a hemi-spherical shape about 0.8 cm in diameter.

Even at a low power input, 150 to 200 watts, the initial outgassing of the niobium sample was sufficient to raise the pressure in the vacuum chamber from less than 1×10^{-8} torr to 1×10^{-5} torr. However, the pressure soon fell by a factor of ten and the niobium could be heated further. At a power input of about 1000 watts the niobium would melt and it was held just above the melting point for about 4 hours. During this time there would be some evaporation of the niobium, about 4×10^{-5} gm min^{-1} and the pressure would fall to less than 1×10^{-8} torr.

Increasing the power input to 2000 watts would increase the evaporation rate of the niobium to about 0.15 gm min^{-1} and initially raise the pressure to 1×10^{-7} torr. As the gettering action of the freshly deposited niobium on the chamber surfaces increased the pressure fell to about 5×10^{-8} torr.

The electron beam evaporator was switched off and the chamber allowed to cool, after about 2 hours the pressure had fallen to $< 1 \times 10^{-9}$ torr. This pressure could be maintained indefinitely with no further evaporation of niobium.

To achieve a niobium deposition rate of 250 $\overset{\circ}{A}$ min^{-1} on a substrate positioned 20 cm from the evaporation source, required an evaporation rate of about 0.08 gm min^{-1}. To evaporate the niobium at this rate an electron beam current of 420 mA was needed. The rate could be varied from 0.01 to 0.15 gm min^{-1} by varying the electron beam current between 400 to 500 mA.

As previously mentioned, initially only very low rates of evaporation, 0.005 gm min^{-1}, were possible even when running the evaporator at 2200 watts. This was found to be due to the amount of the electron beam striking the sample. Ideally the contact area should be of the order of 0.6 cm x 0.3 cm, in fact it was found to be 2 cm x 0.5 cm and a considerable proportion of the electron beam was missing the niobium sample and dissipating directly on the crucible. The installation of the 'overspray' shield had the effect of concentrating the beam onto the sample and raised the evaporation rate from 0.005 gm min^{-1} to 0.15 gm min^{-1}. In terms of film deposition rate this represented an increase from about 15 $\overset{\circ}{A}$ min^{-1} to about 450 $\overset{\circ}{A}$ min^{-1}.

Once the required evaporation rate had been reached the pressure in the chamber was allowed several minutes to stabilize at about 5×10^{-8} torr. At this point the substrate was exposed to the evaporation source, once the required thickness of film had been deposited the shutter was closed.

3.4.4. Determination of Film Thickness

The thickness of the niobium films was measured outside the chamber using a Thin Film Measuring Microscope in conjunction with a Constant Deviation Wavelength Spectrometer, both instruments were supplied by Hilger and Watts Ltd., Figure 29. The method used for determining the thickness followed that suggested by Tolansky[65] using fringes of equal chromatic order.

Consider an overlaid film beneath a half silvered flat such that a small parallel air gap exists, Figure 30a. There will exist in the incident beam of white light a frequency such that m (not necessarily integral) wavelengths are contained within the double path length $2y_1$

$$2y_1 = m\lambda + \frac{\delta}{\Pi} \lambda \qquad (3.1)$$

m is the order of the fringe

δ is the phase change on reflection

A shorter wavelength λ^1 also exists such that (m + 1) wavelengths are contained

$$2y_1 = (m + 1)\lambda^1 + \frac{\delta}{\Pi} \lambda^1 \qquad (3.2)$$

Neglecting the phase term, then an integral number of wavelengths within the gap will result in interference and thus produce a fringe.

From equations (3.1) and (3.2)

$$m = \frac{\lambda^1}{\lambda - \lambda^1} \qquad (3.3)$$

microscope

spectro-
meter

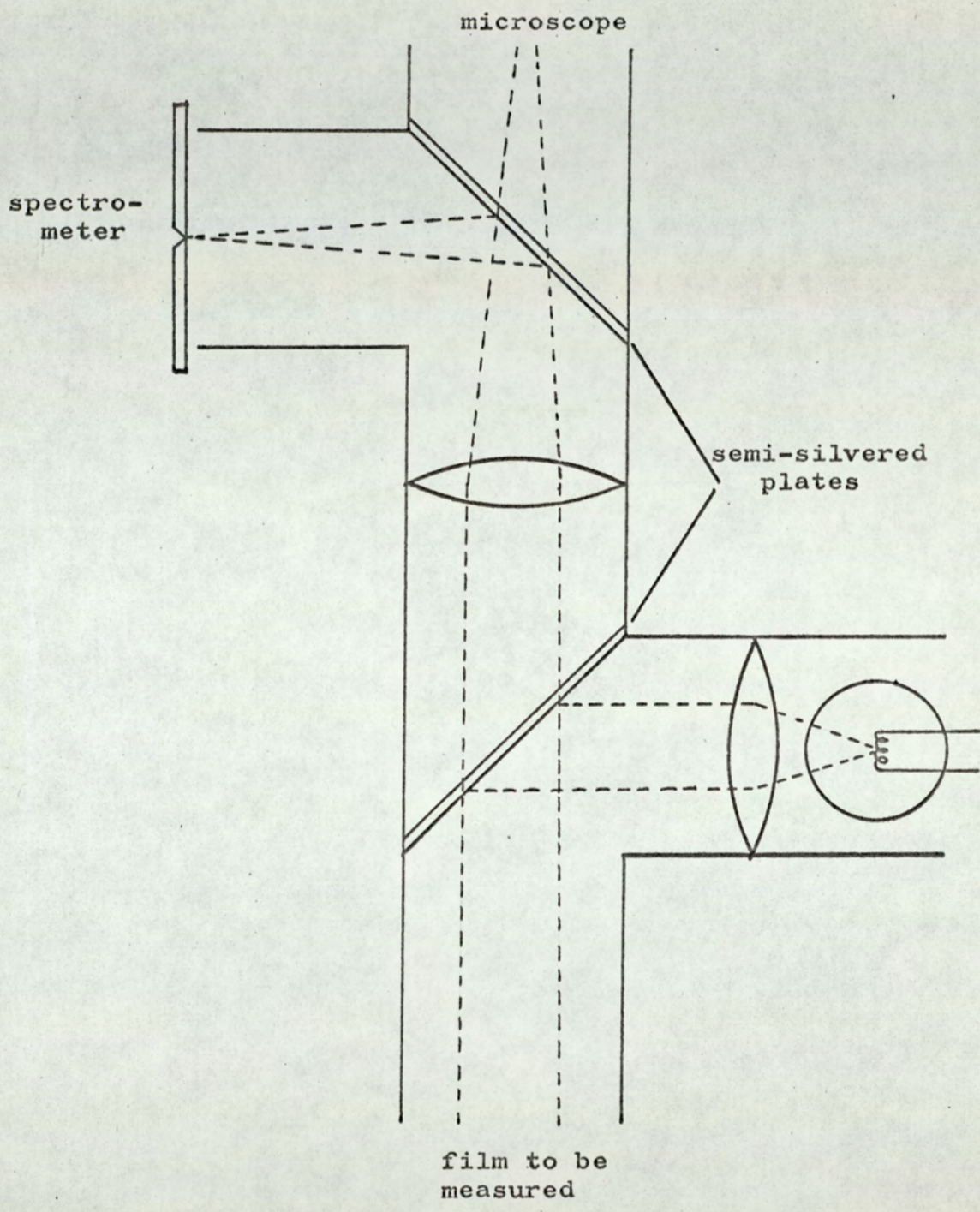semi-silvered
plates

film to be
measured

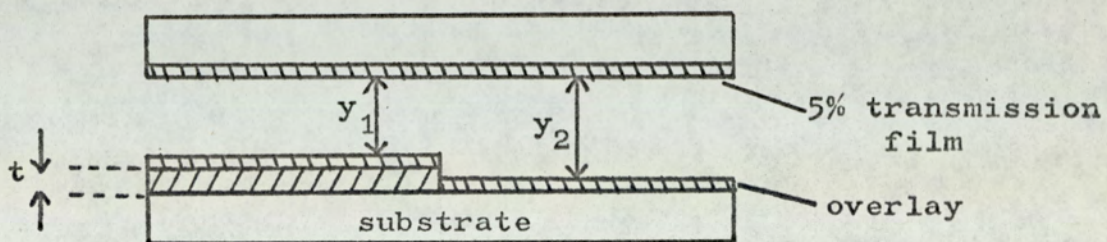Figure 29. Thin film measuring microscope.
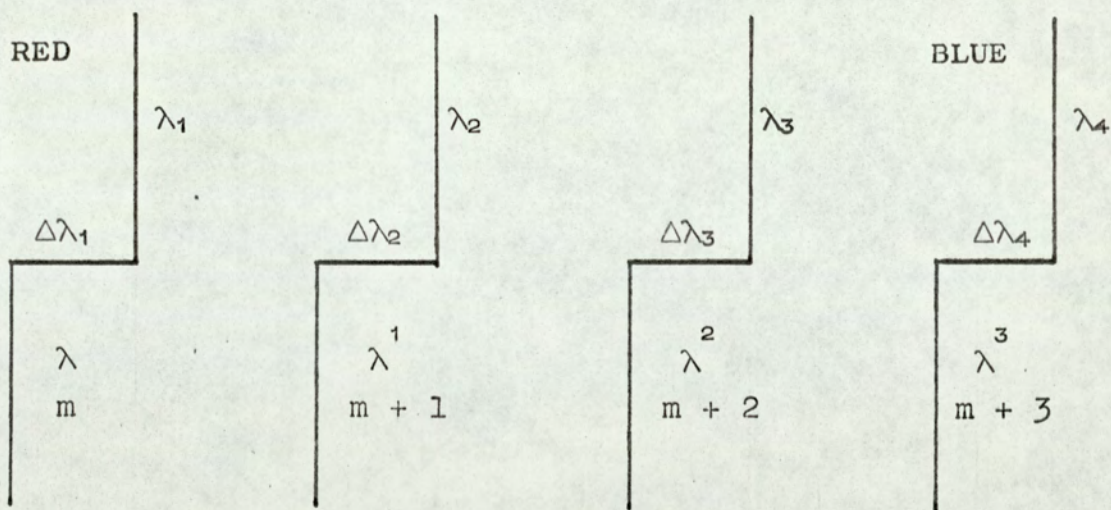
Figure 30a. Fringe formation.

Figure 30b. Field of view showing four orders
of interference.

In a region y_2 where the path length is slightly different to y_1 there will be a slightly different wavelength such that a fringe of the same order m is produced.

$$2y_2 = m\lambda_1 \tag{3.4}$$

The thickness of the film will be given by equations (3.1) and (3.4)

$$t = y_2 - y_1 = \frac{m}{2}(\lambda_1 - \lambda) = \frac{m}{2}\Delta\lambda \tag{3.5}$$

The image in the spectrometer appeared as a series of stepped fringes superimposed on a continuous spectrum, as shown in Figure 30b. By measuring the wavelengths λ^i the order for a number of fringes could be determined and should increase as consecutive integers towards the violet end of the spectrum. A similar measurement of λ_i will yield $\Delta\lambda$ and hence the film thickness.

The phase parameter in equation (3.1) will in general be a function of wavelength, but Koehler[66] has shown this to be nearly constant at 0.97 in the visible spectrum for silver deposit of over 80% reflectivity. Shultz[67] has shown a similar dependence for aluminium. Aluminium overlays were used in preference to silver since aluminium tarnishes less readily.

Errors in the determination of film thicknesses increased as the thickness decreased. For a film of 200 Å the error was about $\pm$ 5%, at 150 Å the error was about $\pm$ 10% and at thicknesses below 120 Å the error could be $\pm$ 50%. For very thin films it was found more accurate to estimate film thickness from the evaporation rate of the niobium and the time taken for the deposition of the film.

3.4.5. Electrical Properties of Films

The normal resistive properties of the films were determined by passing a constant current through the film and observing the voltage developed across the film. Current densities of the order of 10 to 100 A cm^{-2} were used.

Films which were to be examined before removal from the vacuum chamber were deposited onto substrates held at about 500°K. After deposition the films were allowed to cool to about 300°K and the temperature coefficient of resistance was determined over this range. The films were then cooled with liquid nitrogen and the film resistivity at 80°K was measured.

Liquid helium was introduced into the cryostat and the temperature of the film lowered to about 4°K. The superconducting properties of the film were determined by passing a suitable current through the film and raising the temperature by means of the heater coil positioned in the substrate mounting. The temperature at which a resistive transition took place was observed. This procedure was repeated with various values of current until the critical temperature was reached. The film was then warmed up and the temperature coefficient of resistance over the range 10 to 300°K was determined.

Films which were to be examined after removal from the vacuum chamber were also deposited onto substrates held at 500°K. The films were allowed to cool to 300°K before removal and allowed 120 hours for oxide growth before the electrical properties were investigated. Once the films were mounted in the cryostat assembly

the procedure followed was similar to that already described.
The resistance of the films was determined at 300°K and 80°K.
The critical currents were determined at various temperatures
and the critical temperature was determined before the temperature
coefficient of resistance was observed over the range 10 to 300°K.

3.4.6. Study of Optical Properties

Because of the initially rapid growth of oxide on the films
it was essential that the shortest possible time should elapse
between removal from the vacuum chamber and installation in the
ellipsometer. In practice it was found that this interval could
be as little as ten minutes which was considered to be satisfactory.

Initial readings to determine ψ and $\triangle$ were taken at half
hourly periods until the rate of change of the readings dropped
sufficiently for hourly readings. Readings were taken after
progressively longer intervals over a period of ten days.

The procedure followed for determination of the optical
constants and hence the oxide growth has been described in
section 2.5.

CHAPTER 4

Experimental Results

4.1. Introduction

The experimental results were determined from a total of over sixty niobium films fabricated during this programme of work. Of these sixty films, forty were examined 'in situ' and the remainder were examined after removal from the deposition chamber.

Many of the 'in situ' films were found to have electrical characteristics widely different from those expected of niobium films. Some examples are quoted to illustrate the effects of deposition rate, vacuum and substrate temperature on the electrical properties of niobium films.

The results obtained from the electrical measurements on the normal and superconducting states of all the niobium films examined after removal from the deposition chamber are presented. The values of film thickness calculated from the electrical measurements are compared with the thickness determined optically.

The oxide growth on the films as determined by ellipsometry is presented together with the corrected film thickness measurements obtained. The structure of the films and the grain size as determined by electron microscopy and X-ray diffraction is also presented.

4.2. Film Resistance and Resistivity

4.2.1. 'In situ' Measurement of Film Resistance

As mentioned in section 3.4.5. some films were examined before removal from the deposition chamber. The film resistance was normally determined by observing the voltage developed across the film, by the passage of a constant current through the film, while

the temperature was varied between 10°K and 300°K. Current densities of the order of 10 to 100 A cm^{-2} were used. For thick films the actual current was 1 mA, for thin films the current was reduced to 10 μA. The film resistivity was determined from the resistance and was also plotted as a function of temperature.

The resistivity of a film and the temperature dependence of the resistivity can depend on the thickness of the film and the film purity, as determined by imperfections and impurities. The effect of gaseous impurities on the resistivity of niobium films was found to be quite significant.

4.2.2. Effect of Gaseous Impurities on Film Resistivity

A niobium film deposited in a moderate vacuum, 2×10^{-6} torr, and at a low deposition rate, 12 $\overset{\circ}{A}$ min^{-1}, onto a substrate held at 300°K displayed a negative temperature coefficient of resistivity, Figure 31. The resistivity ratio ρ_{300}/ρ_{10} was determined as 0.87, the film would not superconduct at temperatures above 4.0°K. A film deposited under similar conditions but onto a substrate held at 500°K, Figure 32, was found to have a higher resistivity ratio, 0.94 in spite of being a thinner film. This film also retained the normal electrical resistance down to a temperature of 4.0°K.

Raising the deposition rate to 110 $\overset{\circ}{A}$ min^{-1} resulted in a film having a positive temperature coefficient of resistivity and a resistivity ratio of 1.25, Figure 33. However, the resistivity, 99$\mu\Omega$ -cm at 300°K, was high considering a film thickness of 3400 $\overset{\circ}{A}$. This is shown by Figure 34 where a similar thickness film was deposited at 400 $\overset{\circ}{A}$ min^{-1} in a vacuum of 2×10^{-7} torr. The resistivity ratio has been increased to 1.94 and the resistivity at 300°K has been more than halved. Both these films were found to be

superconducting below 8.0°K.

Three films, 230 Å, 2800 Å and 3755 Å thick, were deposited at a rate of about 200 Å min^{-1} in a vacuum of 5×10^{-7} torr onto substrates at 500°K. The results obtained from these films are shown in Figures 35, 36 and 37.

The effect on the resistance of a film by exposure to an atmospheric environment is shown in Figure 38. After determining the resistance of the 230 Å thick film it was exposed to the atmosphere. Once the resistance had stabilised, after about 3 hours, the resistance was redetermined over the temperature range 10°K to 300°K. As can be seen the resistance increased after exposure by about 14%. Assuming that the increase was caused by the transformation of a layer of conducting material into a layer of non-conducting oxide, and that the thickness was inversely proportional to the resistance (over a small range of thickness) the thickness of the oxide layer was estimated to be about 30 Å.

4.2.3. Measurement of Film Resistance after Oxide Growth

After deposition and once the films had been exposed to the atmosphere for 120 hours, to establish the oxide layer, the films were mounted in the auxiliary cryostat assembly. The variation of film resistance over the temperature range 10°K to 300°K was determined as described before. The results obtained from a series of films, deposited under similar conditions, ranging from 45 Å thick to 5440 Å thick are shown in Figures 39-57. The corresponding graphs of film resistivity versus temperature are also illustrated. The variation of resistivity with temperature for a bulk sample of niobium is shown in Figure 58. These results were taken from the experiments of White and Woods [68] on a drawn and annealed niobium

sample of resistivity ratio $\rho_{300}/\rho_{10} = 480$.

4.3. Measurement of Critical Current

The procedure followed for the determination of critical currents was the same for all films. A measured current was passed through the superconducting film and the temperature of the film was raised until a resistive transition was observed. The temperature was determined at this point. The procedure was repeated with progressively smaller currents until the critical temperature of the film was reached. This was taken to be the temperature at which a current density of 10 A cm^{-2} caused a resistive transition.

Films greater than about 100 Å thick were found to have transitions less than 0.035°K wide, the width increased to about 0.1°K for a film 90 Å thick. Widths of 1.0°K and 3.0°K were observed for the transitions of films 50 Å and 45 Å thick, the transitions are shown in Figures 59 and 60. For these films the critical temperature was taken to be the temperature at which the resistance had risen to half the value of the residual resistance.

The results obtained from 'in situ' films are shown in Figures 61 and 62, and the results for films mounted in the auxiliary cryostat are shown in Figure 63.

4.4. Determination of Film Thickness

The interferometer method of measuring film thickness was described in section 3.4.4. Very thin films, of the order of 120 Å or less, produced a very small step in the fringes observed in the spectrometer. Consequently the errors in determining the thickness of these films were large, $\pm 50\%$. It was considered more accurate to determine the thickness from the deposition rate, which was approximately known as 240 Å min^{-1} and the deposition time. Using

this method films of estimated thicknesses 120 Å and 80 Å were deposited.

An electrical method for the determination of film thickness was described in section 1.5. and was given by equation (1.15) as

$$\frac{dR}{dT} = \frac{d\rho_\infty}{dT} \cdot \frac{film\ length}{width \times thickness}$$

Thus the thickness can be expressed as

$$d = \frac{d\rho_\infty}{dT} \cdot \left(\frac{dR}{dT}\right)^{-1} \cdot \frac{L}{W} \qquad (4.1)$$

The variation of the resistivity of bulk material with respect to temperature $d\rho_\infty/dT$, was determined from the data of White and Woods. It was calculated to be $d\rho_\infty/dT = 0.0498\ \mu\Omega$-cm $^{\circ}K^{-1}$ at a temperature of $300^{\circ}K$. The length and width of the films were determined as 1.11 cm and 0.204 cm respectively from measurements of the evaporation mask using a travelling microscope. The term $(dR/dT)^{-1}$ was calculated, at a temperature of $300^{\circ}K$, for each film from the graphs of resistance versus temperature, Figures 35-57.

The results of film thickness obtained by the two methods are compared in Table 7. It must be remembered that the interferometer method of determining film thickness measures total film thickness and makes no distinction between the conducting niobium and the non-conducting oxide layer.

4.5. Determination of oxide thickness by Ellipsometry

For measurements of oxide growth on films it is a requirement of this technique that the substrate, in this case the niobium film, should be opaque to the wavelength of light used. This requirement limited the minimum thickness of film available for

investigation to about 400 Å. The results presented here are obtained from three films, one of about the minimum thickness, 420 Å and the others of 1660 Å and 3530 Å.

Observations on all films were commenced about 10 minutes after removal from the vacuum chamber and continued over a period of days. The reduction in the value of $\triangle$, due to the growth of the oxide layer, with respect to time is shown in Figure 64, for two of the films, at the same wavelength of 5478 Å. By extrapolating the graph of Figure 64 to zero time, a value of $\triangle$ for an oxide free film can be determined and the corresponding value of ψ estimated from Figure 65. Using these values of $\triangle$ and ψ and assuming the optical constants of the oxide to be n = 2.37 and k = 0.00 as determined by Young and Zobel[69] for a wavelength of 5461 Å. The variation of $\triangle$ and ψ with respect to oxide thickness can be computed, using Drude's exact equations (2.39) and (2.40), Table 8, and the optical constants of oxide free niobium determined as n = 2.3074 and k = 2.6963.

One film, 1660 Å thick, was also observed using the wavelengths, 4960 Å and 5760 Å. The results of oxide thickness versus $\triangle$ and ψ are shown in Tables 9 and 10. From these results the optical constants of clean niobium were determined as n = 2.1896 and k = 2.7019 for a wavelength of 4960 Å, and n = 2.5465 and k = 3.5071 for a wavelength of 5760 Å.

The rate of growth of the oxide layer on the niobium film could be determined, Figure 66, by combining the results in Table 8 with Figure 64. From this it was established that after 120 hours the oxide layer was approximately 35 Å thick. It was now possible to determine the actual niobium film thickness by subtracting the oxide

thickness from the measured film thickness obtained by interferometry. Table 11 shows the comparison of thicknesses obtained in this way and electrically measured thicknesses.

4.6. Film Structure

To ascertain the structure of the niobium films some of the films were examined by electron microscopy. A carbon film was deposited onto electron microscope grids which were placed in the evaporation chamber. After the deposition of a niobium film the grids were transferred to the electron microscope (Phillips EM 200). No discernable structure was visible but a ring pattern obtained from one film, about 200 Å thick, is shown in Figure 67. Computed values of the 'd' spacing obtained from the pattern are compared to the known values in Table 12, together with the appropriate index for the rings. As can be seen the results indicated that the film was polycrystalline body centred cubic niobium.

Some films were stripped from the glass substrates with sellotape after first loosening the film with hydrofluoric acid. The films were mounted in the electron microscope in an attempt to ascertain the relationship between film thickness and grain size. It was found that at the required magnification, about 50,000, the image was so weak and the contrast so poor, that no detail of the film structure could be determined.

An alternative method of determining grain size was attempted. Grain sizes less than 5×10^4 Å produce line broadening of X-ray diffraction patterns. Assuming that the grains are perfect and randomly orientated, the integral breadth of a diffraction line, B (integrated intensity/maximum intensity) is given by the Schemer formula[70,71] as:

$$B = \lambda / L.d \cos \theta_o \qquad (4.2)$$

λ is the wavelength of the X-rays

L is the average particle size, dimensions in units of d.

d is the interplanar spacing of (hkl) in $\mathring{A}$

θ_o is the Bragg angle

The integral breadth is defined as

$$B = \int \frac{I(x) \, dx}{I \max} \qquad (4.3)$$

The patterns obtained from some of the films are shown in Figure 68. The photographs were scanned with a microdensitometer to produce a trace as shown in Figure 69, from which B could be determined. The results of grain sizes determined in this way are shown in Table 13.
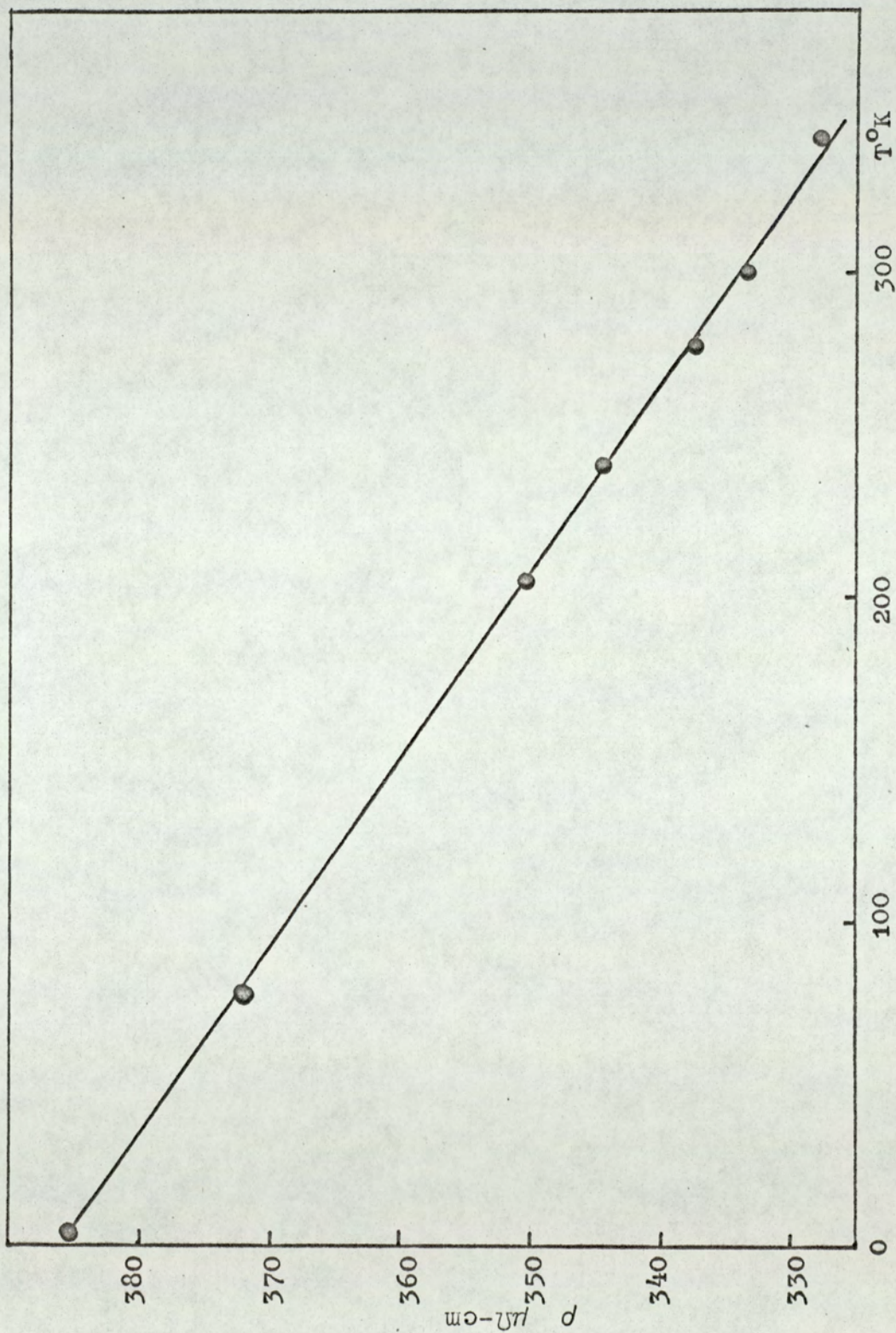
Figure 31. Film 2000 Å thick, deposited at a slow rate onto a substate at $300°K$ in a vacuum of 2×10^{-6}.
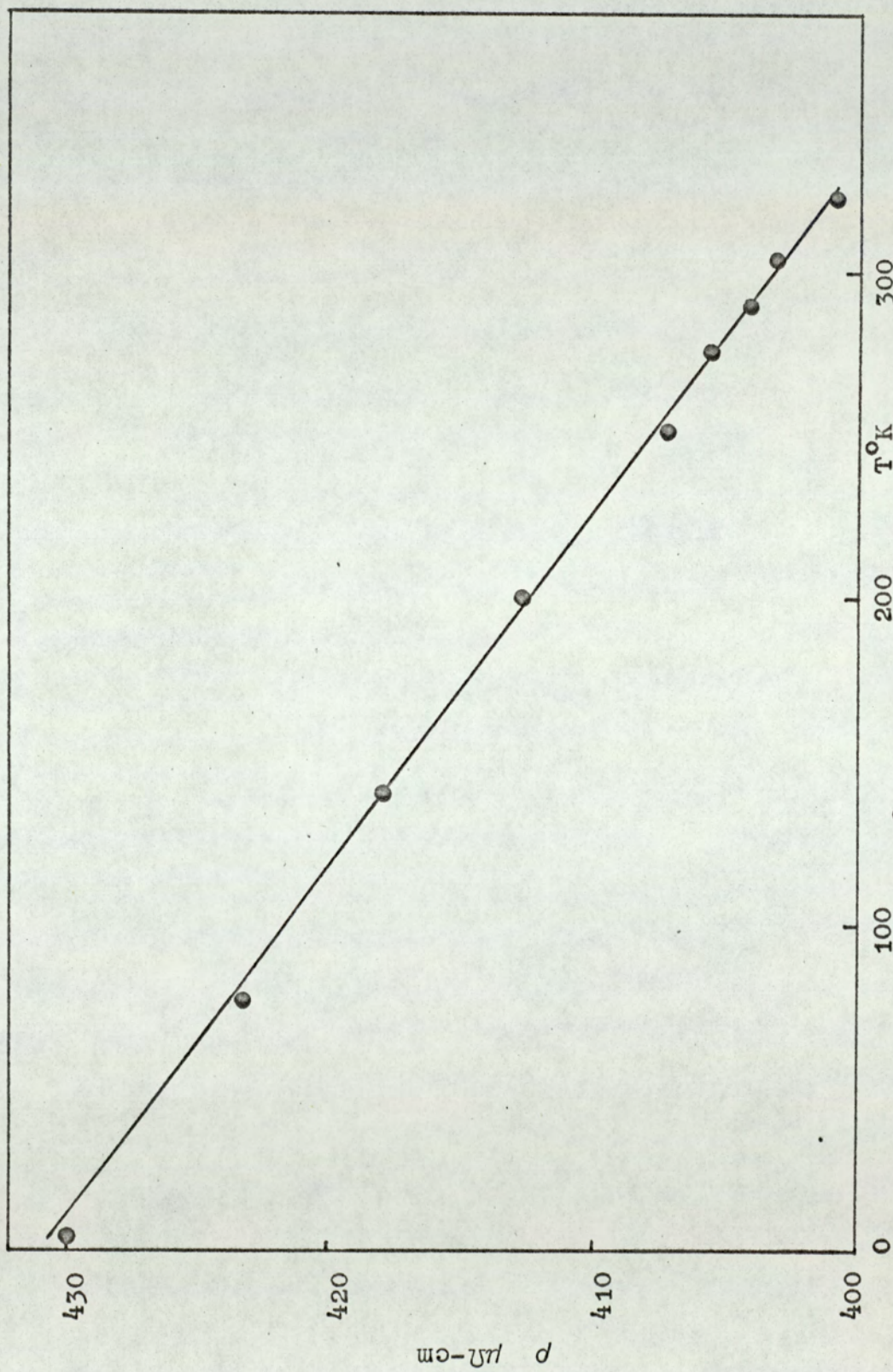
Figure 32. Film 1500 Å thick, deposited onto a substrate held at 500°K in a vacuum of 2 x 10⁻⁶ torr.
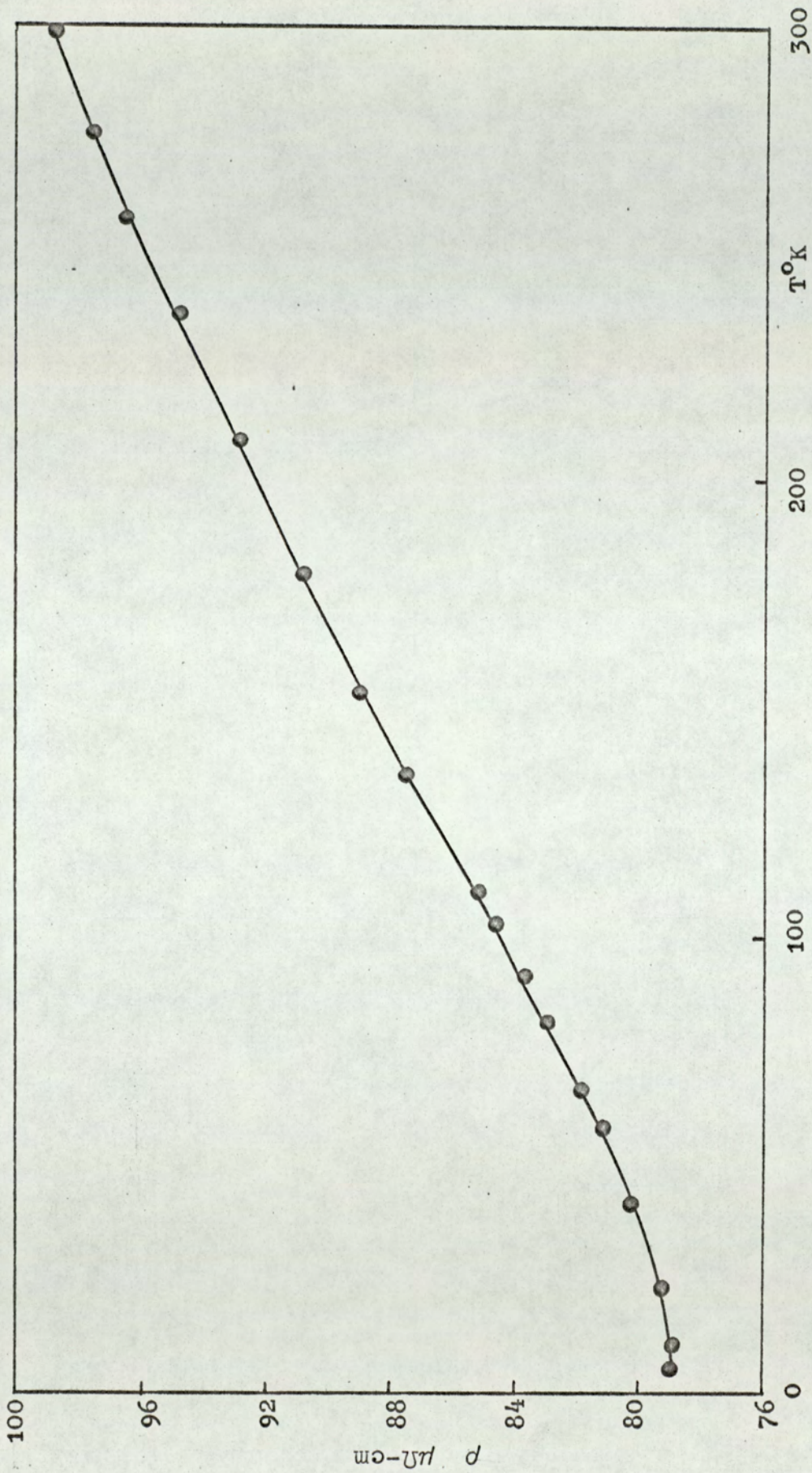
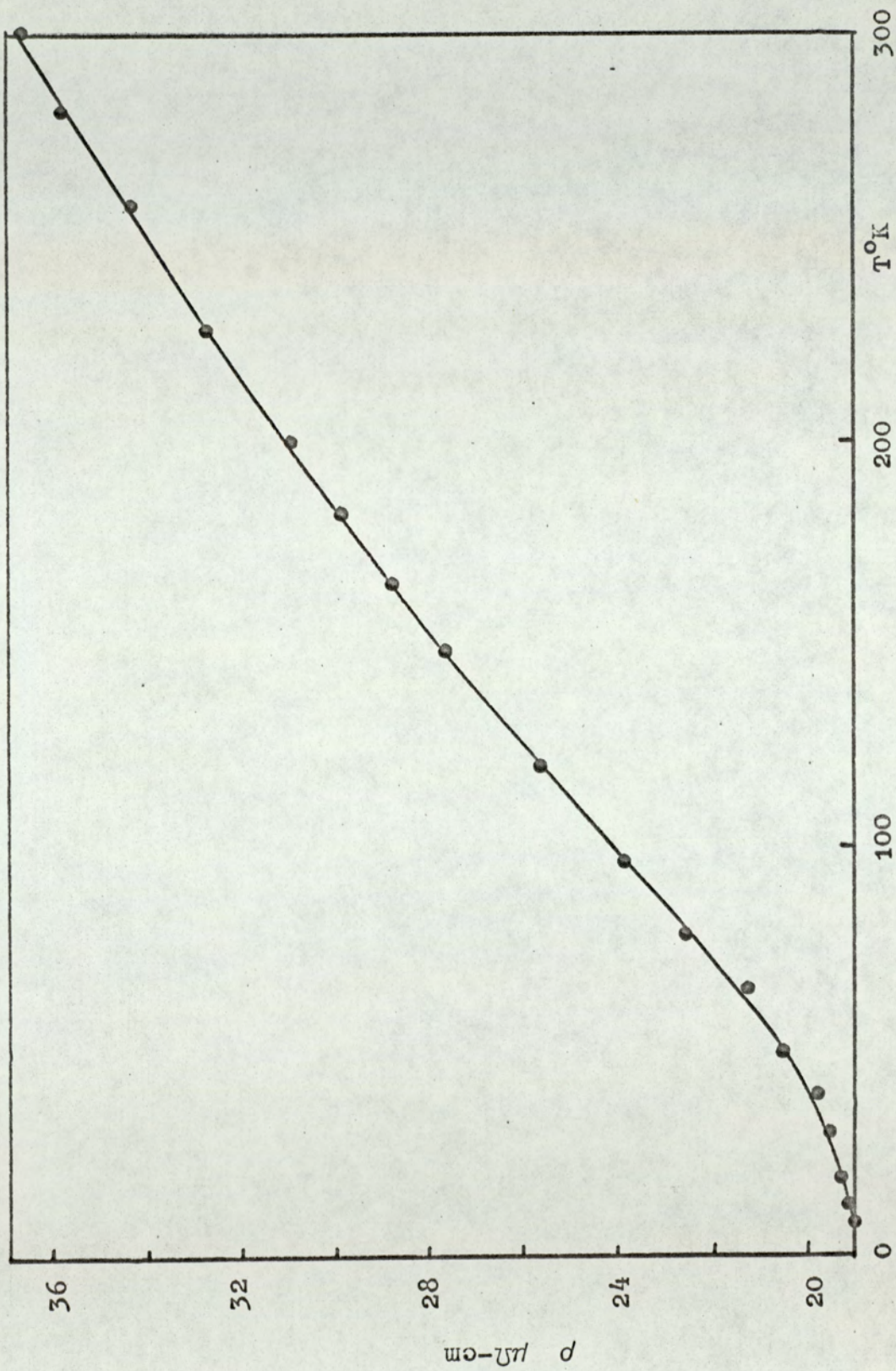Figure 33. Film 3400 Å thick, deposited at 110 Å min⁻¹ onto a substrate held at 500°K in a vacuum of 1 x 10⁻⁶ torr.

Figure 34. Film 3610 Å thick, deposited at 400 Å min^{-1} onto a substrate held at 500°K in a vacuum of 2 x 10^{-7} torr.
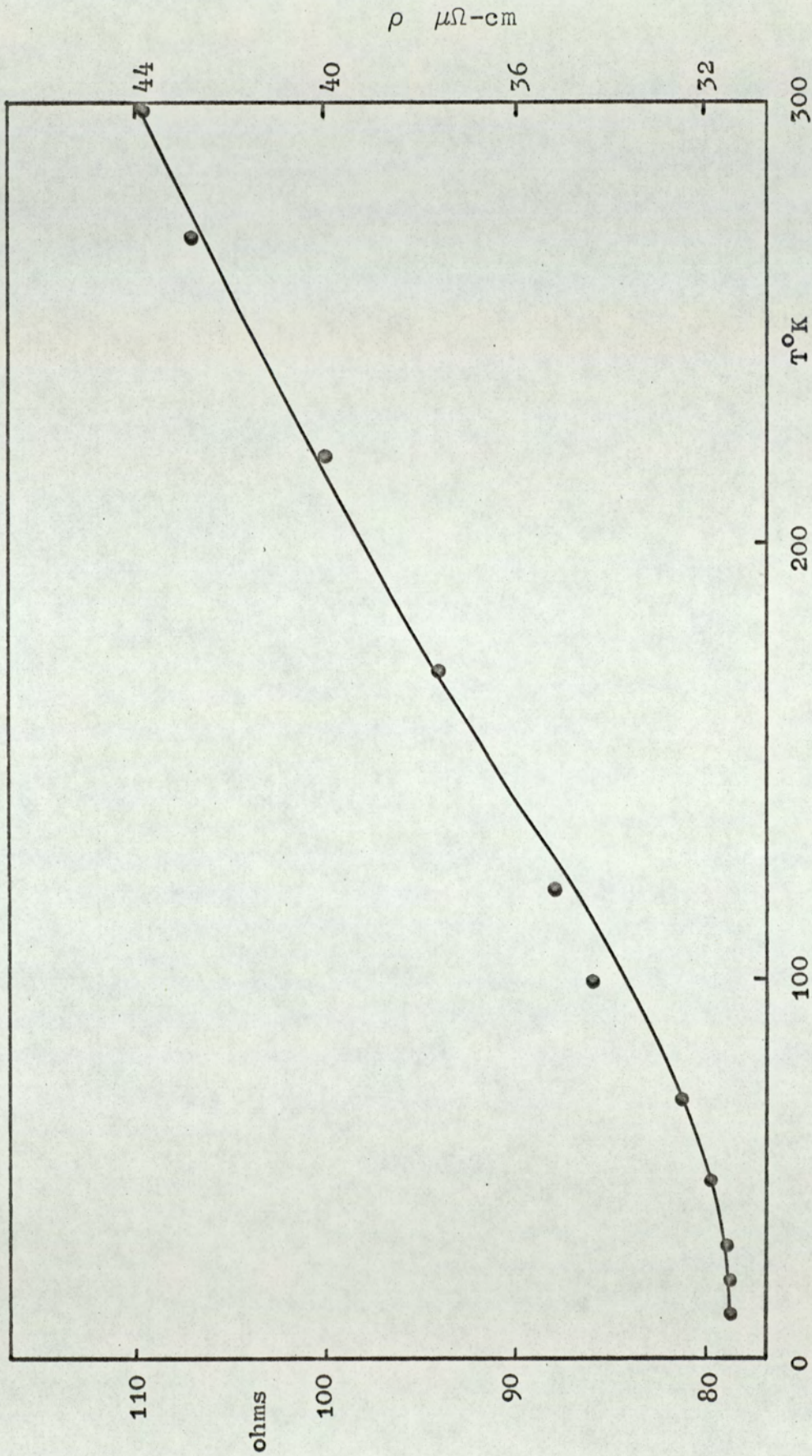
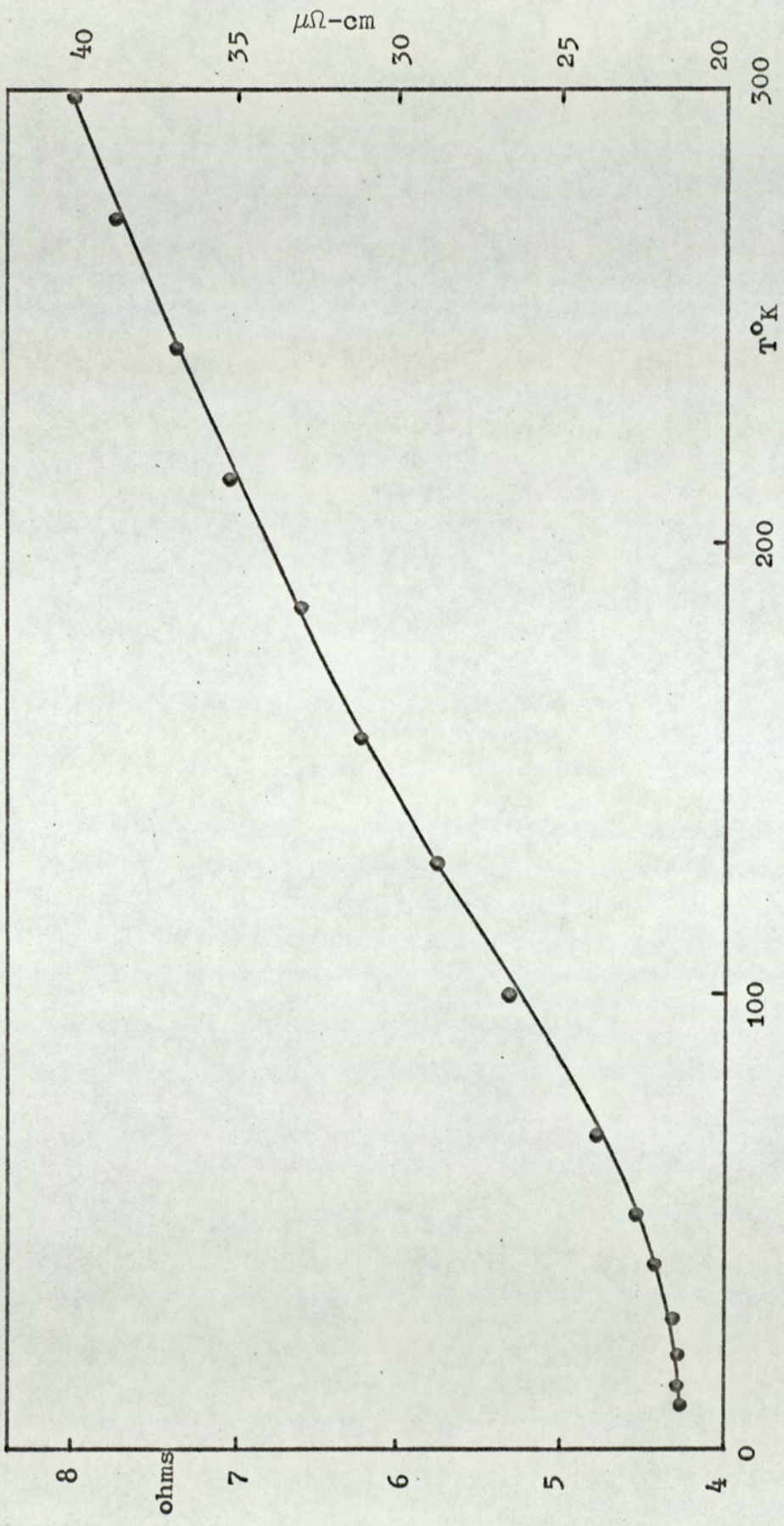Figure 35. Film 230 Å thick. Resistance and resistivity vs temperature.

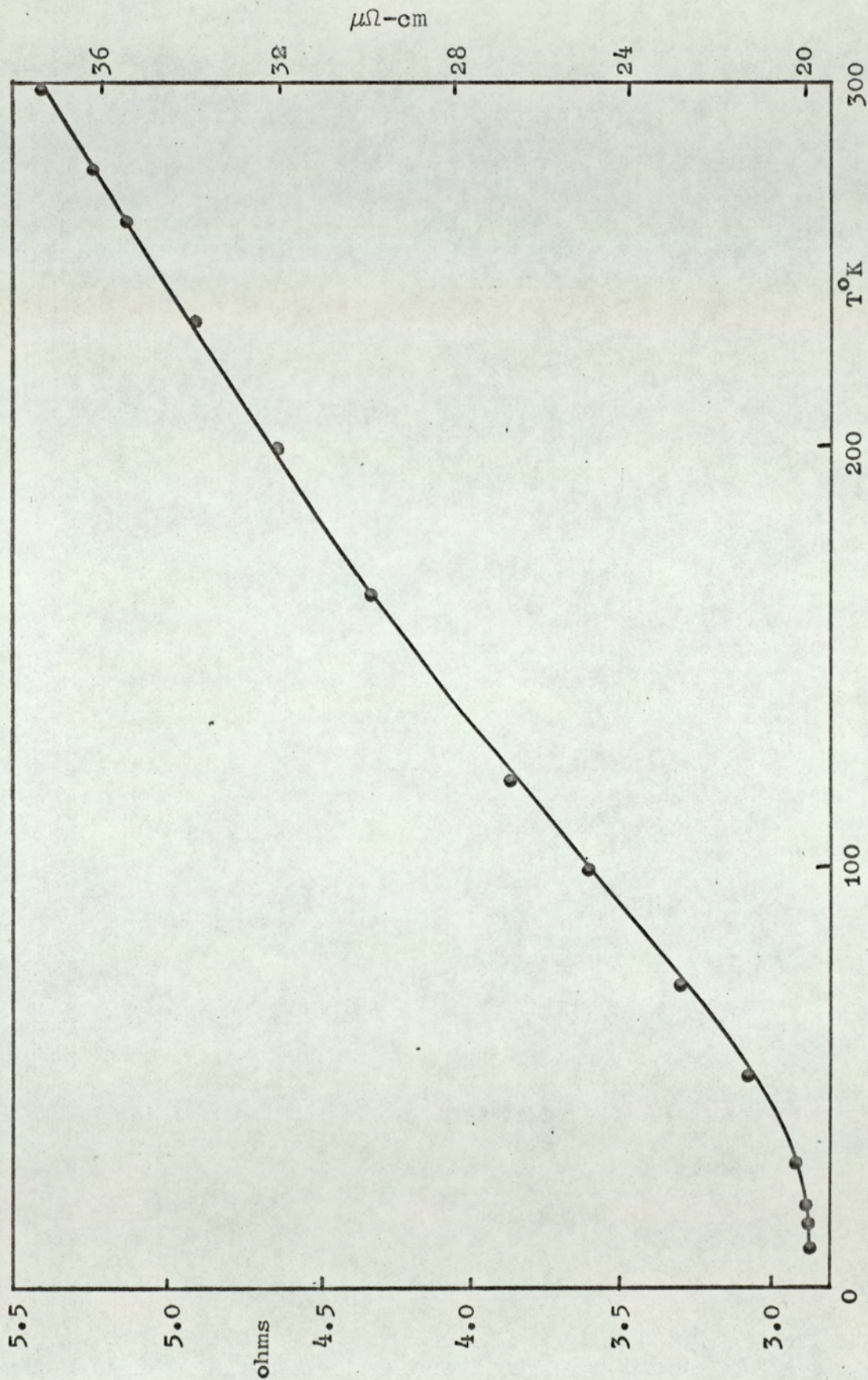Figure 36. Film 2800 Å thick. Resistance and resistivity vs temperature.

Figure 37. Film 3755 Å thick. Resistance and resistivity vs temperature.
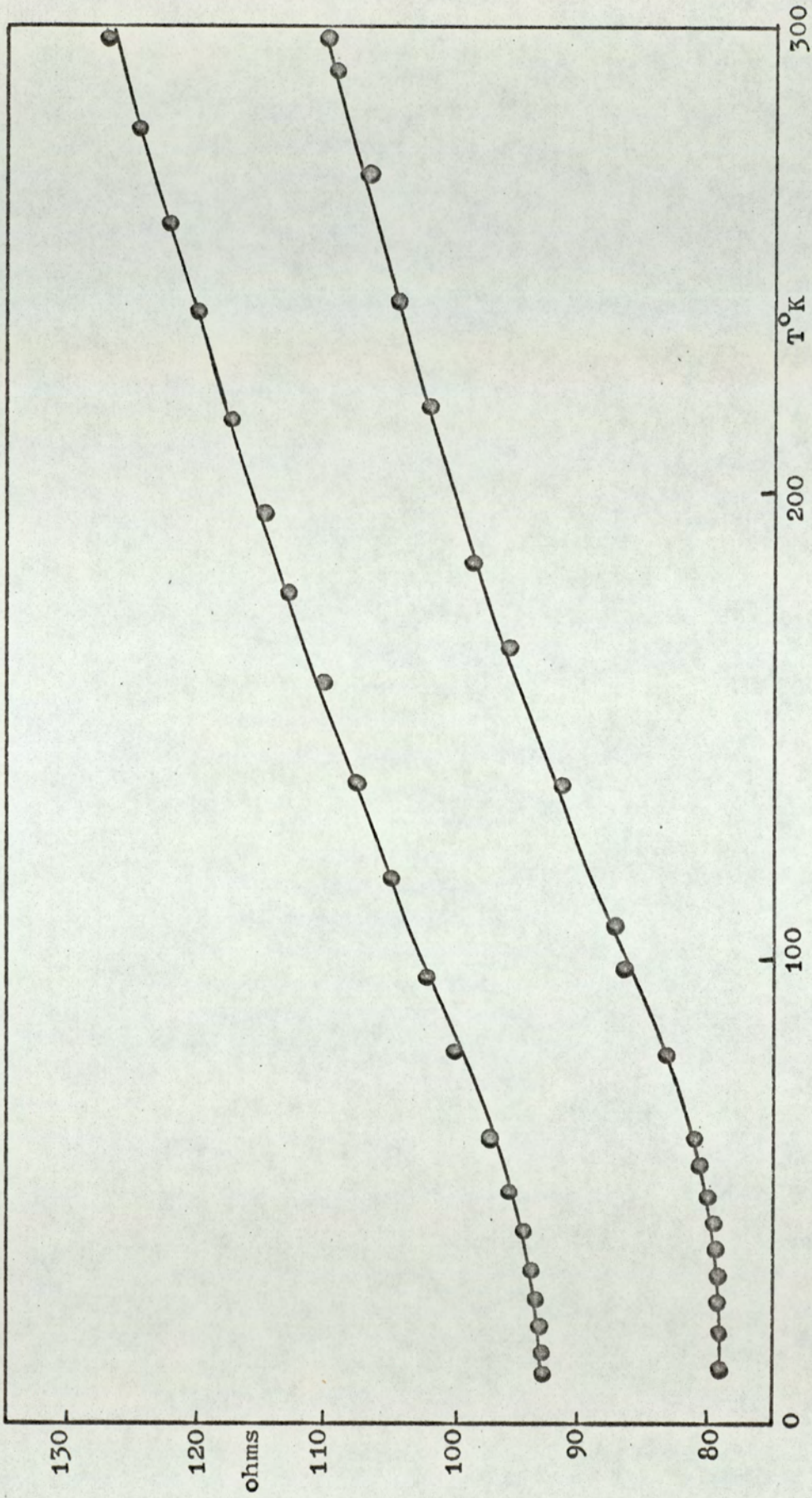
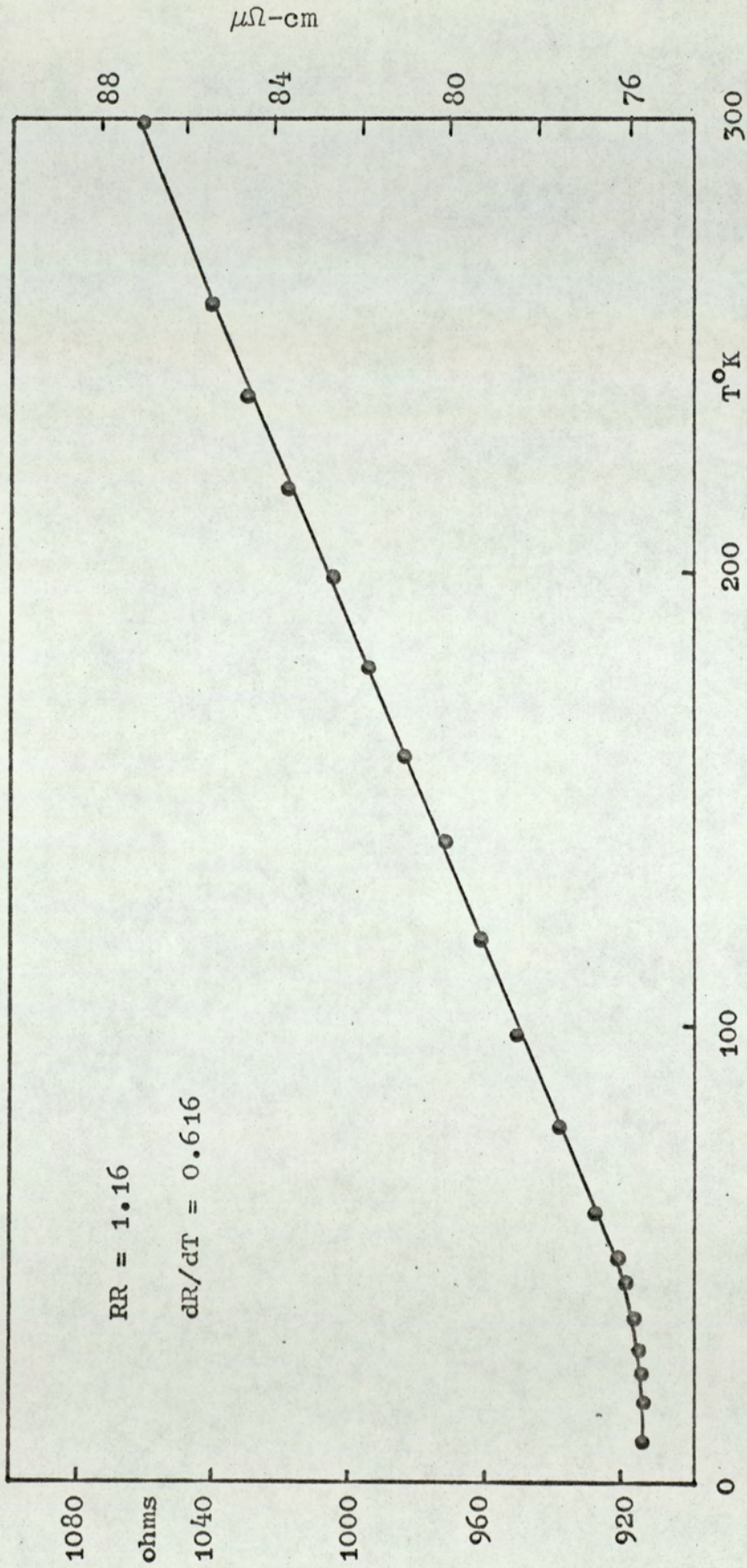Figure 38. Resistance of film 230 Å thick, before and after exposure to atmosphere.

Figure 39. Film 45 Å thick. Resistance and resistivity vs temperature.
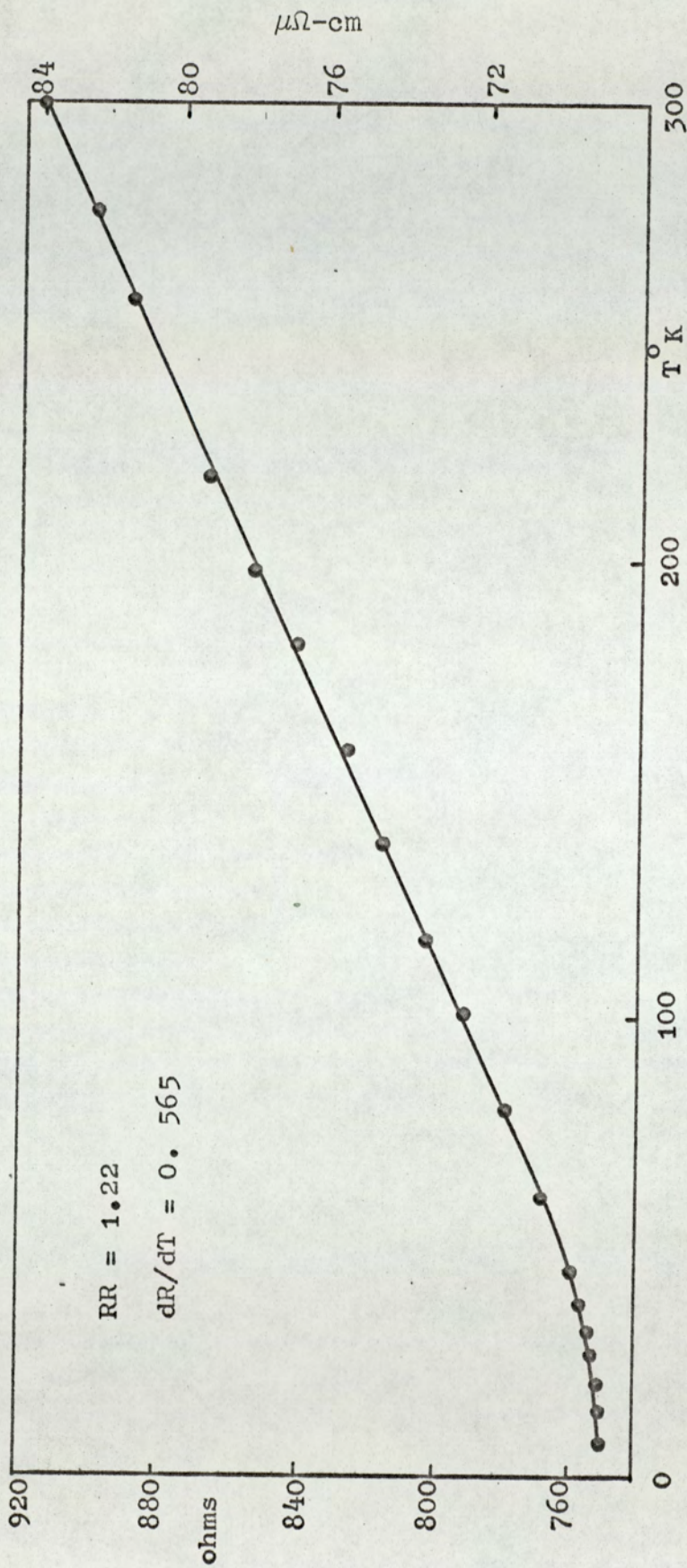
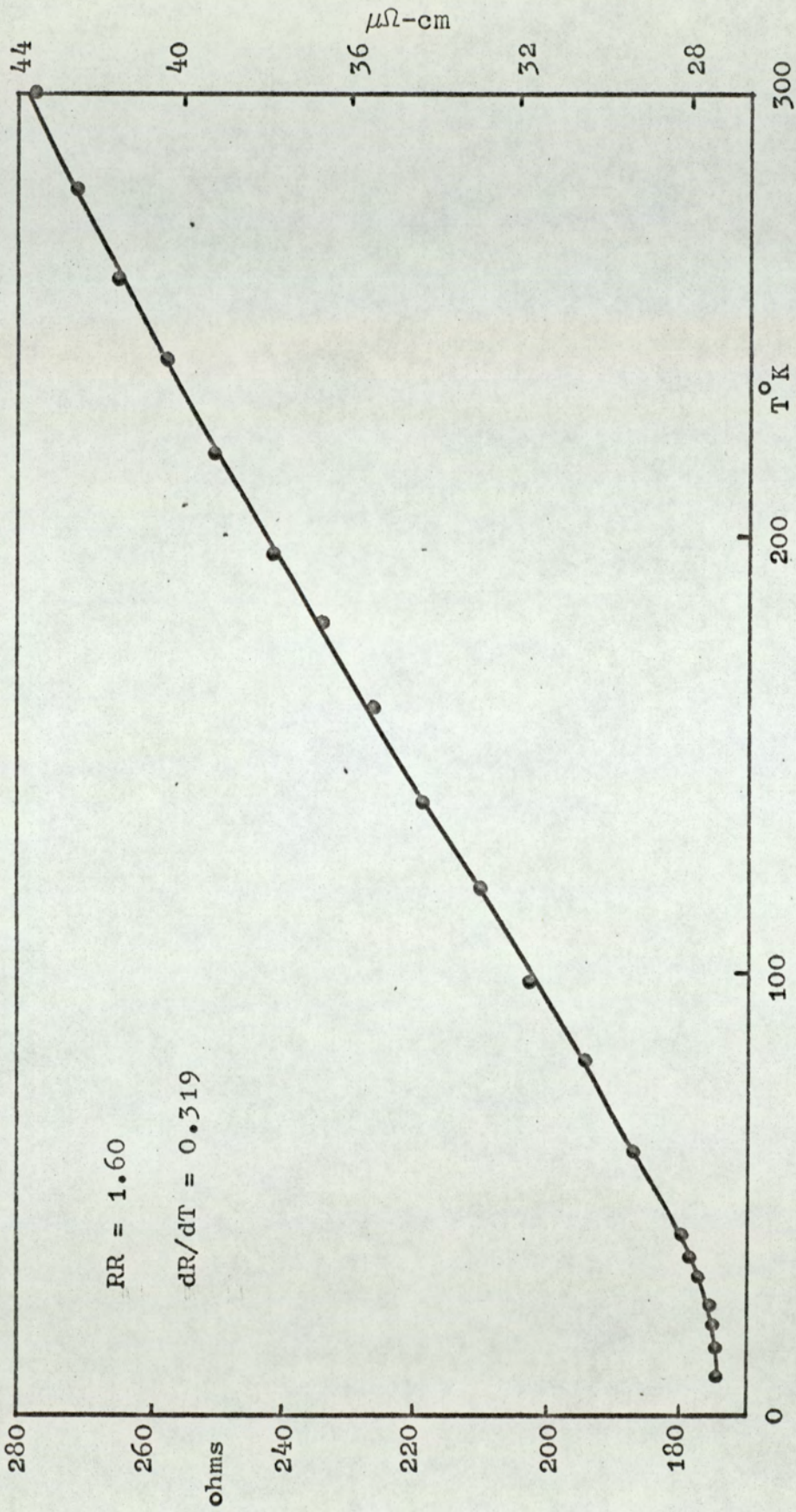Figure 40. Film 50 Å thick. Resistance and resistivity vs temperature.

Figure 41. Film 85 Å thick. Resistance and resistivity vs temperature.

Figure 42. Film 90 Å thick. Resistance and resistivity vs temperature.

Figure 43. Film 130 Å thick. Resistance and resistivity vs temperature.

RR = 1.97

dR/dT = 0.209

Figure 44. Film 150 Å thick. Resistance and resistivity vs temperature.

Figure 45. Film 165 Å thick. Resistance and resistivity vs temperature.

RR = 2.05

dR/dT = 0.170

Figure 46. Film 175 Å thick. Resistance and resistivity vs temperature.
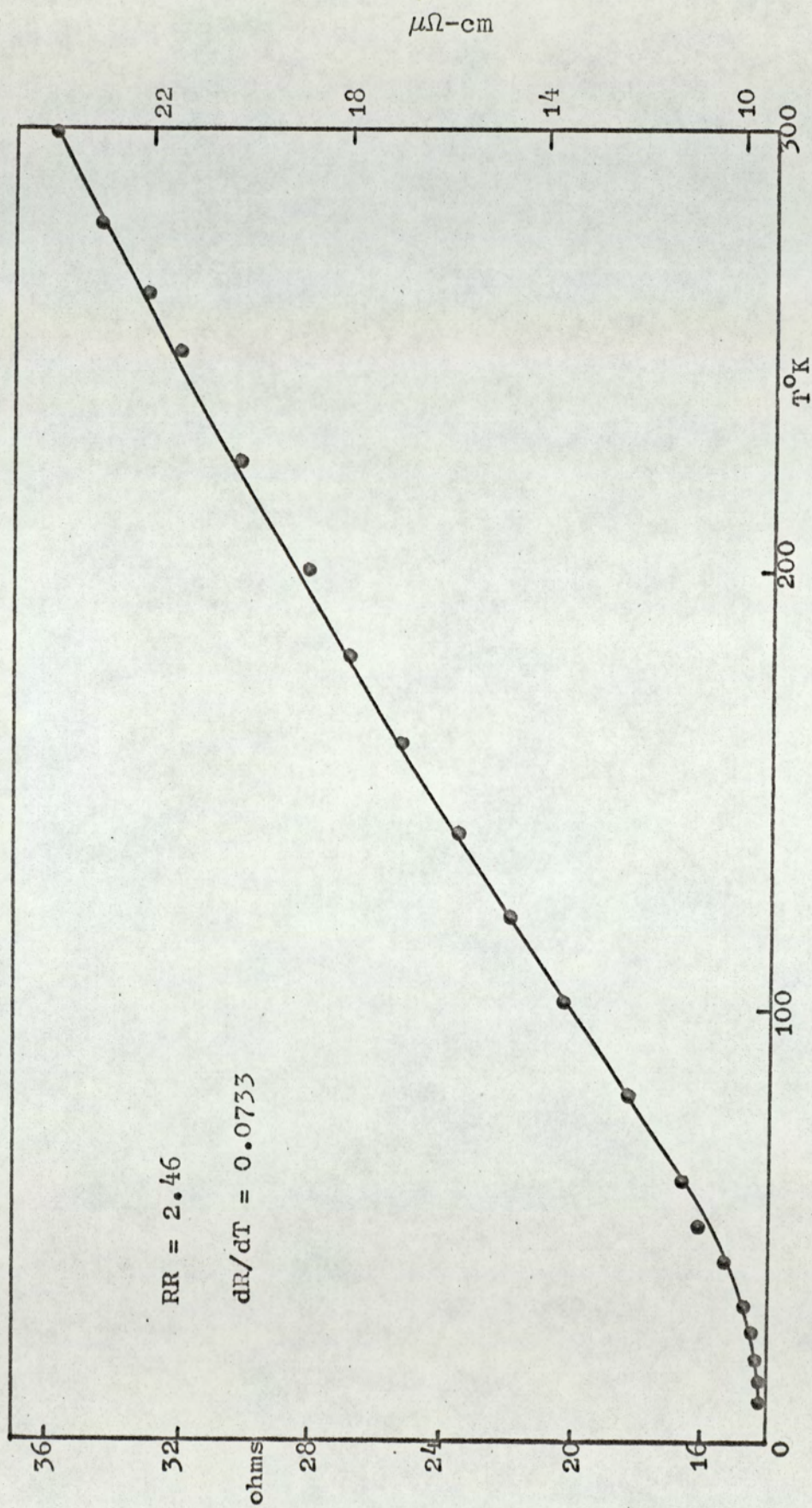
Figure 47. Film 365 Å thick. Resistance and resistivity vs temperature.
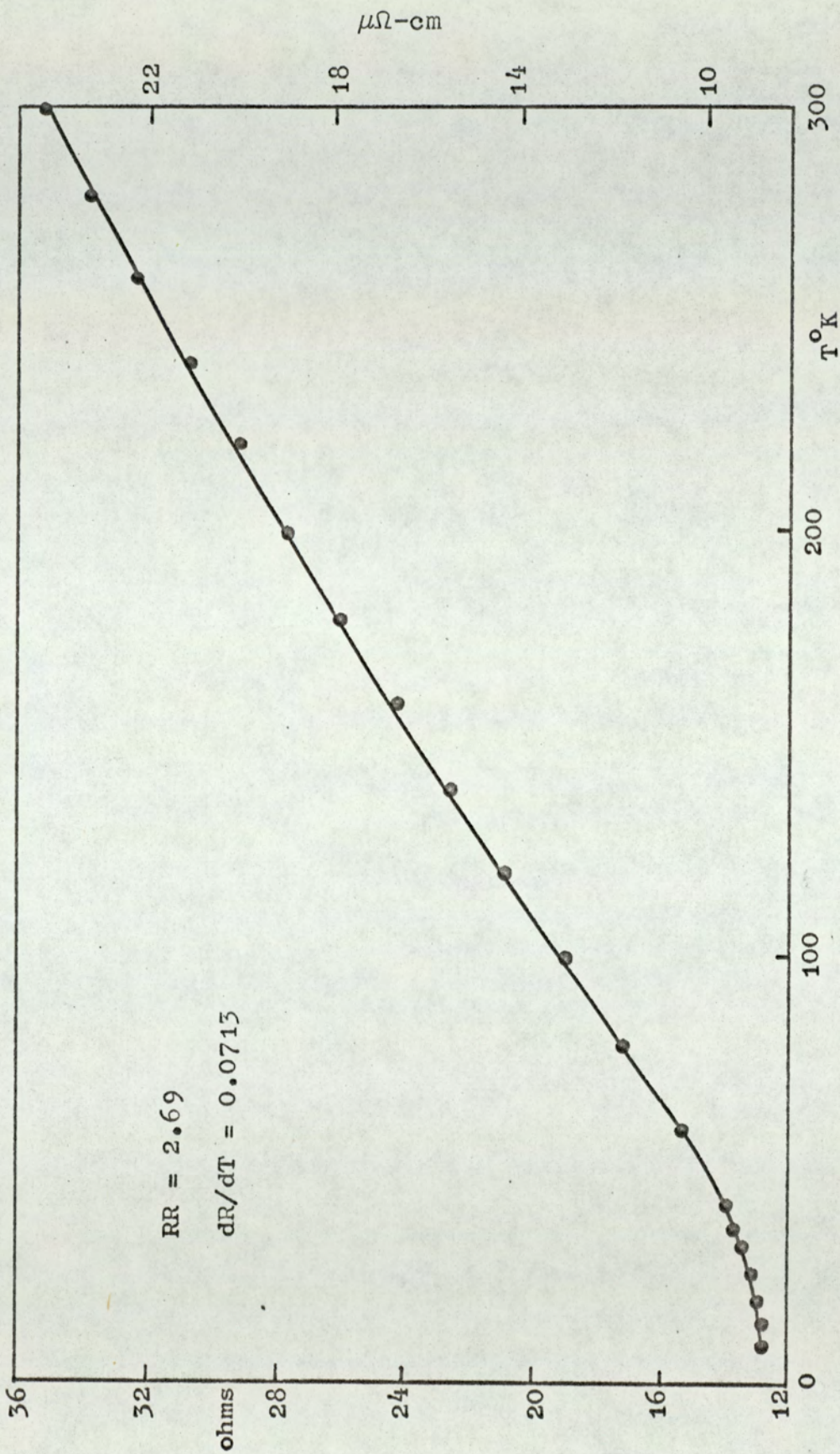
Figure 48. Film 375 Å thick. Resistance and resistivity vs temperature.
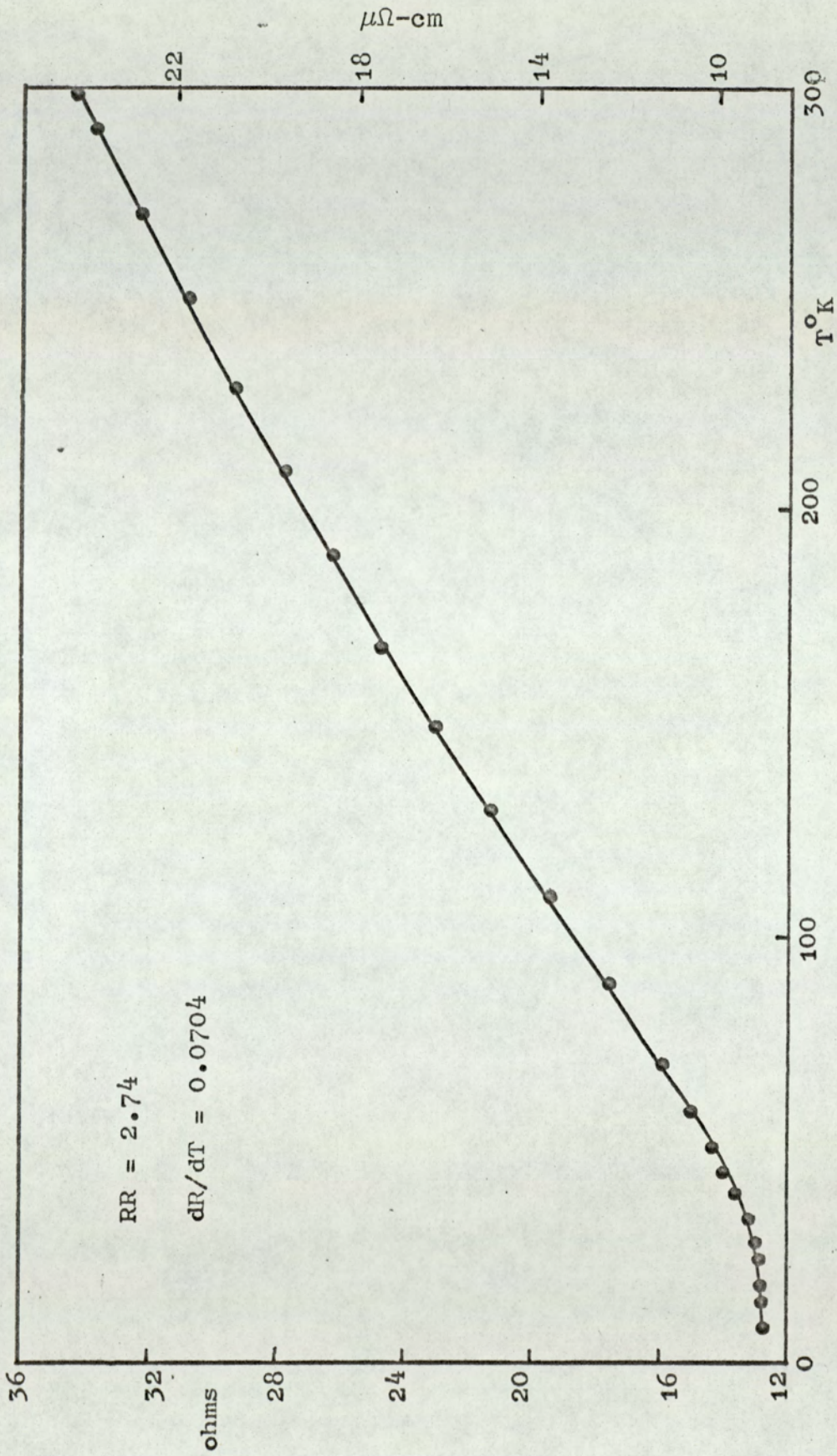
Figure 49. Film 385 Å thick. Resistance and resistivity vs temperature.
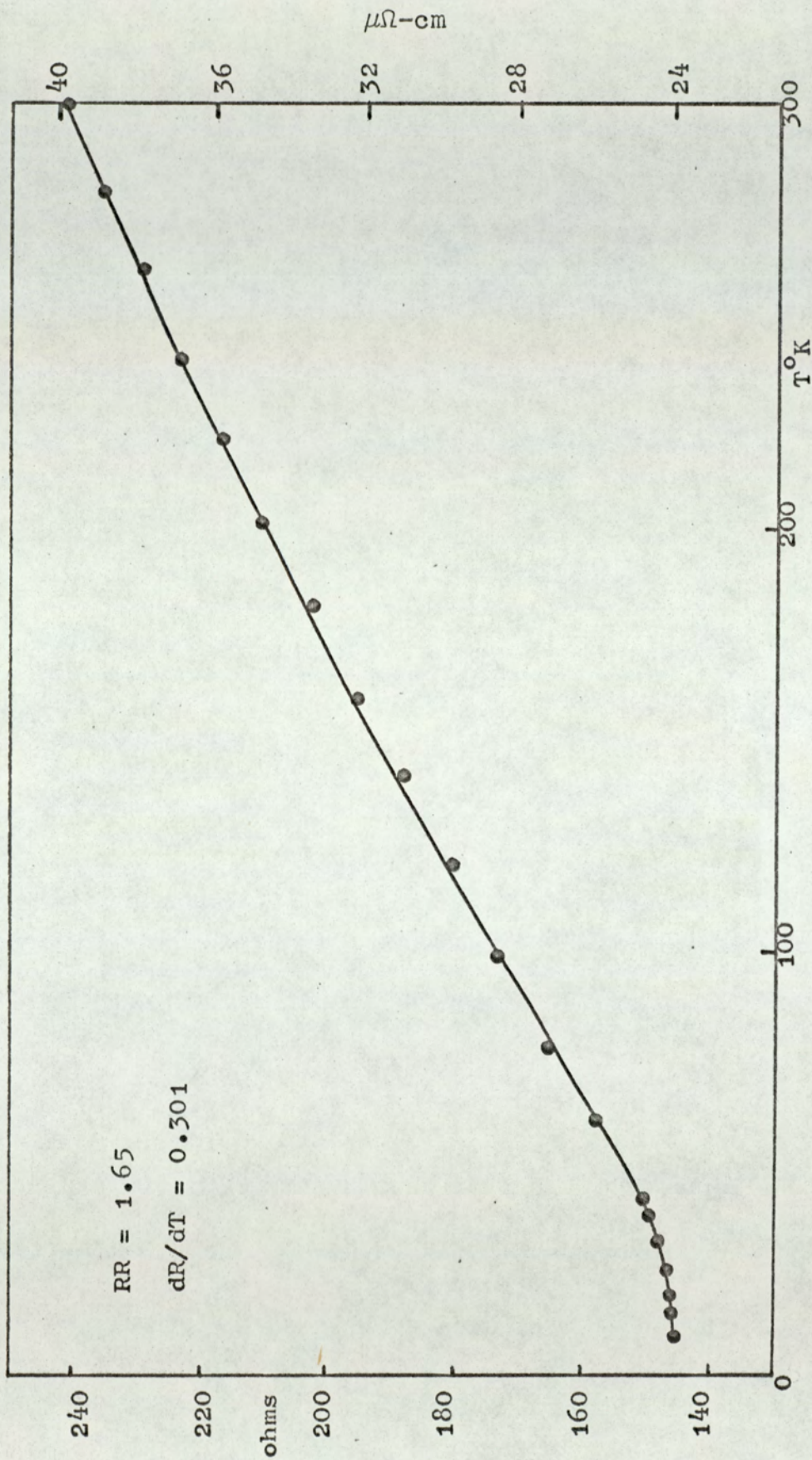
RR = 2.74

dR/dT = 0.0704
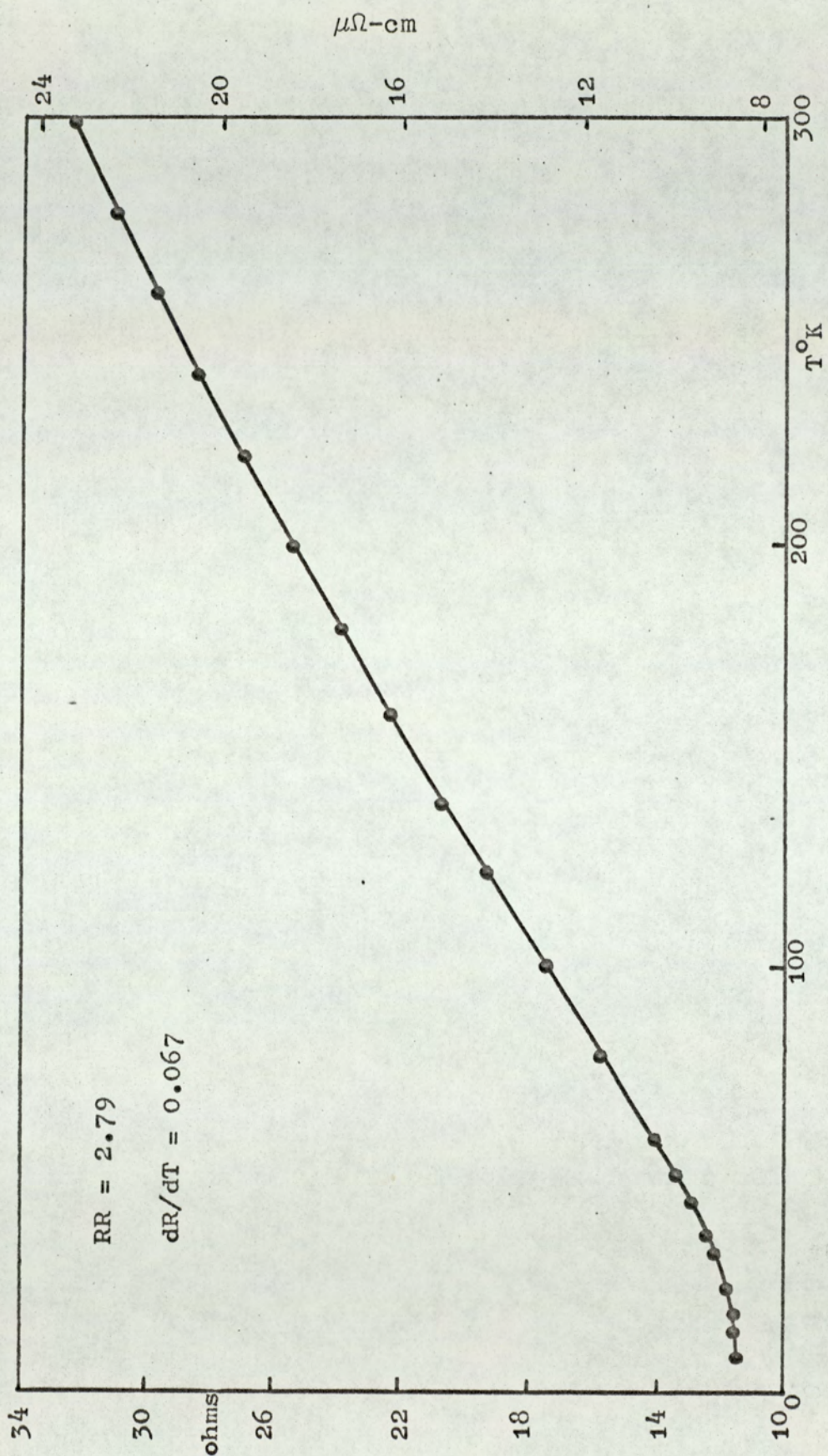
Figure 50. Film 390 Å thick. Resistance and resistivity vs temperature.
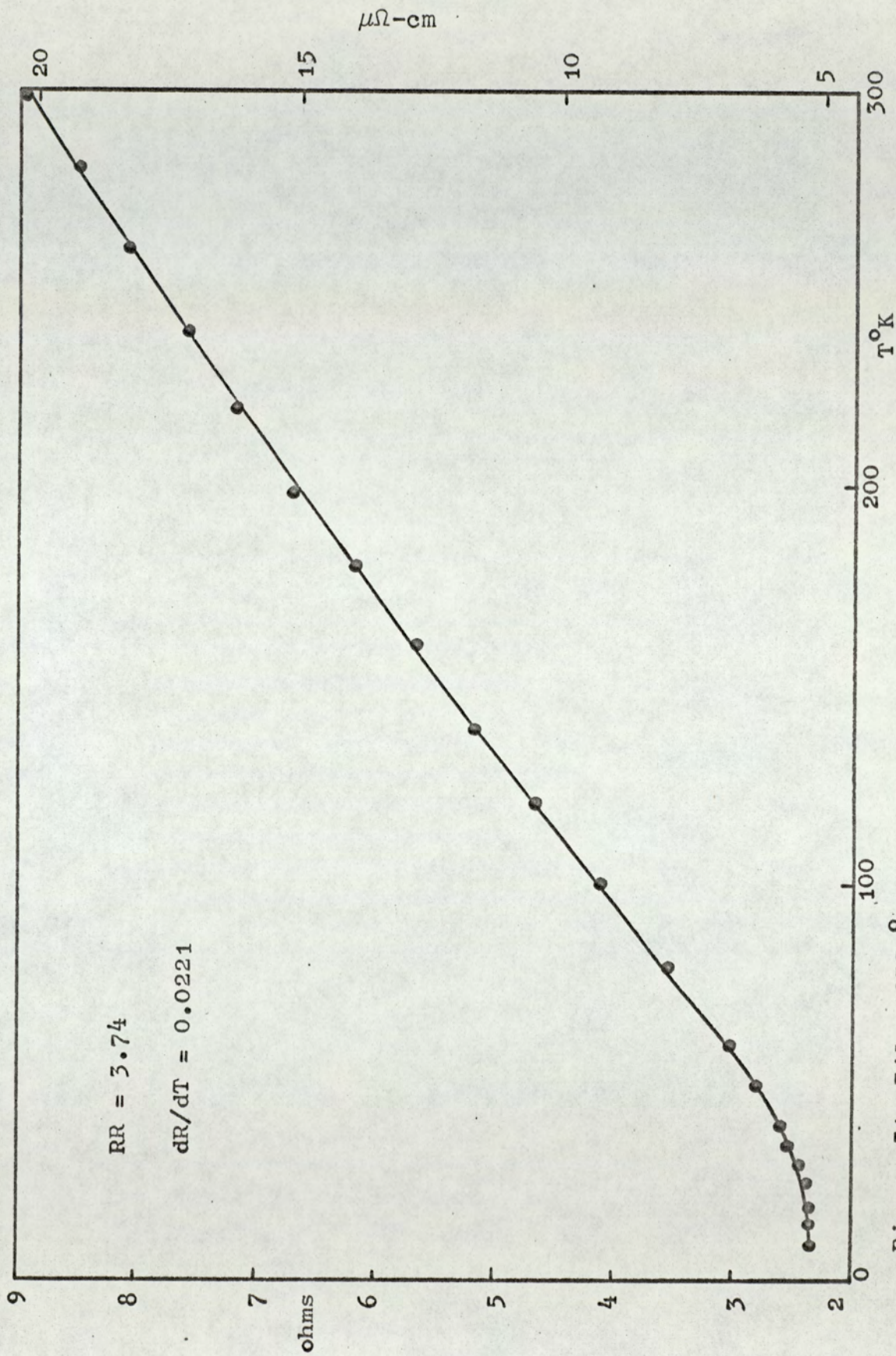
Figure 51. Film 1235 Å thick. Resistance and resistivity vs temperature.

RR = 3.74

dR/dT = 0.0221

μΩ−cm

ohms

T°K
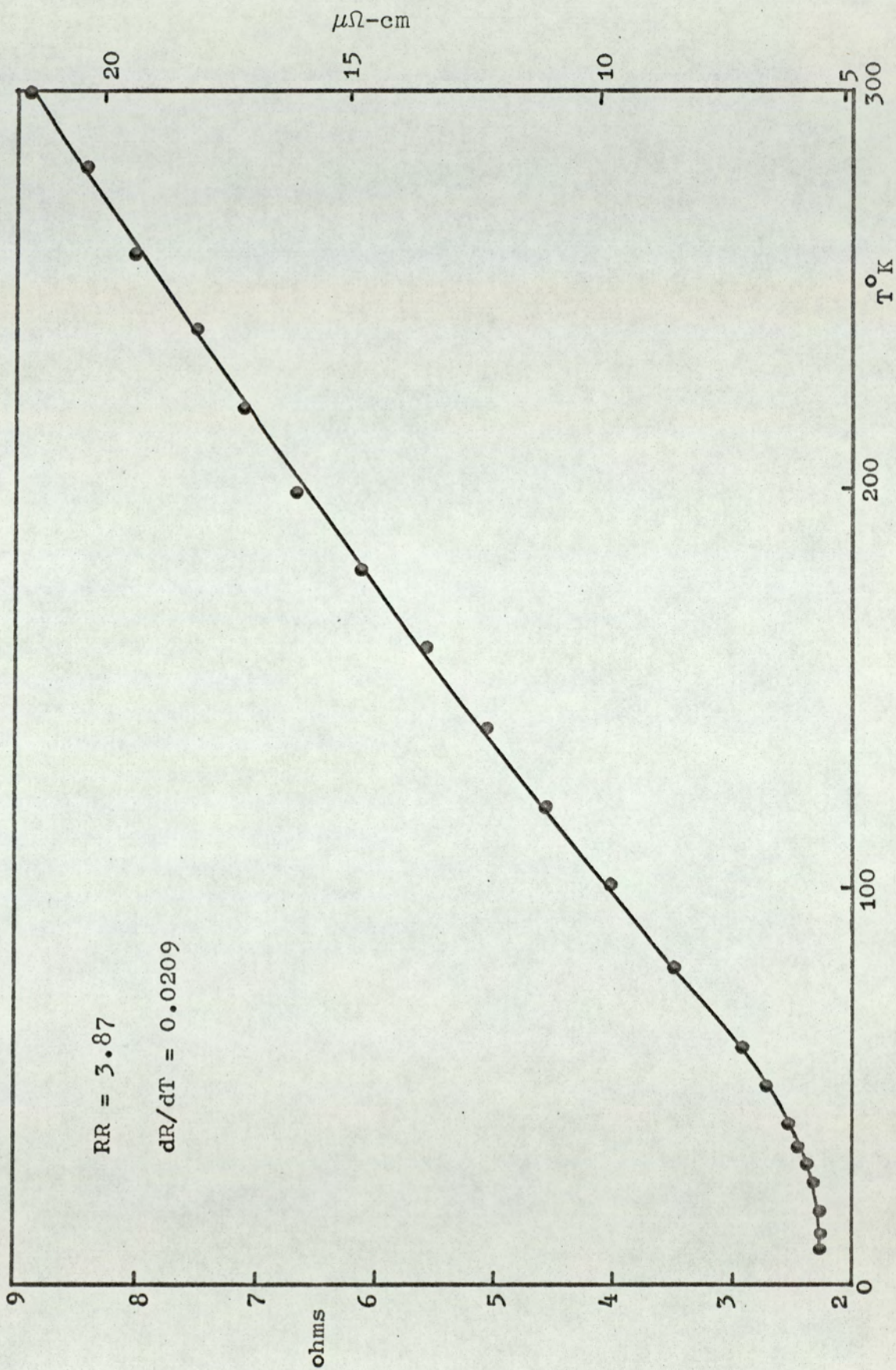
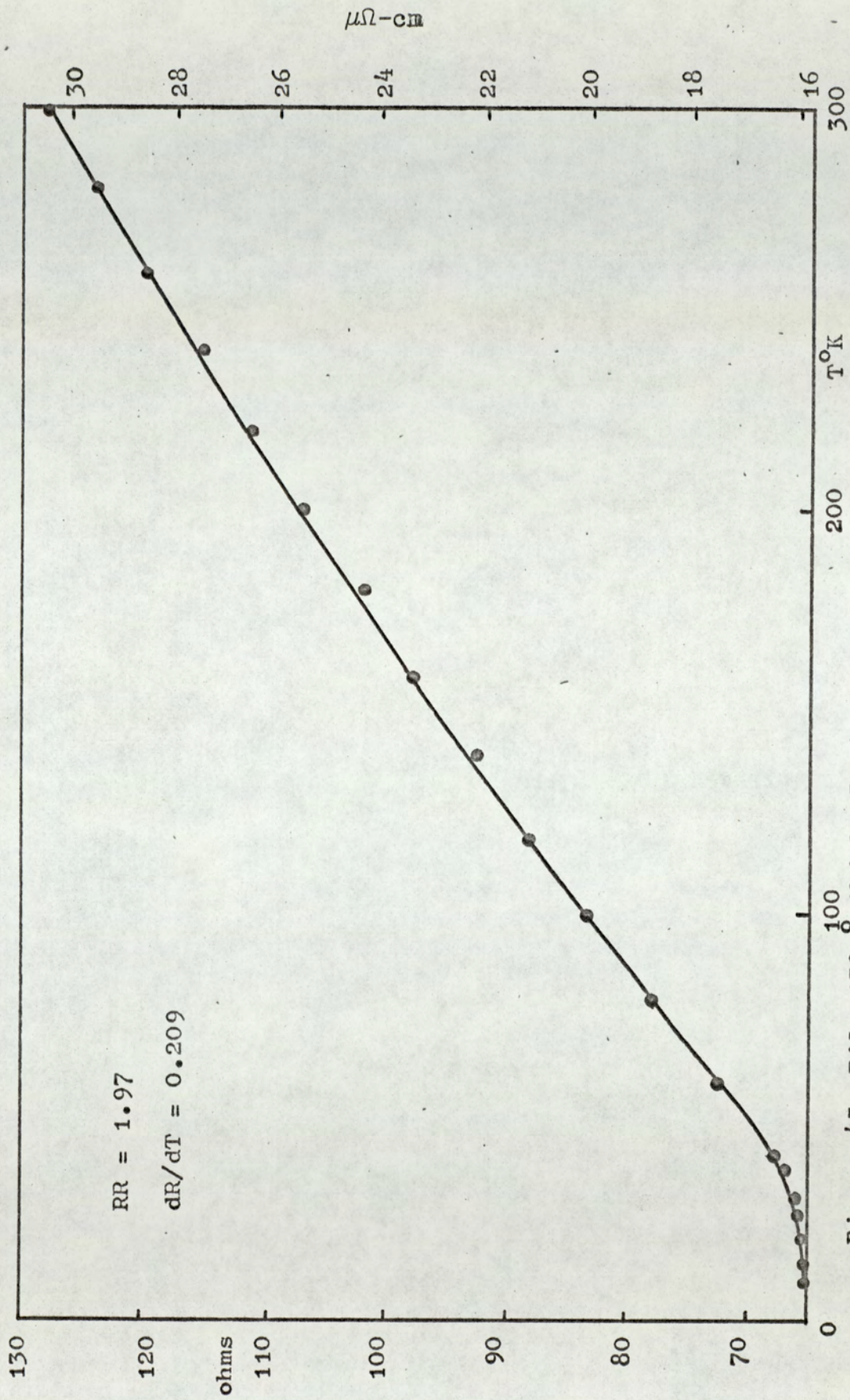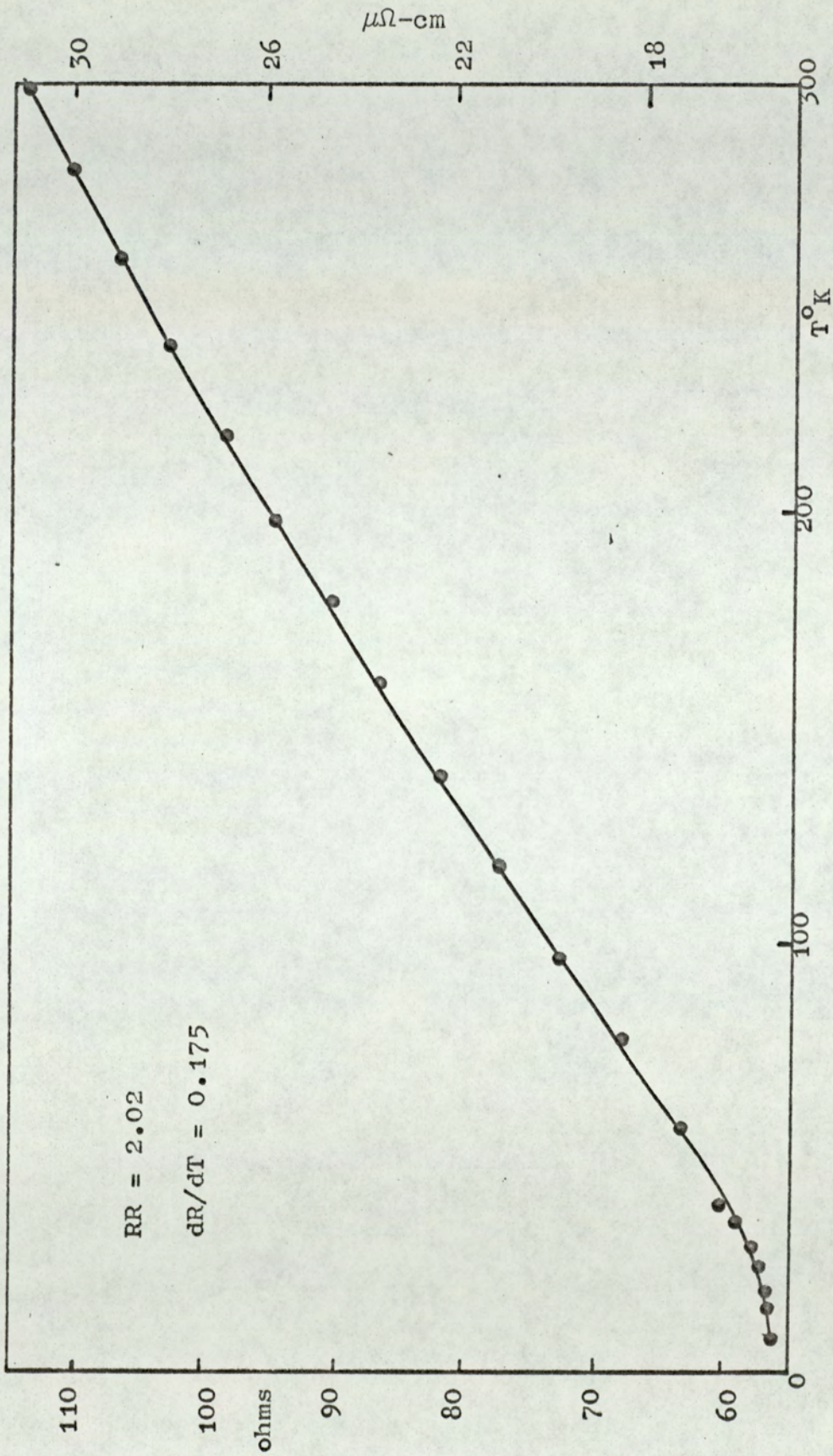Figure 52. Film 1315 Å thick. Resistance and resistivity vs temperature.
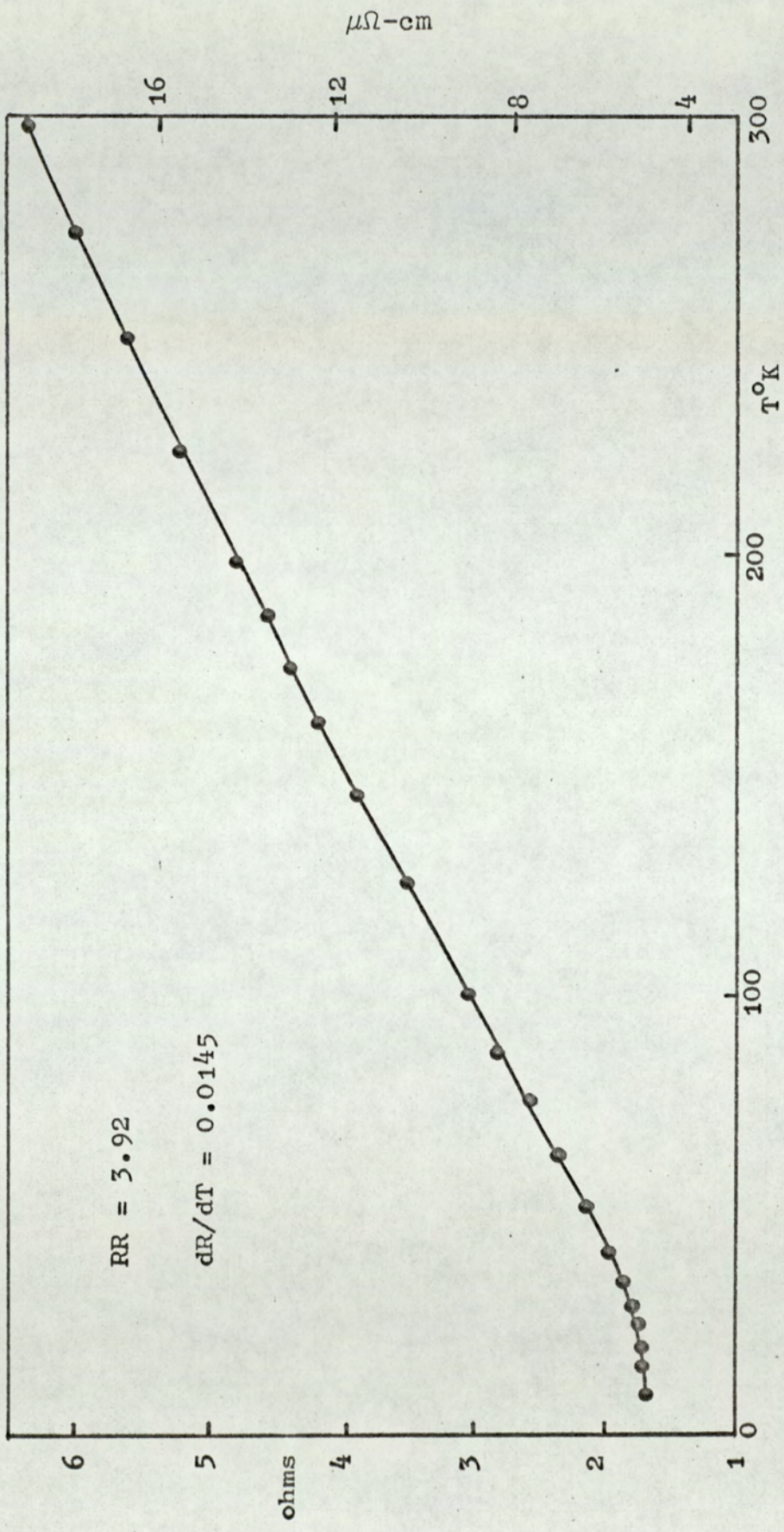
Figure 53. Film 1870 Å thick. Resistance and resistivity vs temperature.
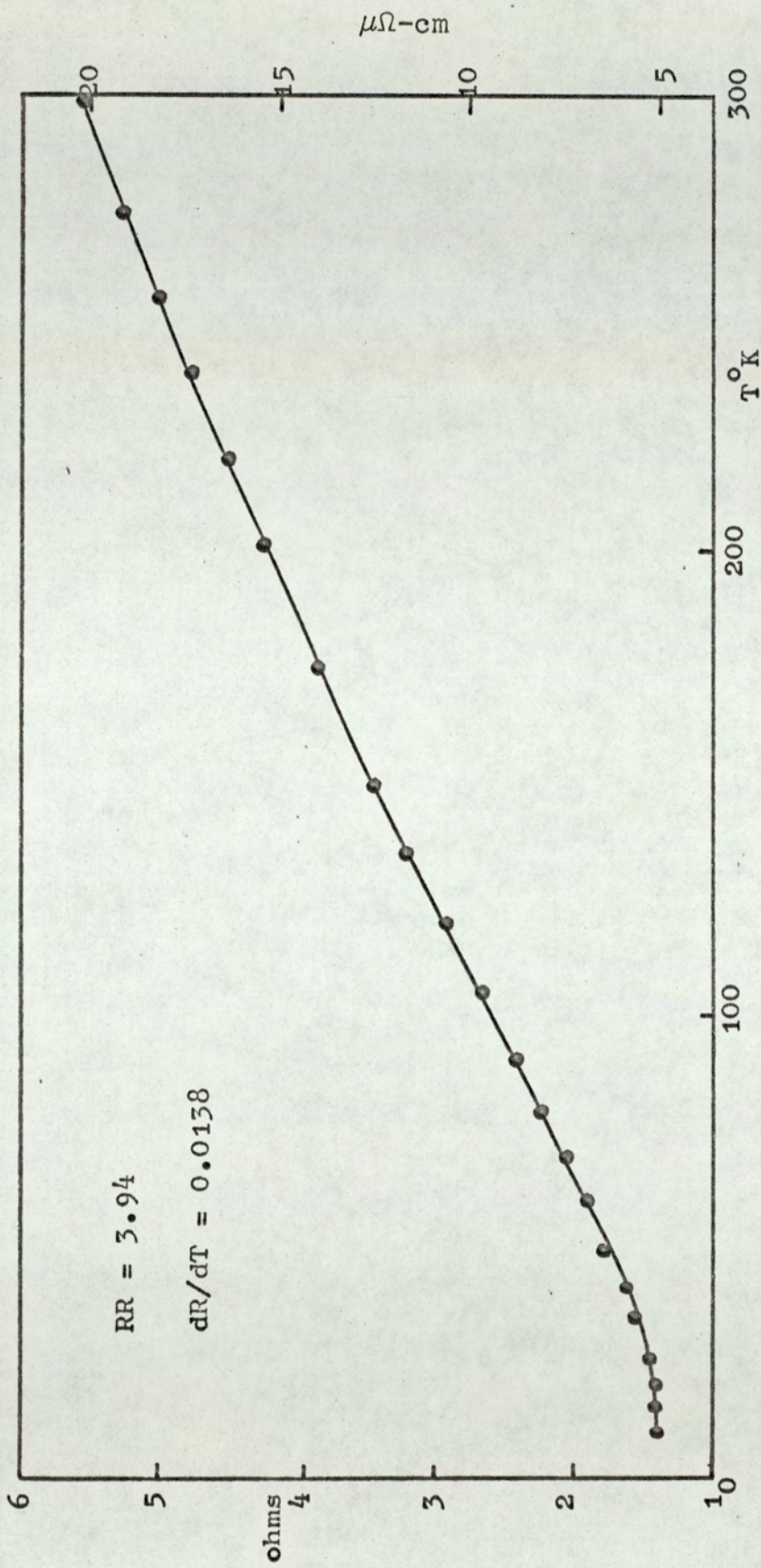
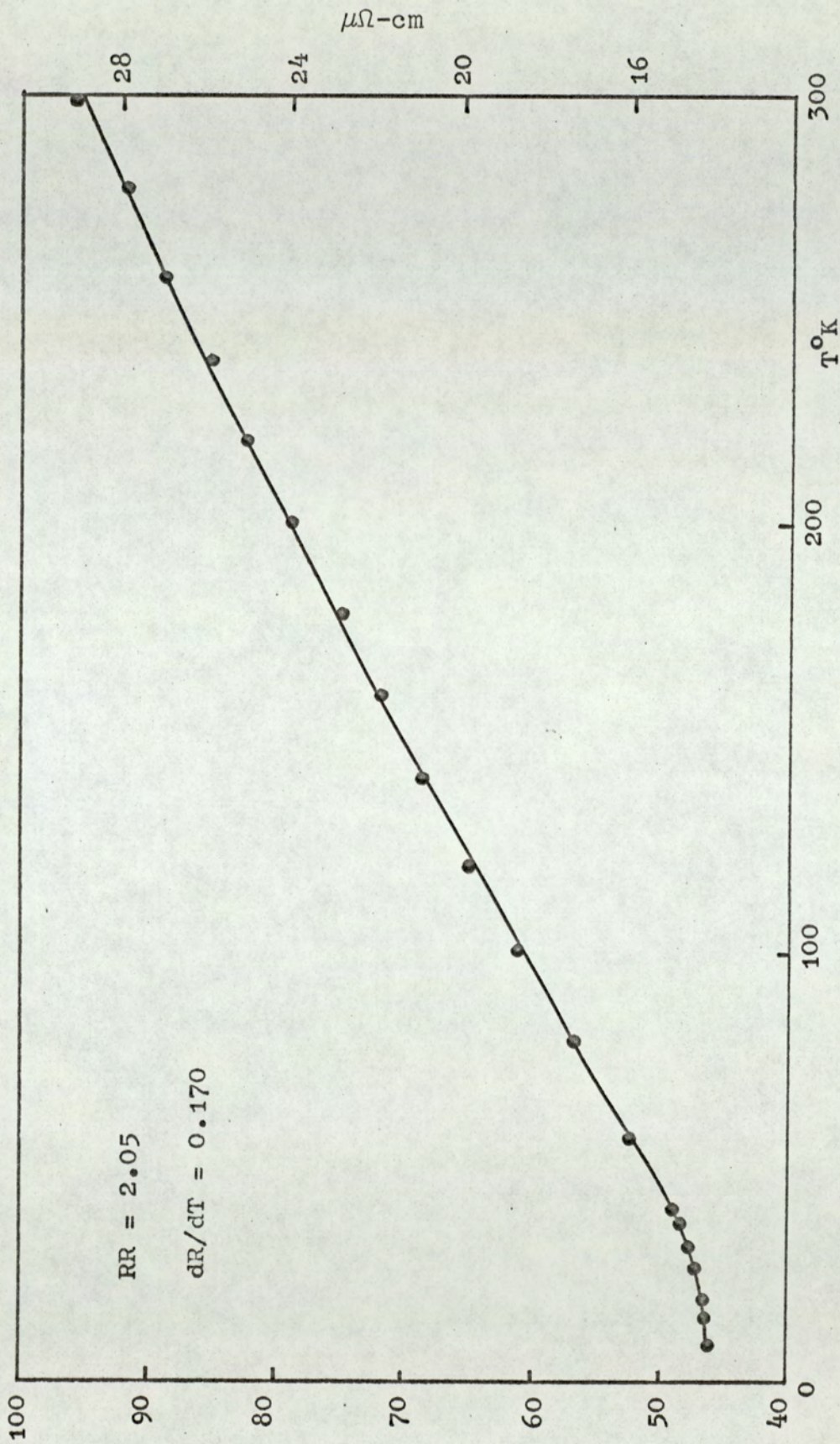Figure 54. Film 1985 Å thick. Resistance and resistivity vs temperature.

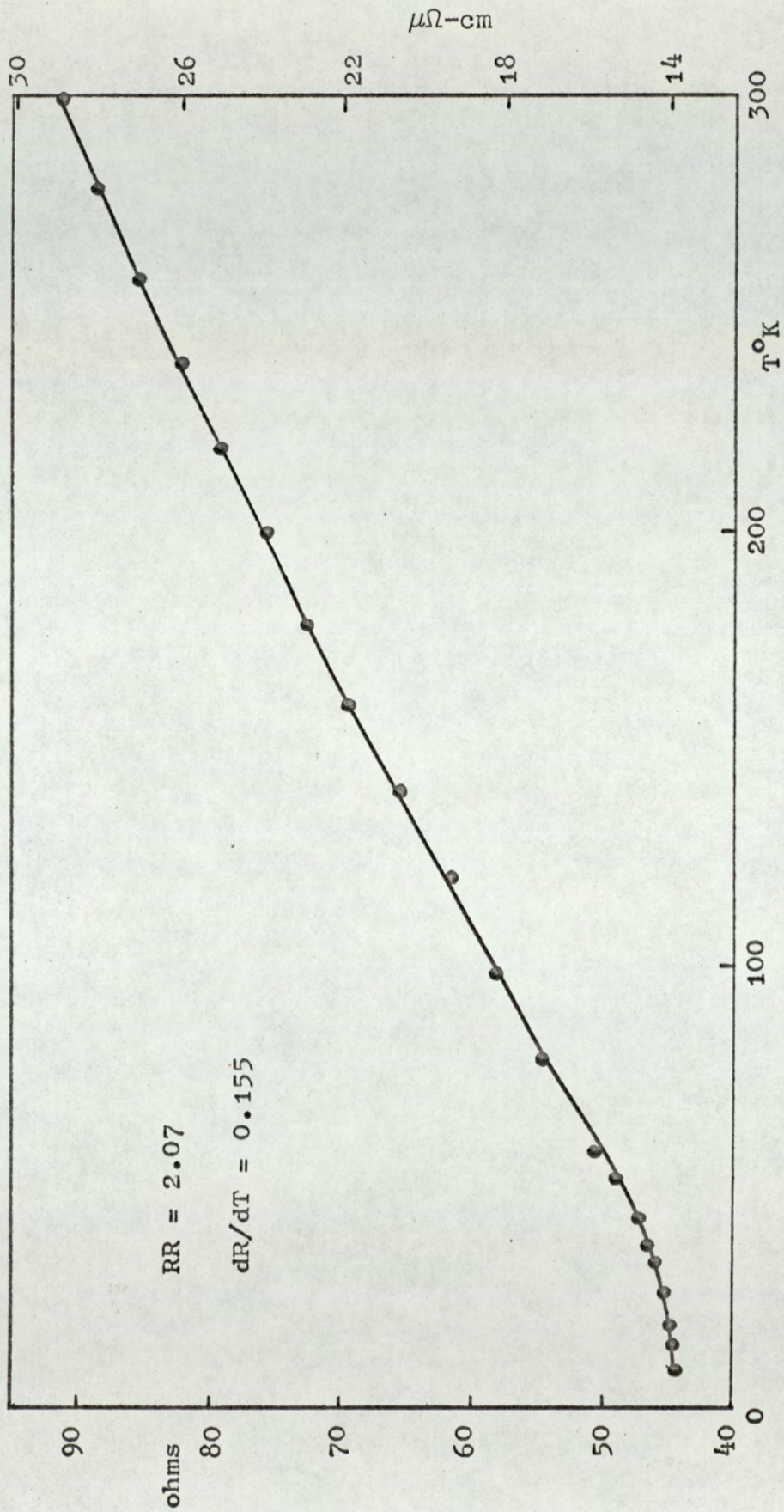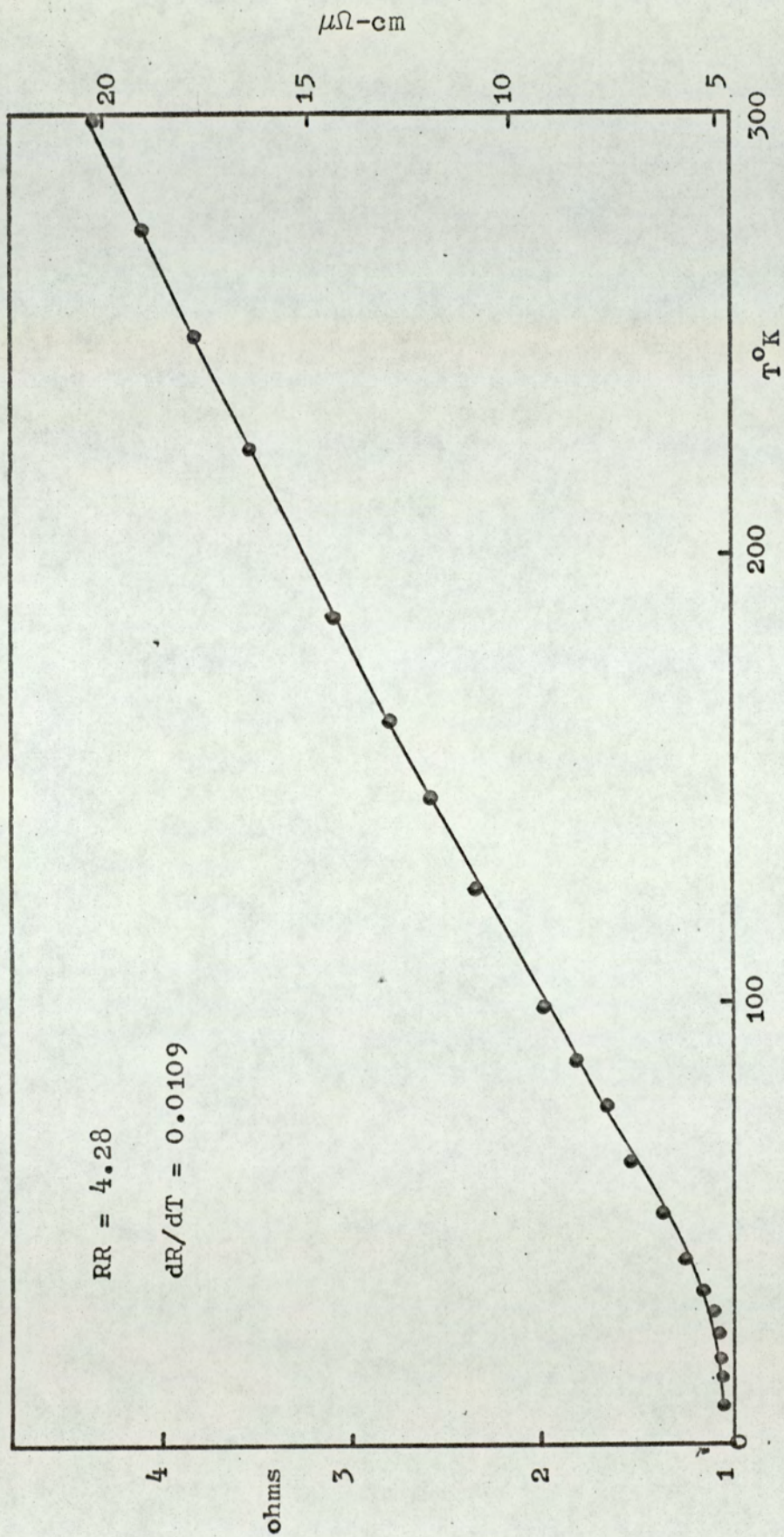Figure 55. Film 2505 Å thick. Resistance and resistivity vs temperature.
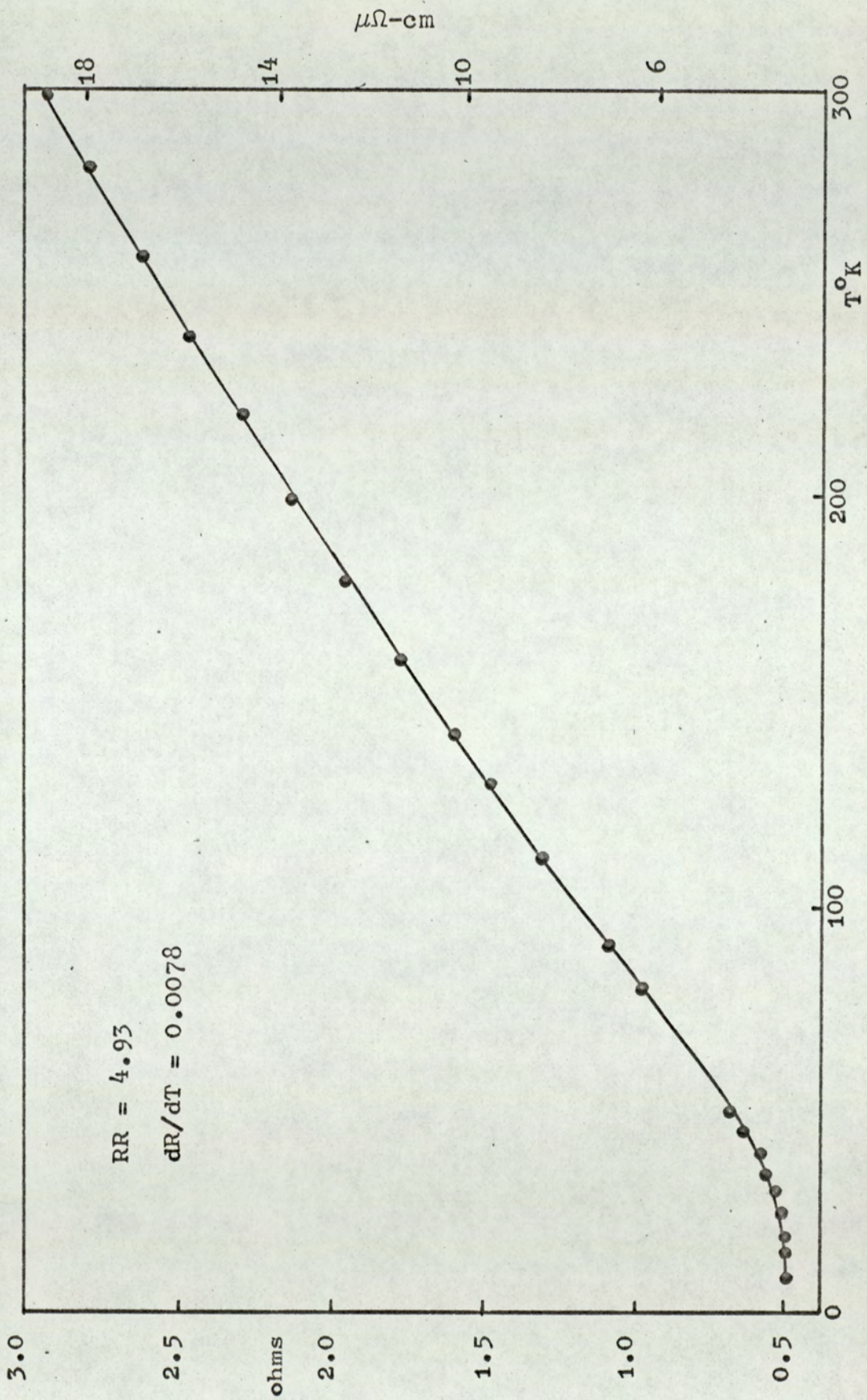
Figure 56. Film 3495 Å thick. Resistance and resistivity vs temperature.

RR = 4.93

dR/dT = 0.0078
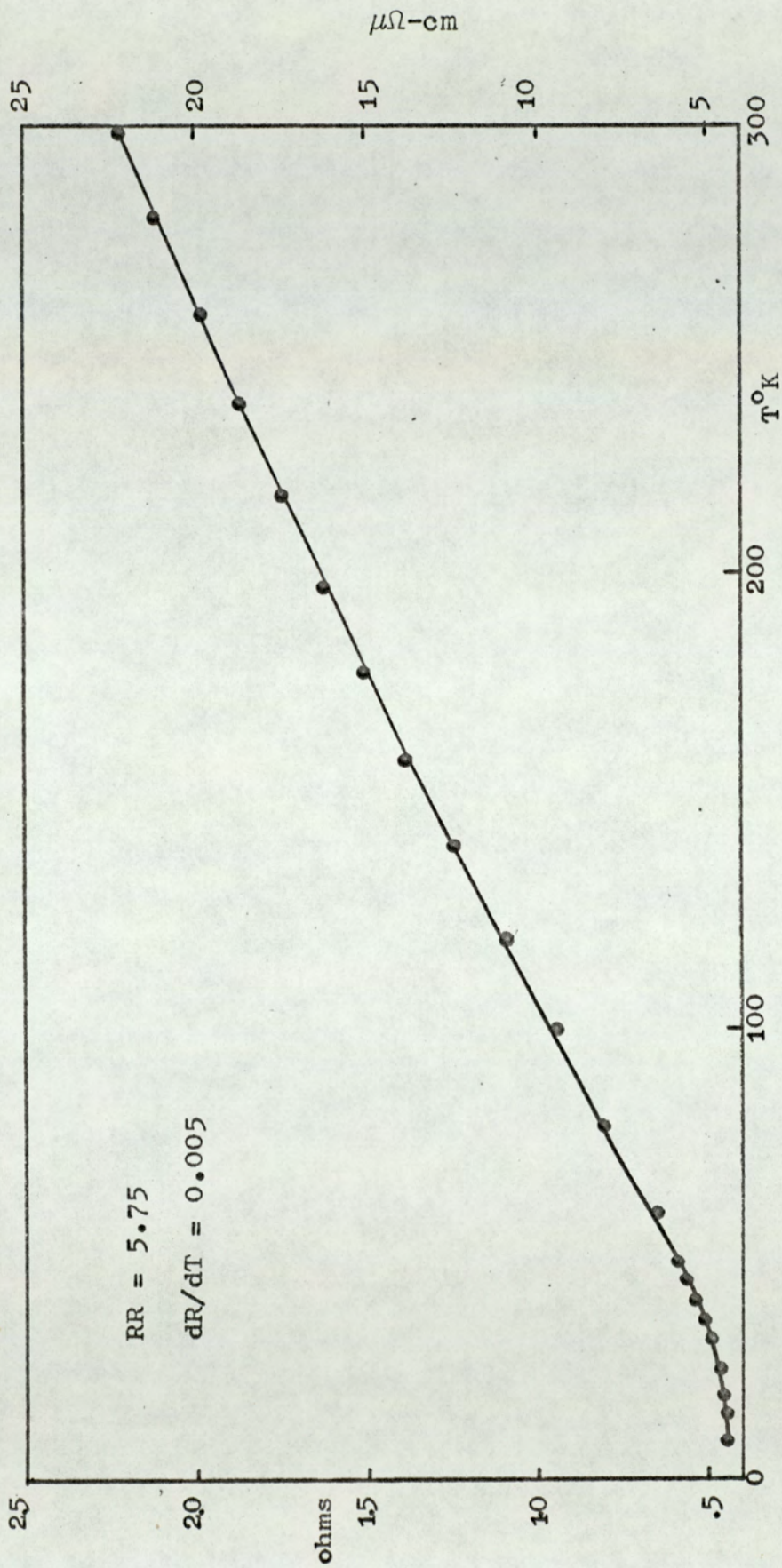
Figure 57. Film 5440 Å thick. Resistance and resistivity vs temperature.

$RR = 4.80$

$d\rho/dT = 0.049 \times 10^{-6} \ \Omega\text{-cm}$

$\mu\Omega\text{-cm}$

$T\,^{\circ}K$
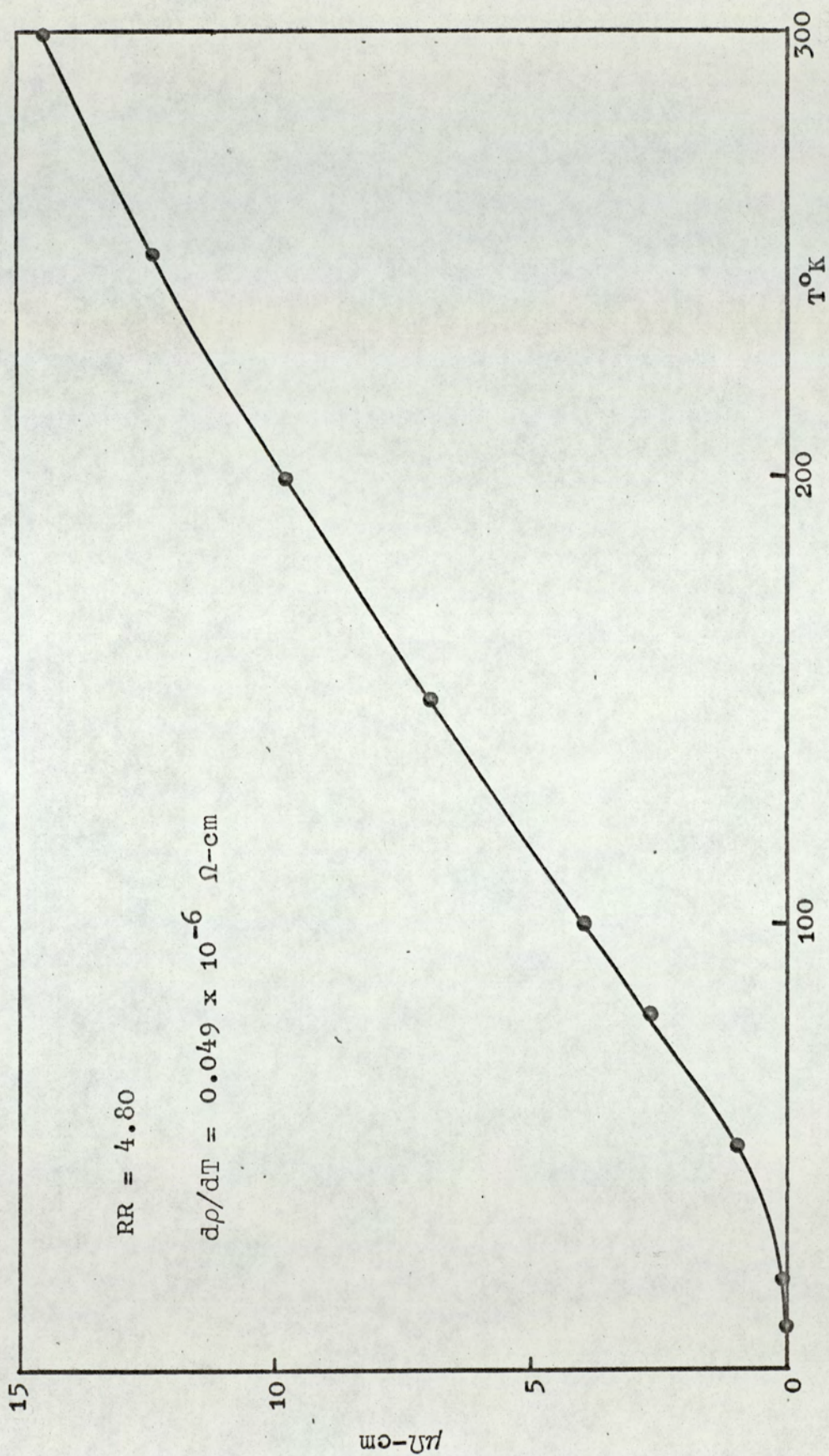
Figure 58. Bulk niobium. Resistivity versus temperature.
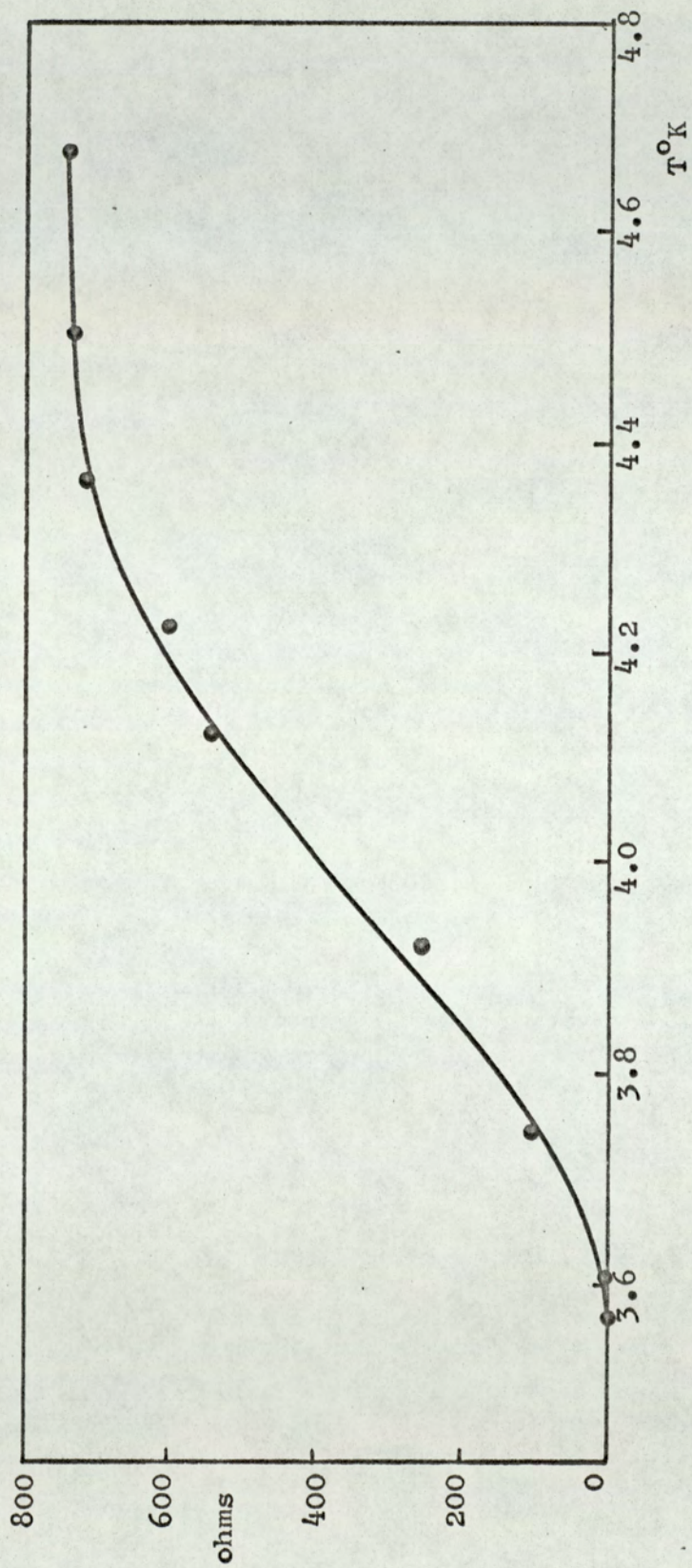
Figure 59. Resistive transition of film 50 Å thick.
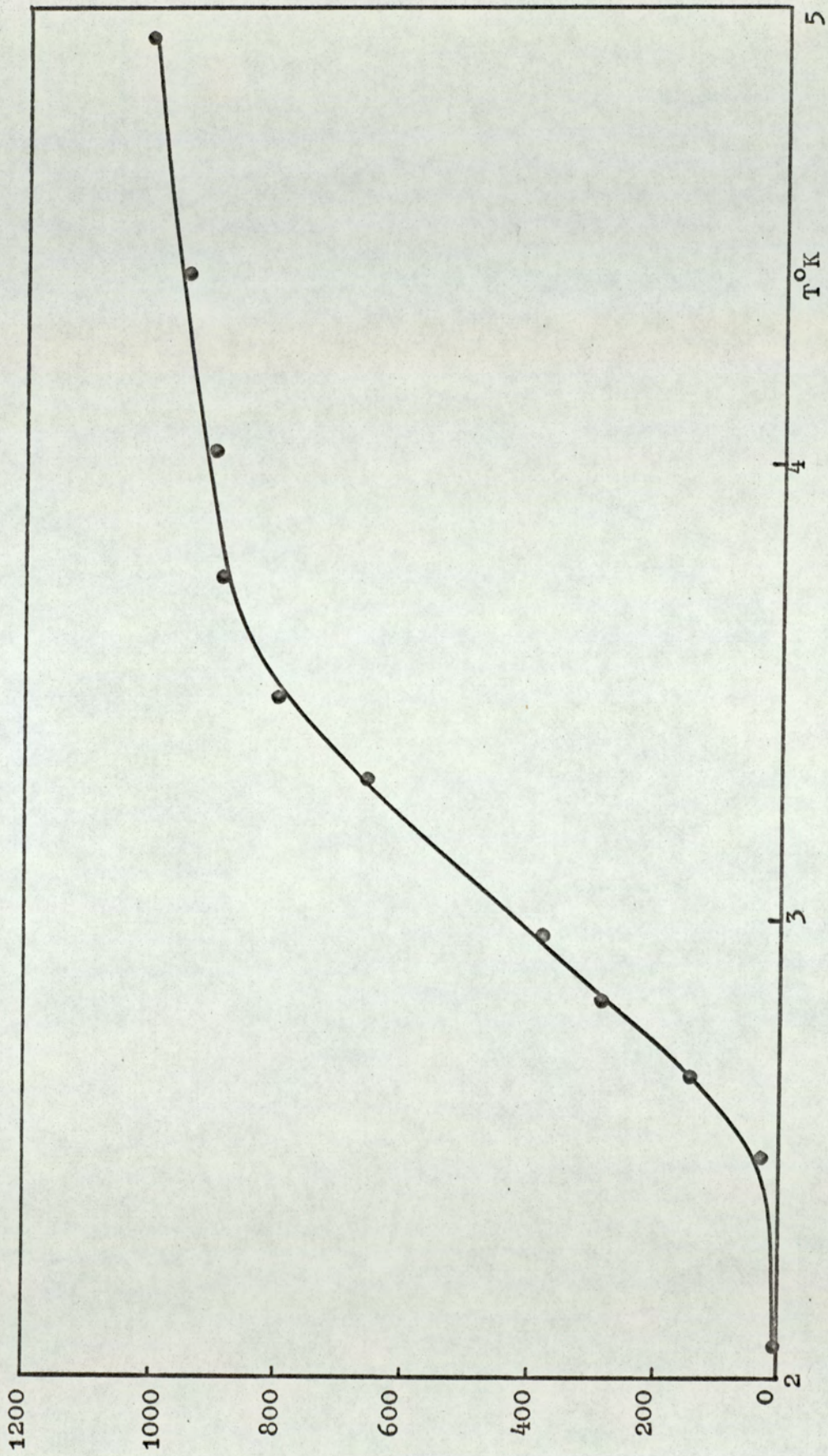
Figure 60. Resistive transition of film 45 Å thick.
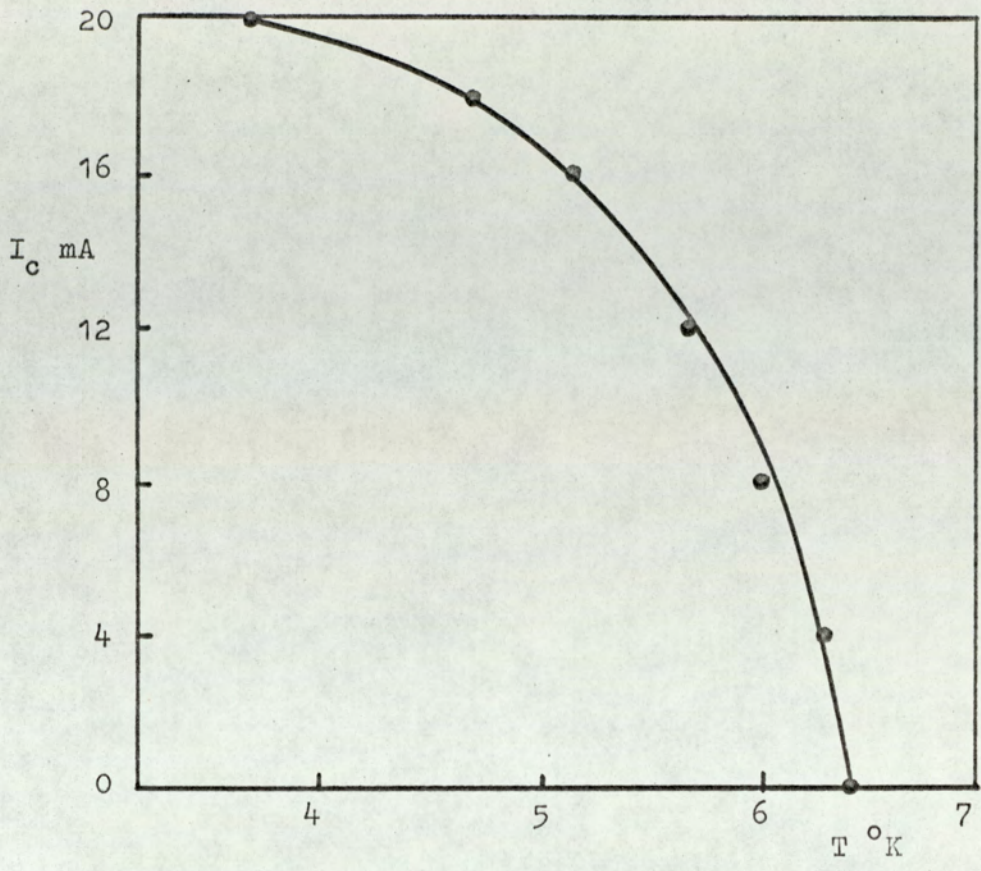
Figure 61. Film 230 Å thick. Critical current vs temperature
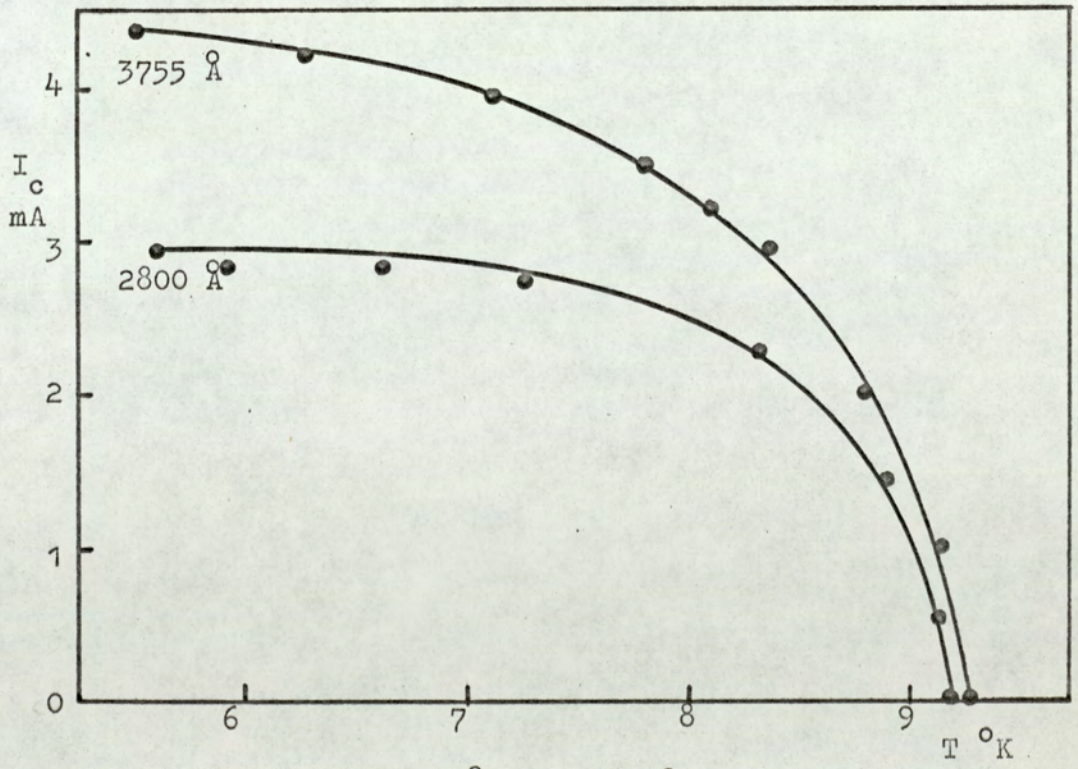
Figure 62. Films 3755 Å and 2800 Å thick. Critical
current versus temperature.
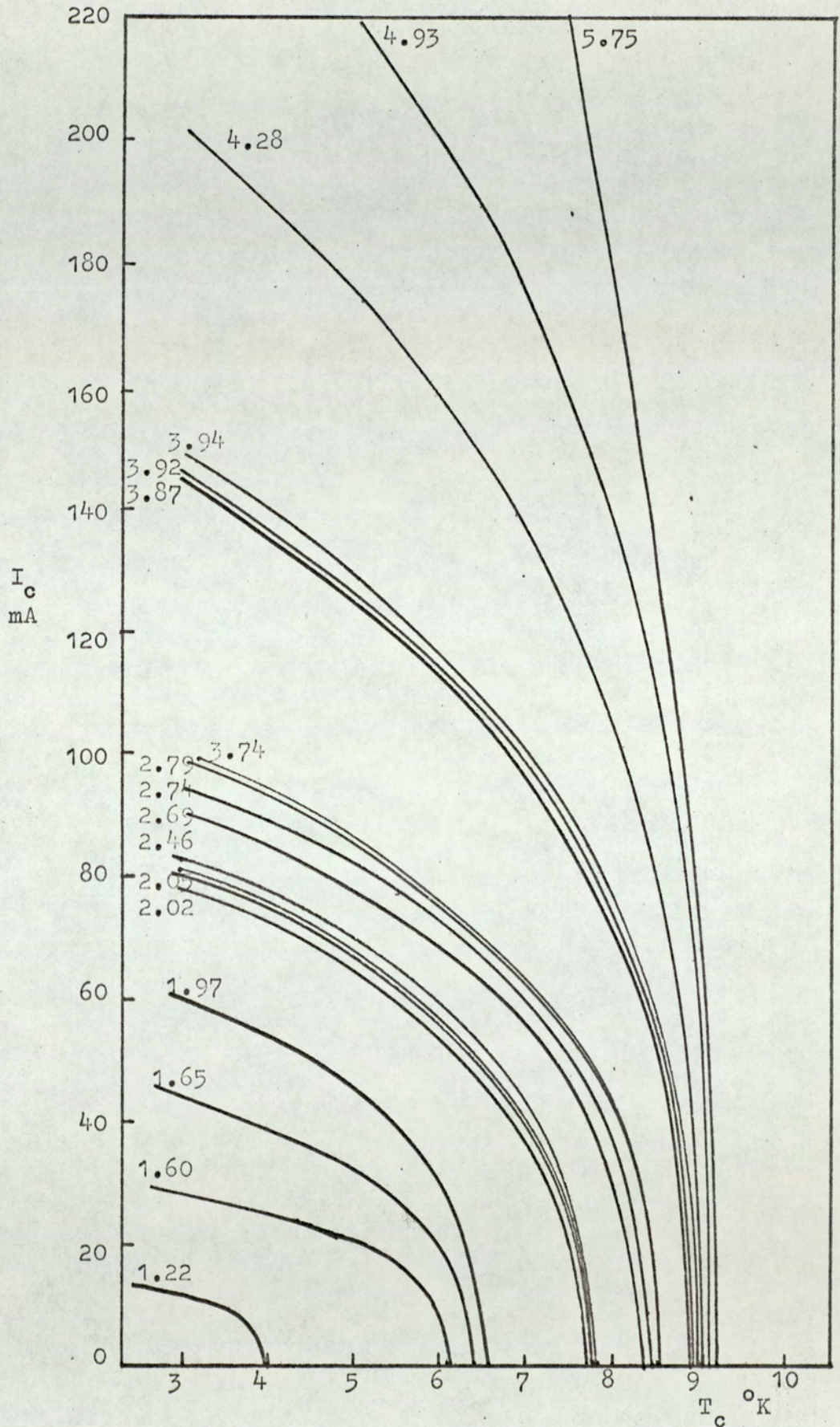
Figure 63. Critical current versus temperature.
Films are designated by the resistivity ratio.

Table 7. Comparison of film thickness measurement.

Film	Film Thickness Å	
	Interferometer	Electrical
60	80*	44
59	80*	48
62	120*	85
61	120*	90
64	165 ± 15	130
63	185 ± 15	155
65	200 ± 10	160
66	210 ± 10	175
70	400 ± 10	370
56	410 ± 10	380
55	420 ± 10	385
57	425 ± 10	405
68	1270 ± 20	1230
67	1350 ± 20	1300
53	1910 ± 20	1870
54	2020 ± 20	1965
71	2540 ± 20	2500
58	3530 ± 20	3470
69	5475 ± 20	5420
42	230 ± 10	225
43	2800 ± 20	2340
50	3755 ± 20	3450

*estimated from deposition rate.
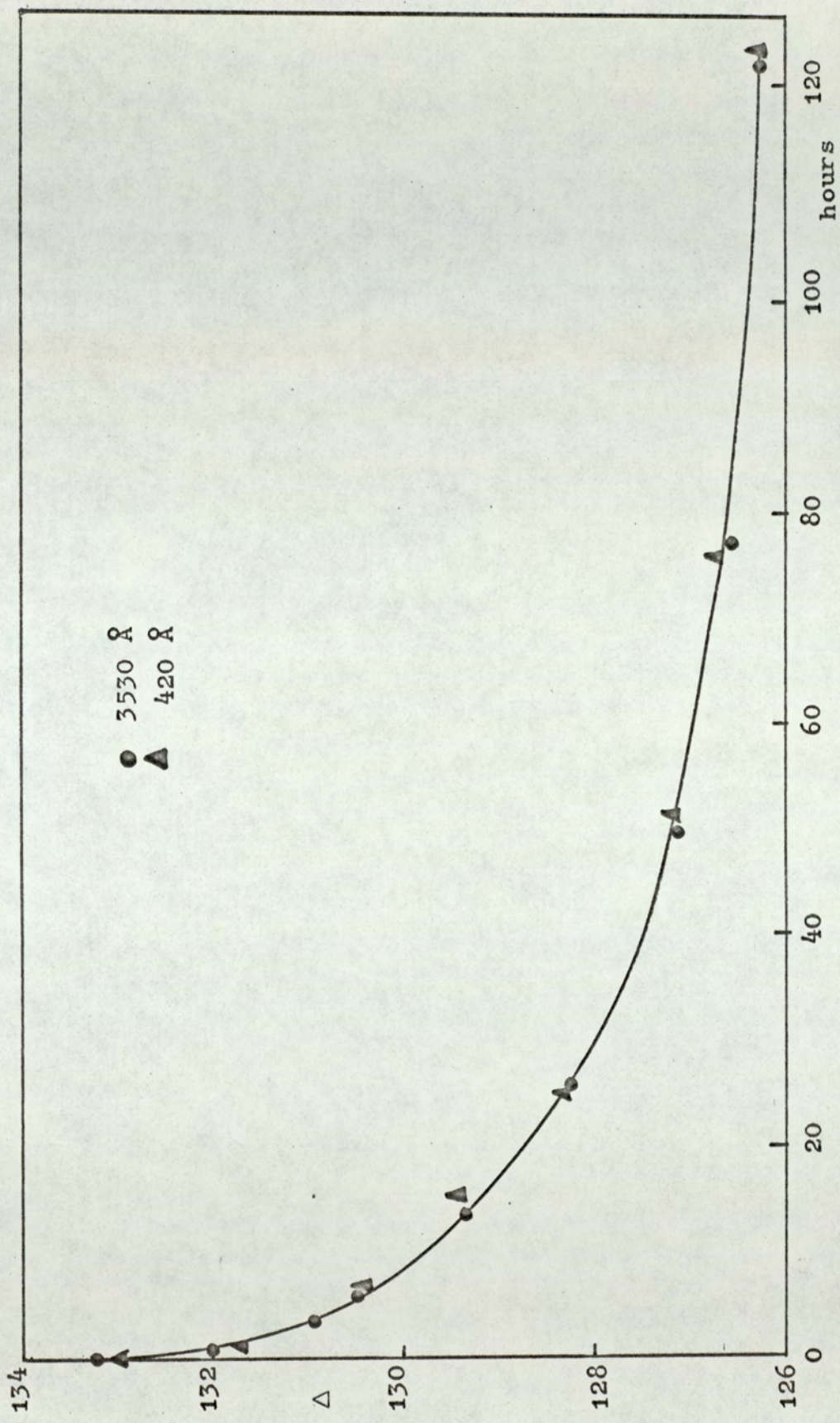
Figure 64. Reduction of Δ due to oxide growth.
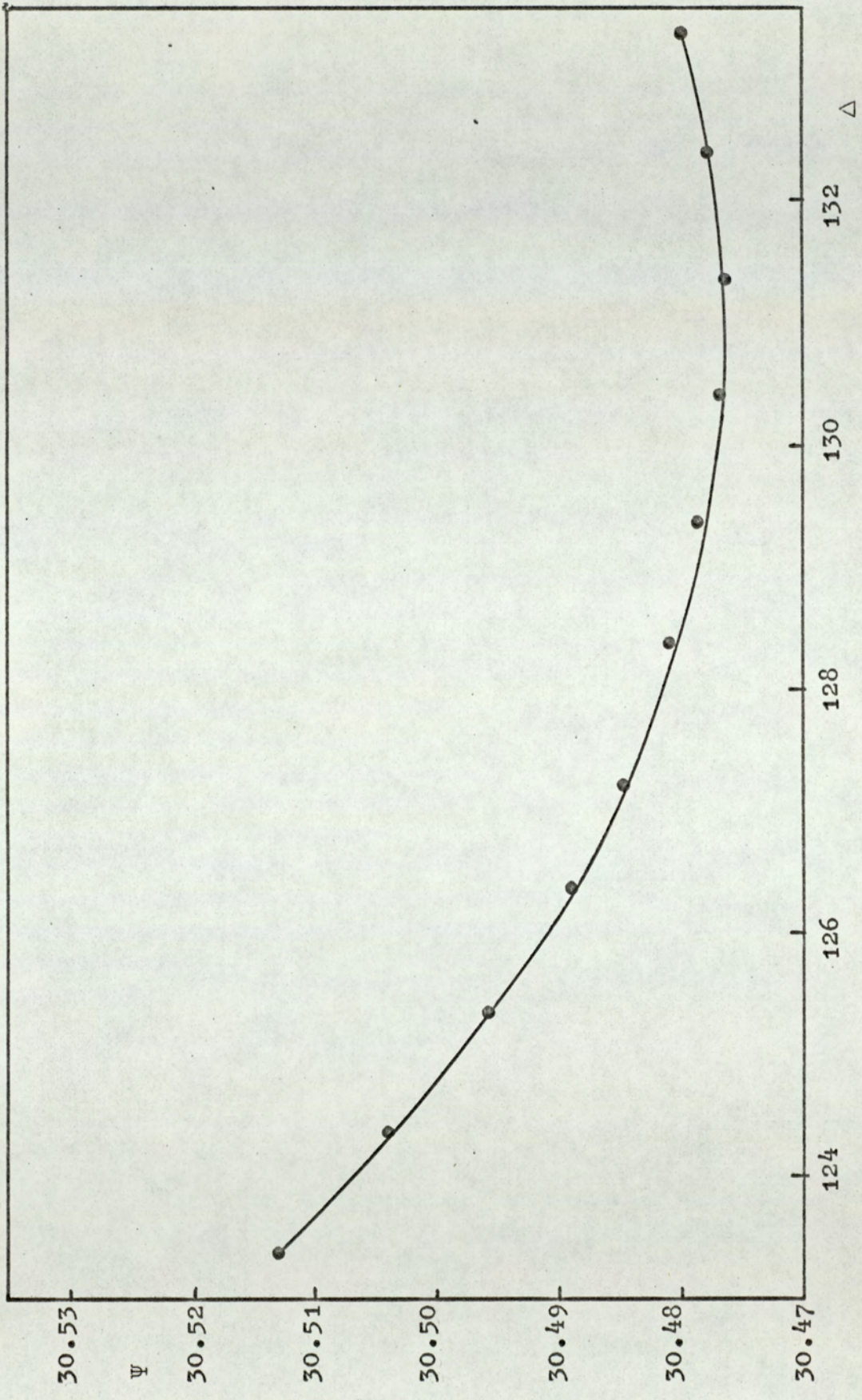
Figure 65. Variation of Ψ with respect to Δ
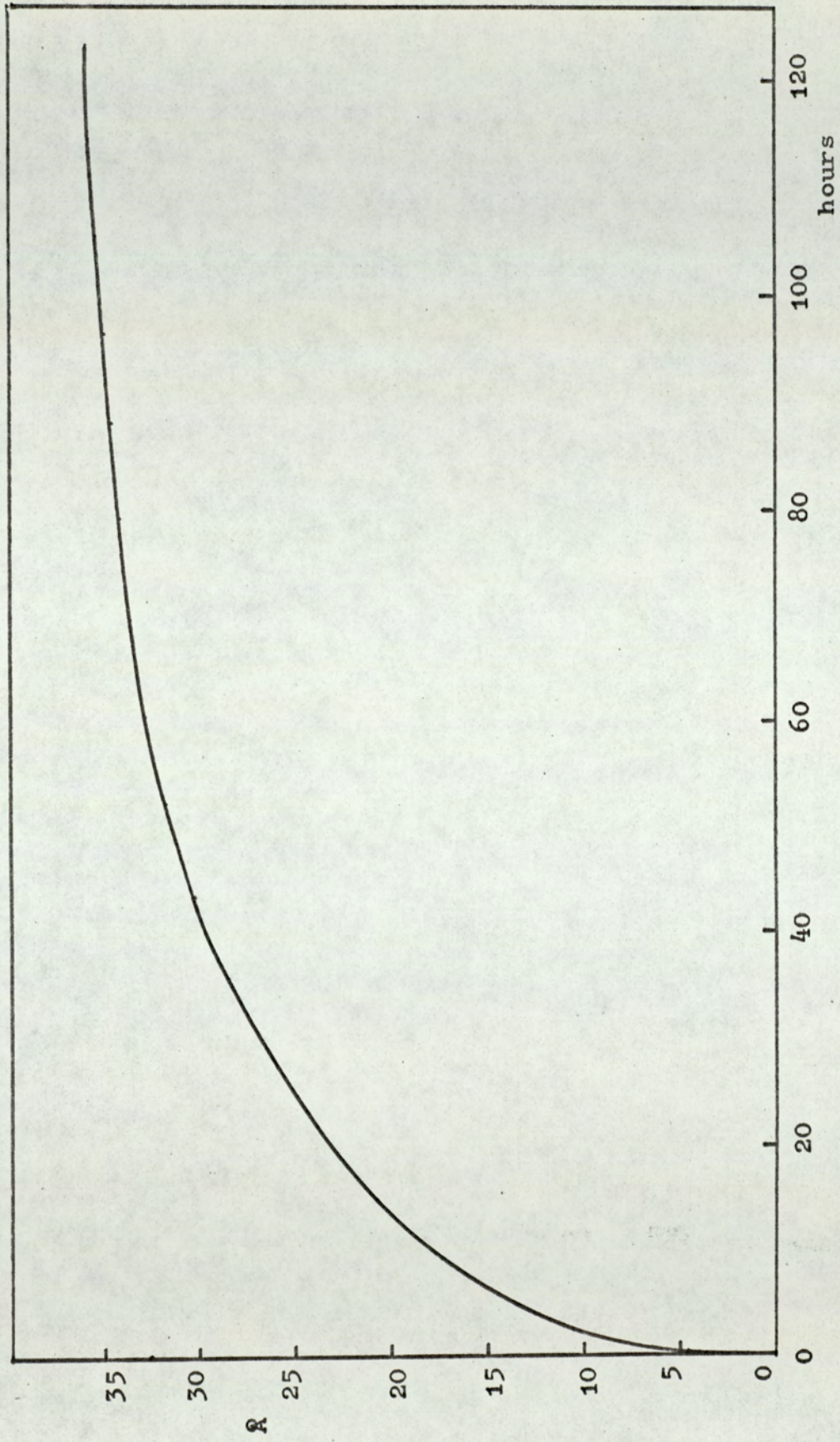
Figure 66. Rate of growth of oxide layer.

<u>Table 8</u>. Variation of $\triangle$ and ψ with respect
            to oxide thickness for a film 3530 Å
            thick

Wavelength 5478 Å

Oxide Thickness	$\triangle$	ψ
0	133.372	30.480
5	132377	30.478
10	131.382	30.477
15	130.385	30.477
20	129.388	30.478
25	128.390	30.481
30	127.389	30.485
35	126.388	30.489
40	125.386	30.496
45	124.382	30.504
50	123.378	30.513

Table 9. Variation of Δ and ψ with respect
to oxide thickness for a film 1660 Å
thick

Wavelength 4960 Å

Oxide Thickness	Δ	ψ
0	132.124	30.121
5	131.011	30.119
10	129.899	30.118
15	128.787	30.117
20	127.674	30.118
25	126.562	30.121
30	125.449	30.125
35	124.337	30.132
40	123.225	30.140
45	122.112	30.149
50	121.001	30.161

<u>Table 10.</u> Variation of $\triangle$ and ψ with respect
to oxide thickness for a film 1660 $\overset{\circ}{A}$
thick

Wavelength 5760 $\overset{\circ}{A}$

Oxide Thickness	$\triangle$	ψ
0	133.611	31.654
5	132.633	31.651
10	131.656	31.650
15	130.679	31.652
20	129.702	31.653
25	128.724	31.654
30	127.746	31.658
35	126.768	31.663
40	125.790	31.670
45	124.811	31.678
50	123.832	31.687

Table 11. Comparison of film thickness measurement.

Film	Film Thickness Å		
	Interferometer	Less Oxide	Electrical
60	80*	45	44
59	80*	45	48
62	120*	85	85
61	120*	85	90
64	165	130	130
63	185	150	155
65	200	165	160
66	210	175	175
70	400	365	370
56	410	375	380
55	420	385	385
57	425	395	405
68	1270	1235	1230
67	1350	1315	1300
53	1910	1875	1870
54	2020	1985	1965
71	2540	2505	2500
58	3530	3495	3470
69	5475	5440	5420
*estimated from deposition rate.			

Figure 67. Electron diffraction pattern of
200 Å thick film
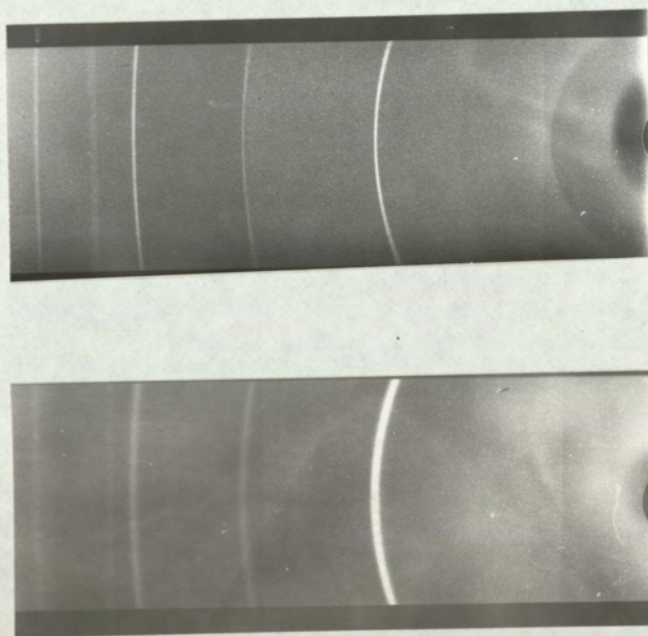
Figure 68. Comparison of X-ray diffraction patterns
for films 5440 Å and 375 Å thick.

Table 12. Comparison of 'd' spacing for 200 $\overset{\circ}{A}$ thick niobium film to known 'd' values

Diameter of rings (cm)	Ratio to first ring	Computed values d($\overset{\circ}{A}$)	Known values d($\overset{\circ}{A}$)	(hkl)
1.672	1.0000	2.33	2.33	(110)
2.378	0.7031	1.64	1.65	(200)
2.894	0.5770	1.34	1.34	(211)
3.356	0.4980	1.16	1.16	(220)
3.774	0.4430	1.03	1.04	(310)
4.100	0.4080	0.951	0.95	(222)
4.50	0.3760	0.876	0.88	(321)
5.050	0.3310	0.770	0.78	(411) (330)
5.300	0.3150	0.734	0.74	(420)
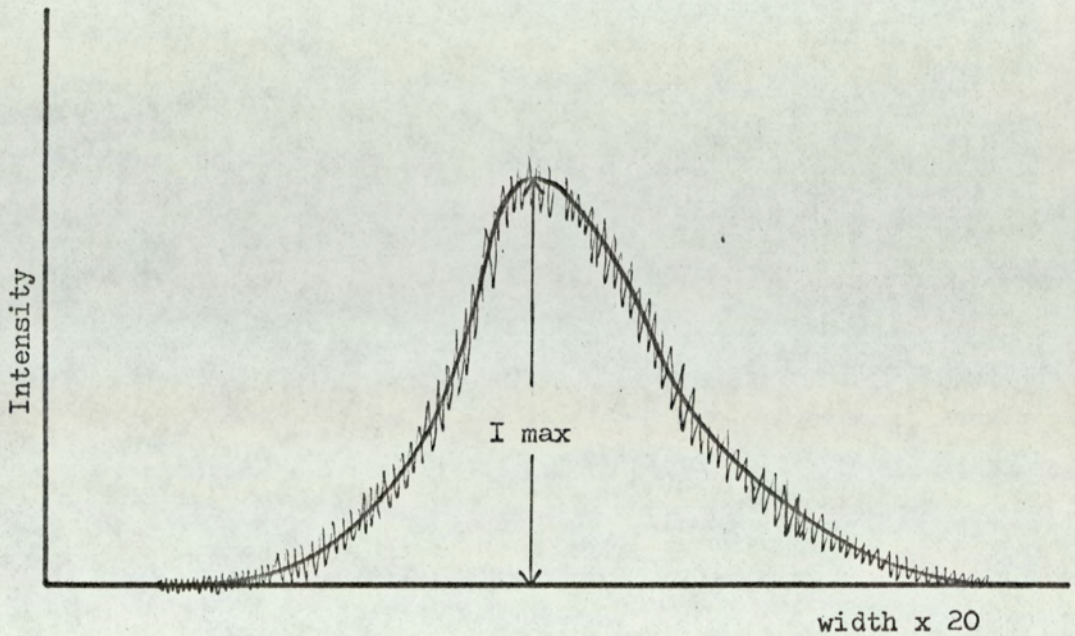
<u>Figure 69.</u>   Densitometer trace obtained from diffraction
line of a film 365 Å thick

<u>Table 13.</u>   Grain sizes of various films as determined
by diffraction line broadening

Film Thickness	Resistivity Ratio	Transition Temperature °K	Grain Size Å
5440	5.75	9.07	210 $\pm$ 5
3495	4.94	9.04	180 $\pm$ 5
1315	3.88	8.92	116 $\pm$ 5
375	2.68	8.42	77 $\pm$ 5
85	1.60	6.60	42 $\pm$ 6
45	1.16	3.00	30 $\pm$ 10

CHAPTER 5

Interpretation and Discussion of Results

5.1. Introduction

The present work offered the possibility of studying the electrical properties of niobium films, prepared by thermal evaporation, over a wide range of thickness.

Measurements of the normal electrical properties of the films are compared with the results reported by other authors, for niobium films prepared by thermal evaporation and sputtering. From the present results an estimate was made of the electron mean free path and the fraction of electrons that suffer specular scattering at the film boundaries.

By applying the McMillan equation (2.5) to the present films it is postulated that modifications to the phonon spectrum may be responsible for the observed reduction in the transition temperature of very thin films. A correlation between grain size, resistivity ratio and transition temperature is also presented.

An estimate is made of the superconducting critical current densities for these films and the results are compared with the work of other authors for films prepared by evaporation and sputtering.

5.2. Film Growth and Structure

5.2.1. Growth

During the initial stage of film growth, when the average thickness of the film is only a few tens of Angströms, the film will have a granular or island like structure consisting of discrete particles. As the film becomes thicker some coalescence

of the particles takes place and a network is formed of particles joined by bridges and separated by gaps. Further growth results in the filling of the gaps until a continuous film is formed.

Each stage of growth has distinctive electrical properties. The resistivity of a granular film is several orders of magnitude greater than that of the bulk material and is generally characterized by a negative temperature coefficient of resistivity. The conductivity is found to vary exponentially with the inverse of temperature, suggesting that the conduction mechanism is thermally activated and can take the form

$$\sigma = \frac{1}{\rho} \ \alpha \ \exp \left(\frac{-\epsilon}{kT} \right) \qquad (5.1)$$

where ϵ is an activation energy.

This dependence has been reported by Neugebauer and Webb[72] for platinum, gold and nickel, Milgram and Lu[73] for chromium, Bashara and Weitzenkamp[74] for gold and Vodar[75] for platinum and tungsten.

When the film becomes slightly thick and some coalescence has taken place, the film may have a positive or negative temperature coefficient of resistivity. There are positive contributions to the resistivity by the metallic particles and bridges and negative contributions to the resistivity from the thermally activated gaps. A distribution of activation energies and therefore a non-linear log conductivity versus $1/T$ dependence is usually observed in these slightly thicker films. It is apparently due to there existing a broader distribution of particle sizes and activation energies than in the thinner films. The results of Neugebauer and Webb are shown in Figures 70 and 71, for both the granular and network
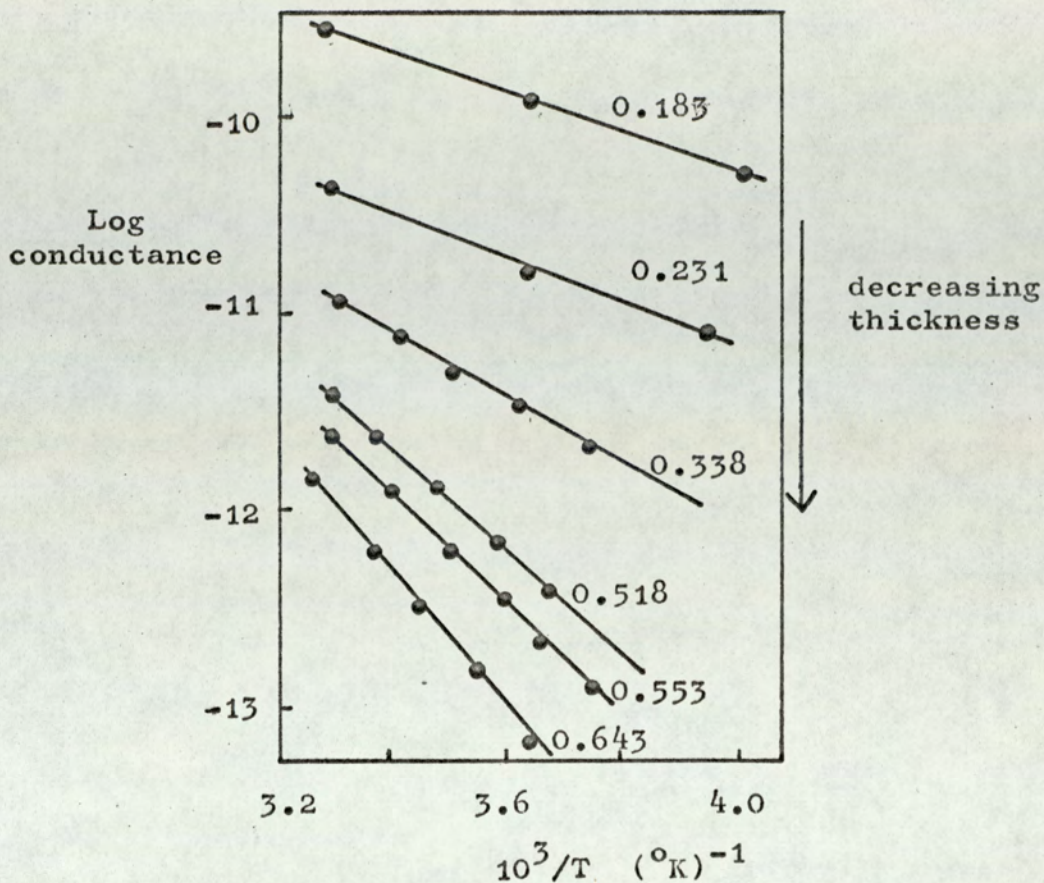
Figure 70. Log conductance vs reciprocal temperature
for discontinuous platinum films. The
activation energies are given for each plot.[72]
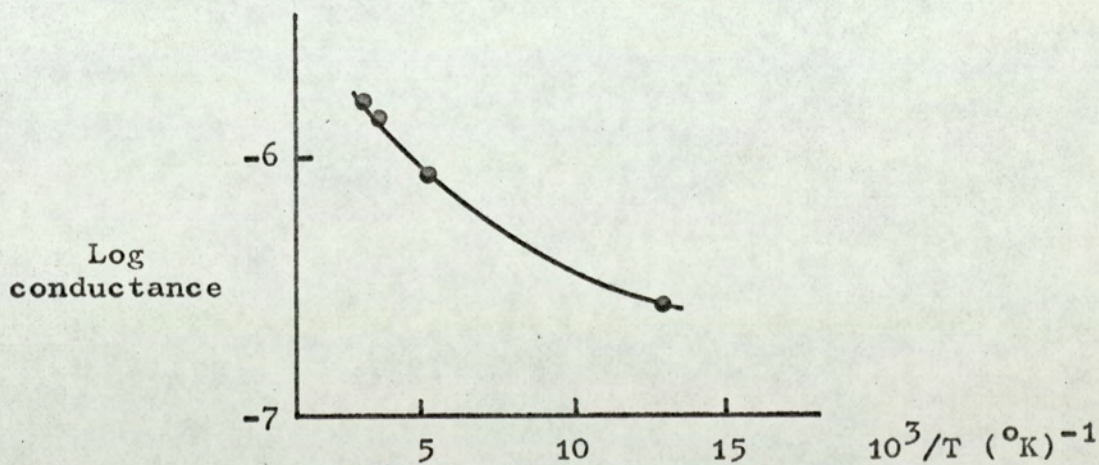
Figure 71. Log conductance vs reciprocal temperature
for nickel films, showing a spectrum of
activation energies.[72]
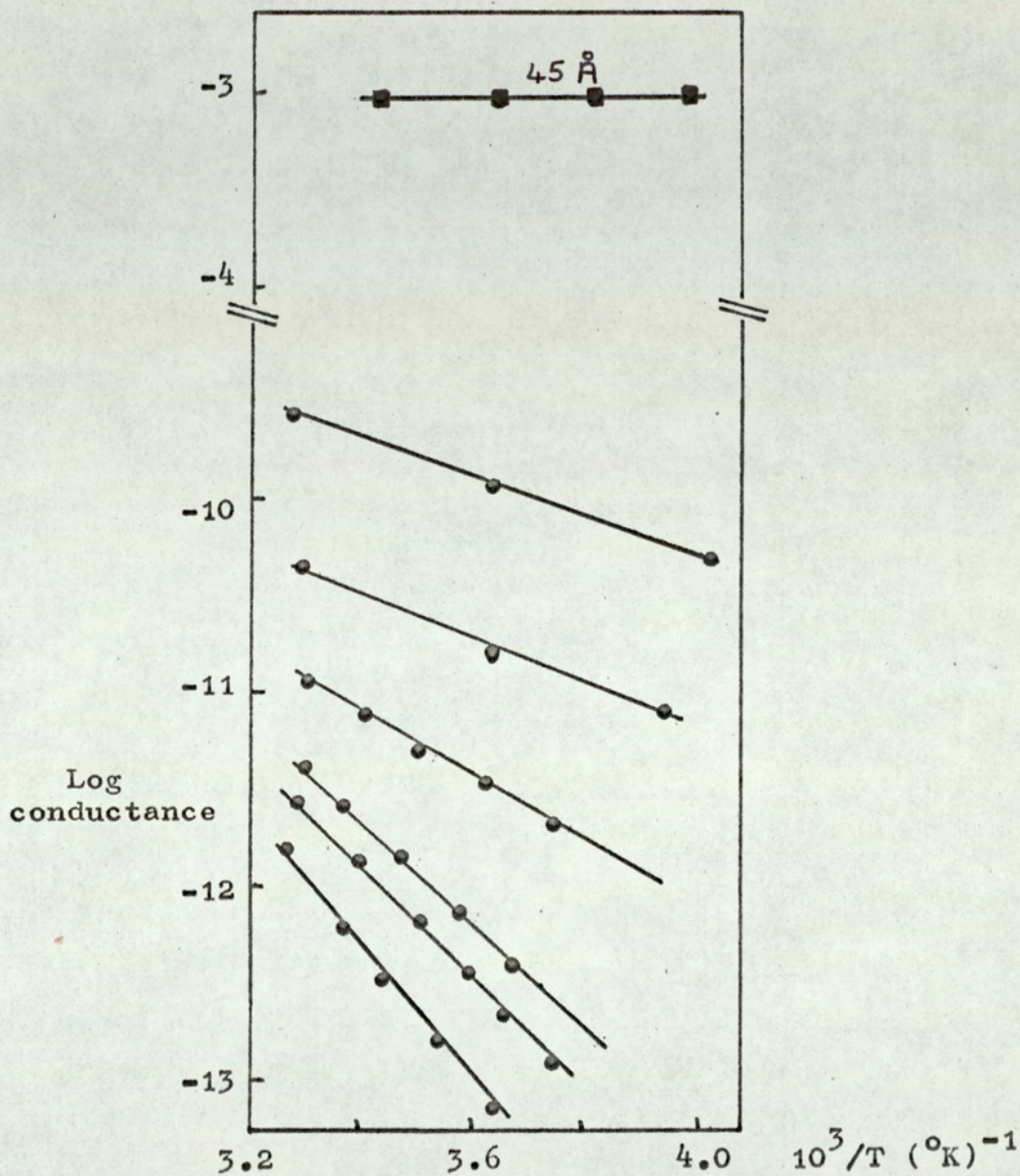
Figure 72.   Comparison of 45 Å thick film with the results of Neugebauer and Webb.[72]

structures of films.

Once the film is continuous, the temperature coefficient of resistivity becomes positive. Any variations from bulk resistivity are due to the dimensions of the film becoming comparable to the mean free path of the electrons. The theory relating to continuous films has been described in section 1.4 and 5.2.

The thinnest niobium film deposited in the present work was 80 Å thick, oxidation reduced the thickness to 45 Å. An examination of the results for this film, Figure 39, reveals that the graph of resistivity versus temperature retains the positive temperature coefficient of resistivity and general shape as displayed by the thicker films and bulk niobium. The resistivity of this film at 300°K was found to be less than a factor of seven greater than for bulk niobium at the same temperature.

A graph of log conductivity versus $^{1}/T$ was plotted for this film, Figure 72. As can be seen by comparison with the results of Neugebauer and Webb, the film neither displays the slope expected for a granular film nor the curve obtained for a porous film. From these observations it was deduced that these niobium films deposited at a thickness greater than 80 Å were continuous.

5.2.2. Structure and Grain Size

Electron and X-ray diffraction patterns of a number of films have been presented, Figures 67 and 68. From these photographs it was determined that in general, niobium films deposited at approximately 250 Å min^{-1}, in a vacuum of 5×10^{-8} torr onto substrates held at 500°K were polycrystalline with a body centred cubic structure.

The exceptions were two very thin films, 50 Å and 90 Å thick, deposited as 80 Å and 120 Å. The X-ray diffraction pattern of the 50 Å thick film revealed that the film had a face centred cubic structure. The pattern obtained from the 90 Å film showed a mixture of face centred cubic and body centred cubic structure. All the films thicker than 160 Å which were examined had the expected body centred cubic structure of niobium. A reasonable assumption would be that the 45 Å thick film was also completely f c c and that the 85 Å thick film was a mixture of fcc and bcc.

These findings are in accordance with the published results and in particular with those of Conella[22] and Hutchinson[20,21] for similar deposition conditions. Although these workers reported that the thin initial layer of fcc niobium was formed only with a substrate temperature of 800°K to 1100°K.

The grain sizes determined by X-ray diffraction line broadening are shown in Table 13. Asada and Nosé[19] determined grain sizes of 100 Å to 200 Å for films ranging in thickness from 500 Å to 7500 Å. Rairden and Neugebauer[18] determined grain sizes from 100 Å to several thousand Angströms for films 2500 Å thick to 25,000 Å thick. Hauser and Theuerer[26] determined a grain size of 100 Å for a film quoted as 37,000 Å thick and a grain size of 30 Å for a film 120 Å thick. Some doubt must be expressed about the reported grain size of the 37,000 Å thick film, in the light of the present measurements and the results quoted by other authors.

5.3. Normal Electrical Resistivity

The effect of gaseous impurities on the resistivity of niobium films has been investigated by many workers, including Rairden and Neugebauer[18], Conella[22], Gerstenberg and Hall[23] and Asada and Nosé[19].

The results obtained from the present work as described in section
4.2.2. confirm these findings. To summarise, the conditions
necessary for the deposition of pure niobium films are, a vacuum
of the order of 5×10^{-8} torr or better, deposition rates of 100 Å
min^{-1} or greater, substrate temperatures of $500°$K or higher. In
extreme cases of poor vacuum, low deposition rates and low substrate
temperatures, films are formed that have negative temperature
coefficients of resistivity.

A comparison of the room temperature and residual resistivities
of the films prepared for this work with the films prepared by other
workers is shown in Tables 14 and 15. As can be seen, in general
the films prepared for this work have lower resistivities than
similar thickness films prepared elsewhere.

The purity of the films reported here, as determined by the
resistivity ratios show a considerable improvement over sputtered
and thermally evaporated films reported earlier. The resistivity
ratios of the present films varied from 1.16 for a film 45 Å thick
to 5.75 for a film 5440 Å thick. Frerichs and Kircher[25] measured
resistivity ratios of less than 1.25 to greater than 4.5 for film
thickness ranging from 700 Å to 3100 Å. Rairden and Neugebauer
obtained a resistivity ratio of 4.2 for a film 2500 Å thick which
is in agreement with the present work. However, they also reported
a similar ratio for a film 5000 Å thick and only a slight increase,
to 4.7 for a film 15,000 Å thick. Fowler determined that an 800 Å
niobium film had a residual resistivity of $26\mu\Omega$-cm and a resistivity
ratio of 2.3. These results are presented in Table 16.

Table 14. Comparison of room temperature resistivity with results of Gerstenberg and Hall.[23]

Film Thickness	Present Work	Gerstenberg and Hall	Film Thickness
5440	18.9	16.9	6000
1985	20.4	21.6	2050
390	24.6	25.4	420

$$\rho_{300} \ \mu\Omega\text{-cm}$$

Table 15. Comparison of residual resistivity with the results of Asada and Nose.[19]

Film Thickness	Present Work	Asada and Nose	Film Thickness
5440	5	7	7500
3495	3.3	13	4500
1235	5.6	54	1050
390	8.75	71	500
390	8.75	88	400

$$\rho_{10} \ \mu\Omega\text{-cm}$$

<u>Table 16</u>. Comparison of film thickness and resistivity ratio

Source	Thickness $\overset{\circ}{A}$	Resistivity Ratio	Present Work
Frerichs and Kircher[25]	700	1.25	2.8–3.8
	3100	4.5	4.9
Rairden and Neugebauer[18]	2500	4.2	4.3
	5000	4.2	5.7
	15000	4.7	—
Fowler[16]	800	2.3	2.8–3.8

5.4. Resistivity and Mean Free Path

The dependence of electron mean free path on film thickness was derived by Fuchs[4] in terms of the reduced resistivity ρ/ρ_∞ and reduced film thickness t/ℓ_∞. Limiting forms of ρ/ρ_∞ for very thick and very thin films were given by equations (1.11) and (1.12).

The assumption made in the equations was that the electron scattering at the film boundaries was entirely diffuse, with complete loss of electron drift velocity. In general, a fraction p of the electrons will suffer specular (elastic) scattering.

The Fuchs-Sondheimer[76] relation modified equations (1.11) and (1.12) to take account of this effect. The limiting forms of the equations now become

$$k \gg 1 \quad \frac{\rho}{\rho_\infty} = 1 + \frac{3}{8k}\ (1 - p) \qquad (5.2)$$

$$k \ll 1 \quad \frac{\rho}{\rho_\infty} = \frac{4\ (1 - p)}{3\ (1 + p)} \frac{1}{k(\text{Ln}\ 1/k + 0.4228)} \qquad (5.3)$$

In fact, as indicated by Chopra[77] equation (5.2) is valid to within 7% even for values of $k \simeq 0.1$. The deviation is even less for values of p greater than zero.

Due to the increase of the electron mean free path as the temperature decreases, it is possible to obtain films that will satisfy $k > 1$ at $300°K$ and $k < 1$ at $10°K$. For such films the combination of equations (5.3) and (5.2) will yield.

$$\frac{(RR)_F}{t} = \frac{3}{4\ \ell}\ (RR)_\infty \frac{1 + p}{1 - p}\ \text{Ln}\ \ell/t \qquad (5.4)$$

$(RR)_F$ is the resistivity ratio of the film

$(RR)_\infty$ is the resistivity of an infinitely thick film

p is the fraction of electrons suffering specular

scattering

Larson and Boiko[78] used equation (5.4) in the study of silver films and Isaeva[79] in the study of copper whiskers. From the plot of $(RR)_F/t$ versus Lnt it is possible to determine a value for the mean free path at $10^\circ K$, and providing the bulk resistivity is known, the fraction p can be calculated.

Figure 73 shows the plot of $(RR)_F/t$ versus Lnt obtained from the present work on niobium films. As can be seen, films of greater thickness than about 400 Å do not satisfy the conditions of equation (5.4). This is because although the films satisfy the condition k≫1 at $300^\circ K$ they do not satisfy the condition k≪1 at $10^\circ K$. The intercept of the straight line at $(RR)_F/t = 0$ gives the value of the bulk film mean free path at $10^\circ K$ as 520 Å.

The fraction p may be calculated from the slope of the graph of Figure 73 providing that the resistivity of an infinitely thick film is known. A value of p = 0.1 was determined from the slope by taking the resistivity of the 5440 Å thick film as being representative of an infinitely thick film. That this assumption was justified is shown in Figure 74. The graph is a plot of equation (5.2) obtained by substituting in it the values ℓ = 520 Å and p = 0.1, as can be seen the experimental points follow the curve fairly closely.

Stronberg and Swenson[79a] determined the mean free path of bulk niobium, of residual resistivity $7 \times 10^{-3} \mu\Omega$-cm, to be 25×10^4 Å. They assumed a Fermi surface area which was 20% of the free electron value for five electrons. By assuming that the product $\rho_\infty \ell_\infty$
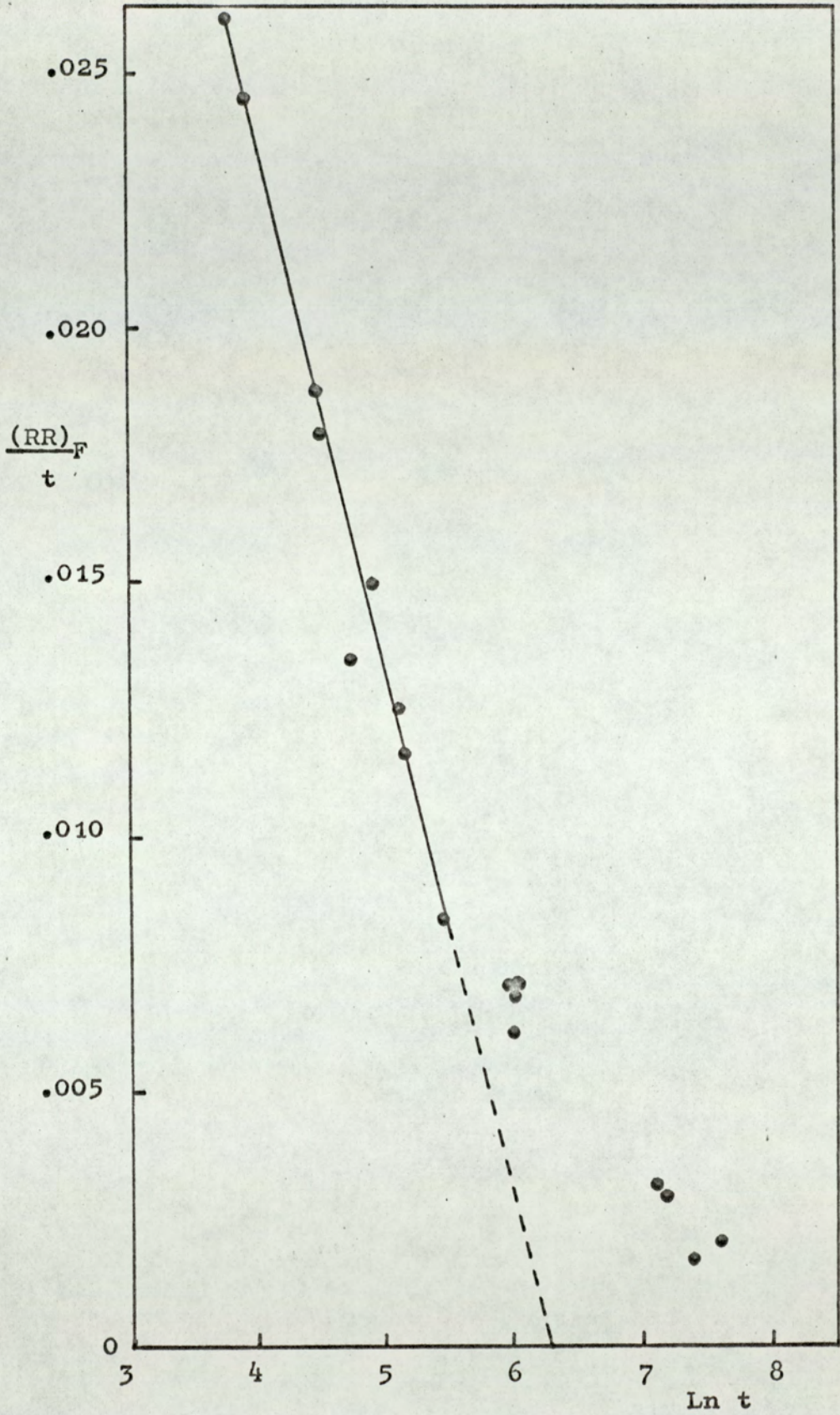
Figure 73. Straight line satisfies k >>1 at
300°K and k<< 1 at 10°K.
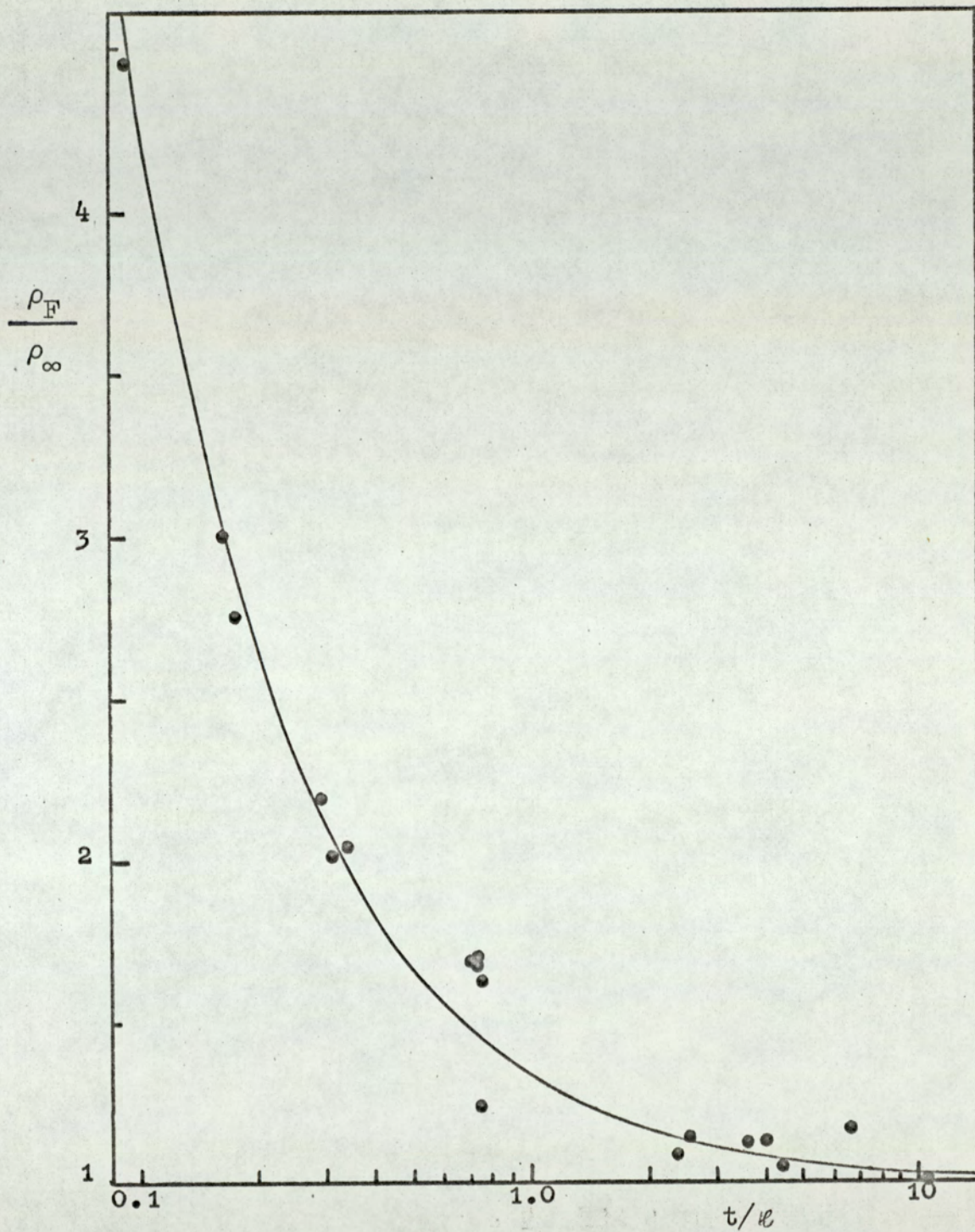
Figure 74. Experimental points compared with plot of equation (5.1), with ℓ =520 $\overset{o}{A}$ and p = 0.1

is constant, then the mean free path of bulk niobium can be estimated.
The residual resistivity of the 5440 Å thick film was $3.24\mu\Omega$ -cm,
hence the mean free path at 10°K was estimated to be 540 Å.

Golovaskin et al[80] determined the mean free path as 310 Å at
4.2°K, 190 Å at 78°K and 40 Å at 293°K from measurements of the
optical constants of electro-polished bulk niobium samples.

5.5. Film Thickness Determination

As described in sections 1.5 and 4.4 an electrical method for
the determination of film thickness was given by equation 4.1 as

$$d = \frac{d\rho_\infty}{dT} \cdot \left(\frac{dR}{dT}\right)^{-1} \cdot \frac{L}{W}$$

As can be seen from Table 11 the agreement between the electrical
determination of thickness and that obtained from the interferometer,
providing a correction is made for the oxide thickness, is very good.
Since equation 4.1 is derived from the thick film equation (1.11) it
might be expected not to be applicable to very thin films, less than
say 100 Å.

However, the value of dR/dT for each film was determined at
300°K, at this temperature the mean free path of niobium has been
determined by Golovaskin et al[80] as about 40 Å. Hence even the
thinnest films, 45 Å and 50 Å thick still satisfy the thick film
condition that the film thickness is greater than the mean free path.

When determining the thickness of films greater than about
1000 Å using equation 4.1, it was found that the calculated thickness
was very sensitive to small changes in $(dR/dT)^{-1}$. For example,
consider the case of the film that had been determined as 5440 Å

thick (less oxide) from the optical measurements. For this film, dR/dT had been determined as $0.005 \ \Omega \ °K^{-1}$, this gave $(dR/dT)^{-1}$ as 200 and the thickness as 5475 Å. An error of only 0.04 Ω in the determination of the resistance change over a 50°K interval resulted in a dR/dT of $0.0058 \ \Omega \ °K^{-1}$. This resulted in $(dR/dT)^{-1}$ having a value of 172 and a thickness determination of 4655 Å. For these thick films the interferometer method of determining film thickness with an error of $\pm$ 20 Å is far more reliable.

However, as the films tend towards thicknesses of 200 Å to 400 Å the thickness becomes far less sensitive to $(dR/dT)^{-1}$. Since the interferometer is still accurate to within about $\pm$ 10 Å, the two methods of thickness determination complement each other.

For films below about 150 Å the interferometer errors become unacceptable, about $\pm$ 50 Å for films less than 100 Å thick. In this region of film thickness the electrical method of determining thickness appears to be far more accurate.

5.6. Resistivity Ratio and Transition Temperature

The observed decreases in the values of the transition temperatures of niobium films has been widely reported for film thickness ranging from 300 Å to 25,000 Å. Rairden and Neugebauer[18], Gerstenberg and Hall[23], Frerichs and Kircher[25] and Asada and Nosé[19], have all attempted to correlate the observed decrease with the work of DeSorbo[33] on the effect of dissolved oxygen in bulk niobium. However, Asada and Nosé reported that a film 490 Å thick had a transition temperature 0.7°K lower than that predicted by DeSorbo with an estimated oxygen contamination of less than 0.7 atomic %. This was accounted for by the suggestion that grain size may also be a factor
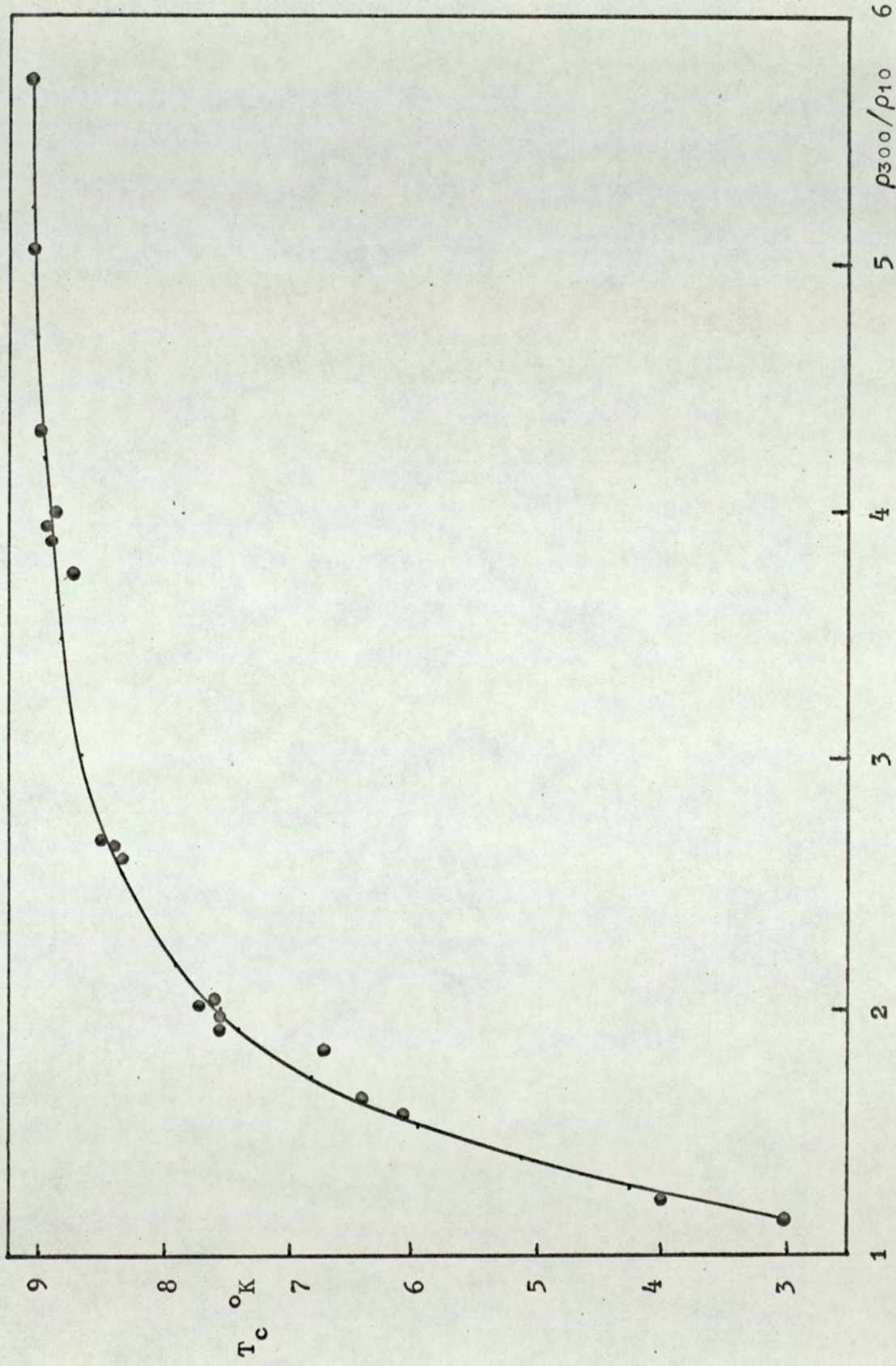
Figure 75a. Variation of transition temperature with resistivity ratio.
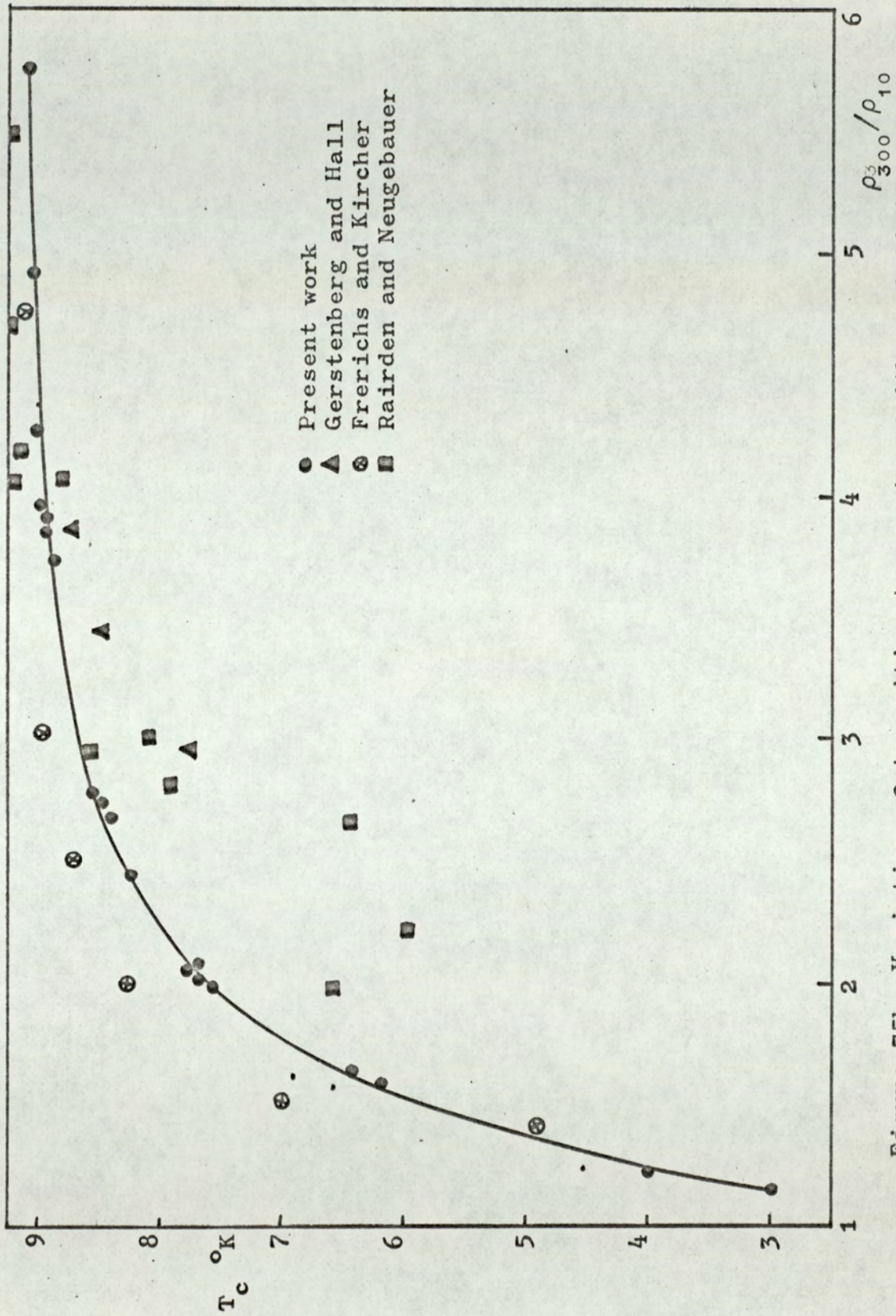
Figure 75b. Variation of transition temperature with resistivity ratio.

affecting the transition temperature.

The results obtained for the present work are compared with the results of Gerstenberg and Hall, Frerichs and Kircher, and Rairden and Neugebauer, in Figure 75. As can be seen some points lie well below the curve. This can be accounted for since the depression of the transition temperature could be a combination of the thickness of the film and oxygen contamination. Severe oxygen contamination would depress the T_c well below the curve. According to DeSorbo an oxygen concentration of 3.83 atomic % would produce a T_c of 5.84°K in bulk niobium.

The results of Rairden and Neugebauer, for thick films, lie above the curve for resistivity ratios greater than 4. This is possibly due to the difference in the measurement of the transition temperature for the bulk material. Rairden and Neugebauer determined the bulk value to be 9.46°K, while for the present work it was measured as 9.22°K.

The results of Frerichs and Kircher in general lie above the curve. Since the reported resistivity ratio of a 700 Å thick film was only 1.25, some caution should be taken in interpreting the results since a film of comparable thickness in the present work gave a resistivity ratio of about 3.0.

The discrepancy may be due to gaseous contamination or it may be due to the fact that the films of Frerichs and Kircher were prepared by sputtering rather than by thermal evaporation.

5.7. Influence of Phonon Spectrum on Transition Temperatures

It has been found that the superconducting transition temperature T_c, of some metals prepared in the form of very thin films or small

grains is appreciably higher than that of the bulk material. This enhancement was observed by Strongin et al[81] for aluminium and tin, Buckel and Hilsch[82] for tin, and Abeles et al[83, 84] for aluminium.

Leger and Klein[85] suggested that the enhancement was due to a modification of the phonon spectrum. From tunnelling characteristics in junctions of granular aluminium the appearance of a low frequency tail to the phonon spectrum was observed. The magnitude of the tail was found to be related to the increase of the transition temperature of the samples. When the average phonon frequency as determined from the experiments was substituted into McMillan's equation, the calculated transition temperature was found to be in good agreement with that observed experimentally.

Rothwarf[86] proposed that for small grains or films the existence of a low frequency phonon cut-off, leads to a reduction in the pair breaking rate and to enhanced transition temperatures. The effect of small grain size on the phonon spectrum was discussed by Theil[87], as an extension to the work of Marshall and Wilenzick[88]. It was suggested that quantization of the phonon wave vector within a small sample could be the cause. For a cubical grain of side length d_o, the smallest wave number permissible was given by

$$q_o = \frac{\Pi}{d_o} \qquad (5.5)$$

In terms of phonon frequency, a cubical grain of side length d_o would cut off all phonons having a frequency ω_c given by

$$\omega_c = c \frac{\Pi}{d_o} \qquad (5.6)$$

where c is the appropriate velocity of sound in the material.

Theil assumed a continuous spherical particle with free bound-
aries, the model assumed by Debye. There are two sorts of small
amplitude volume vibrations possible in a free electron sphere, one
third of the modes belong to longitudinal vibrations and two thirds
of the modes to the transverse vibrations[90]. For simplicity Theil
assumed an average phonon velocity.

Using equation (5.6) to determine the cut-off frequency,
Rothwarf obtained a relationship between transition temperature and
grain size that was in good agreement with the experimental results
of Abeles et al[84] and Strongin et al[47] for aluminium and tin.

5.8. Application of McMillan's Equation to Niobium Films

It was assumed that for the present work involving niobium films
that the McMillan equation as given by equation (2.5) was applicable.
It was further assumed that the phonon spectrum was modified by the
existence of a low frequency phonon cut-off due to the quantization
of the phonon wave vector.

Following McMillan, the coulomb coupling μ^*, was considered
constant and the transition temperature was considered to depend
upon the electron-phonon coupling factor λ, given by equation (2.2)
as

$$\lambda = \int_{o}^{\omega_o} \alpha^2(\omega) \; F(\omega) \; \frac{d\omega}{\omega}$$

The dependence of the transition temperature upon the electron-
phonon coupling is illustrated by the plot of equation (2.5) in
Figure 76. The value of the coulomb coupling μ^* was taken as 0.13
and the characteristic phonon frequency was taken to be the Debye

temperature $\Theta = 277^{\circ}K$. As can be seen, to achieve the decrease of transition temperature observed experimentally, the electron-phonon coupling factor λ must also be reduced.

Values of the electron-phonon coupling factor may be calculated from equation (2.2) provided that the weighting function $\alpha^2(\omega) F(\omega)$ can be determined. McMillan assumed that the function $\alpha^2(\omega)$ was constant over the phonon spectrum and $F(\omega)$ was taken to be the phonon density of states. The neutron scattering experiments of Nakagawa and Woods[91] provided the phonon density of states of bulk niobium.

The experimental results of the phonon distribution are shown in Figure 77, and the subsequent plot of $F(\omega)/\omega$ versus ω that was determined from it is shown in Figure 78. Hence the electron-phonon coupling λ, can be determined from Figure 78 as:

$$\lambda = 2\alpha^2 \int_0^{\omega_o} \frac{F(\omega)}{\omega} . \, d\omega \qquad (5.7)$$

To reduce the magnitude of λ the range of phonon frequencies over which the integration was performed was reduced. By applying Theil's low frequency cut off to the phonon spectrum, the electron-phonon coupling can be determined with progressively higher phonon frequencies cut-off as:

$$\lambda = 2\alpha^2 \int_{\omega_c}^{\omega_o} \frac{F(\omega)}{\omega} \, d\omega \qquad (5.8)$$

The variation of the electron-phonon coupling with respect to the critical frequency is shown in Figure 79. The dependence of the transition temperature upon the phonon cut-off frequency, Figure 80,
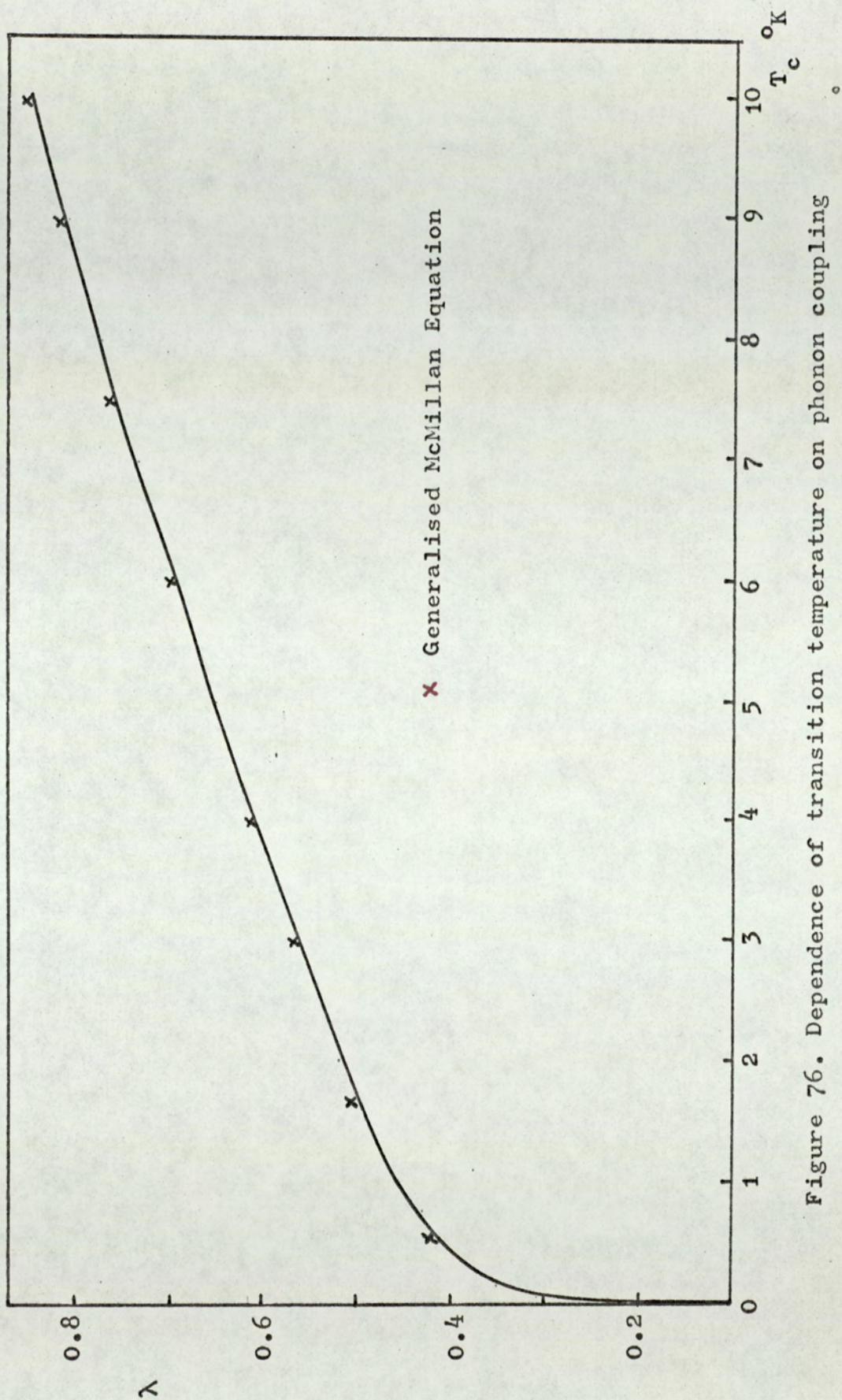
Figure 76. Dependence of transition temperature on phonon coupling
according to the McMillan Equation.
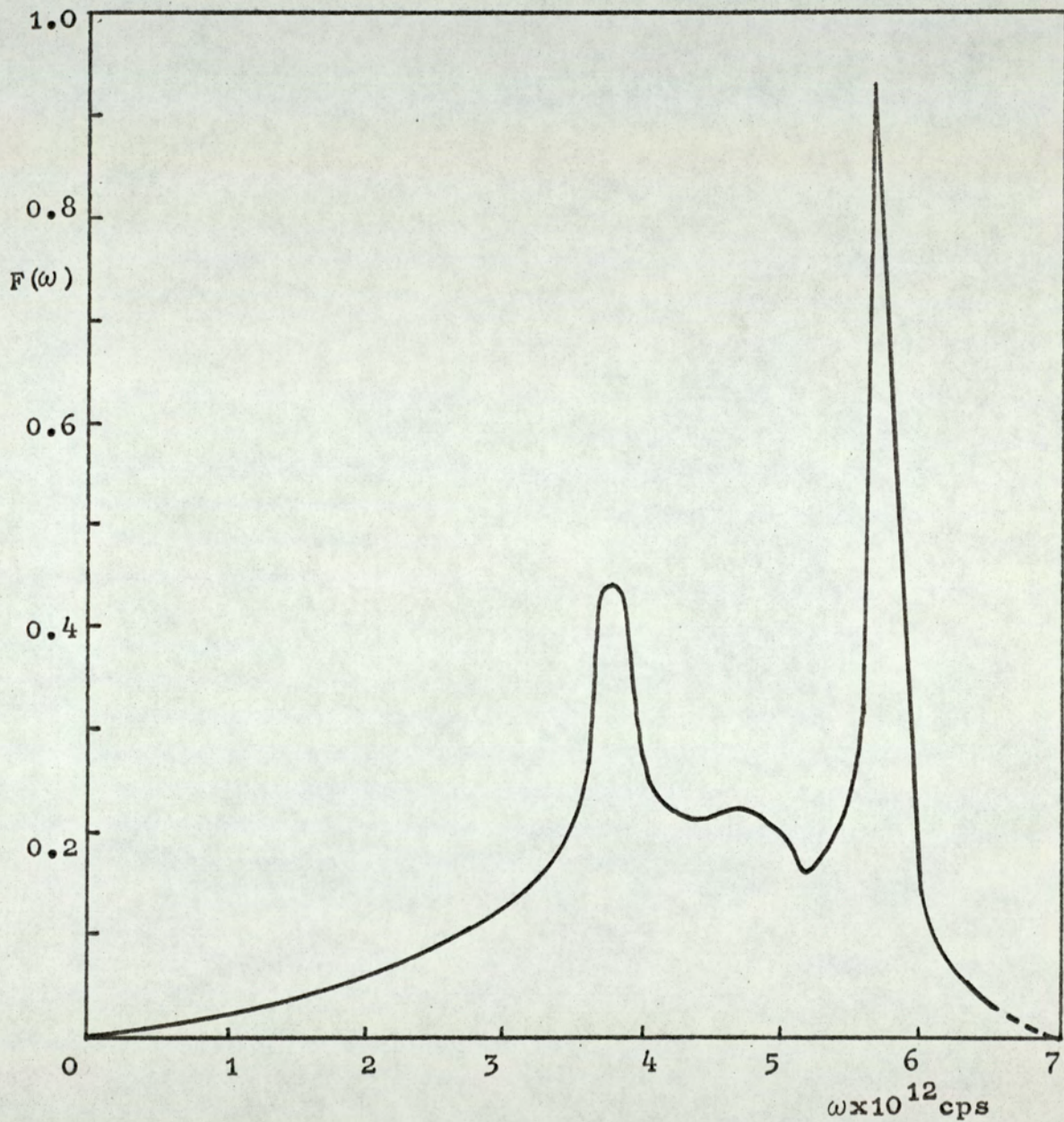
Figure 77, Phonon distribution according to
Nakagawa and Woods.[91]
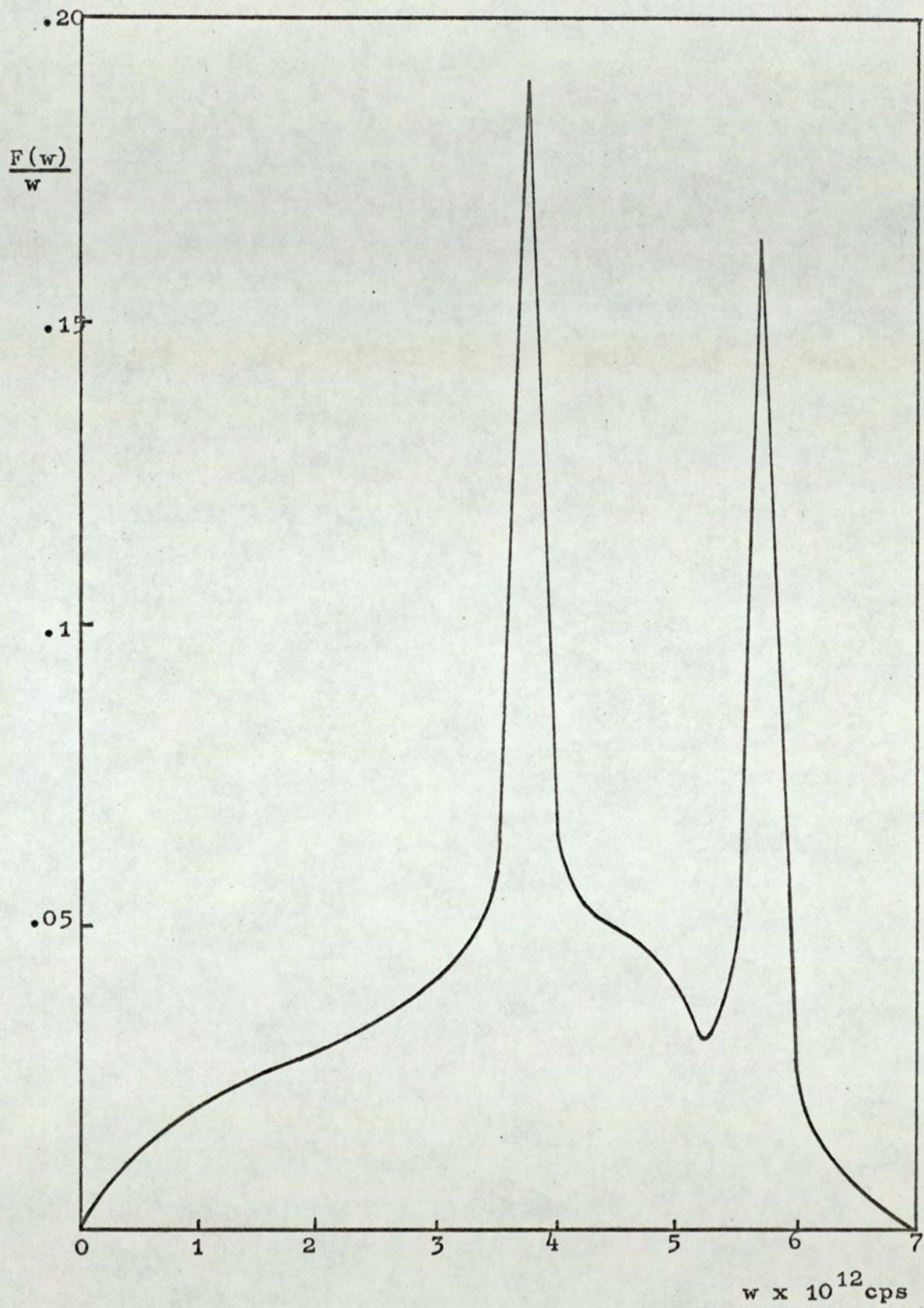
Figure 78. Distribution function derived from the
results of Nakagawa and Woods.[91]
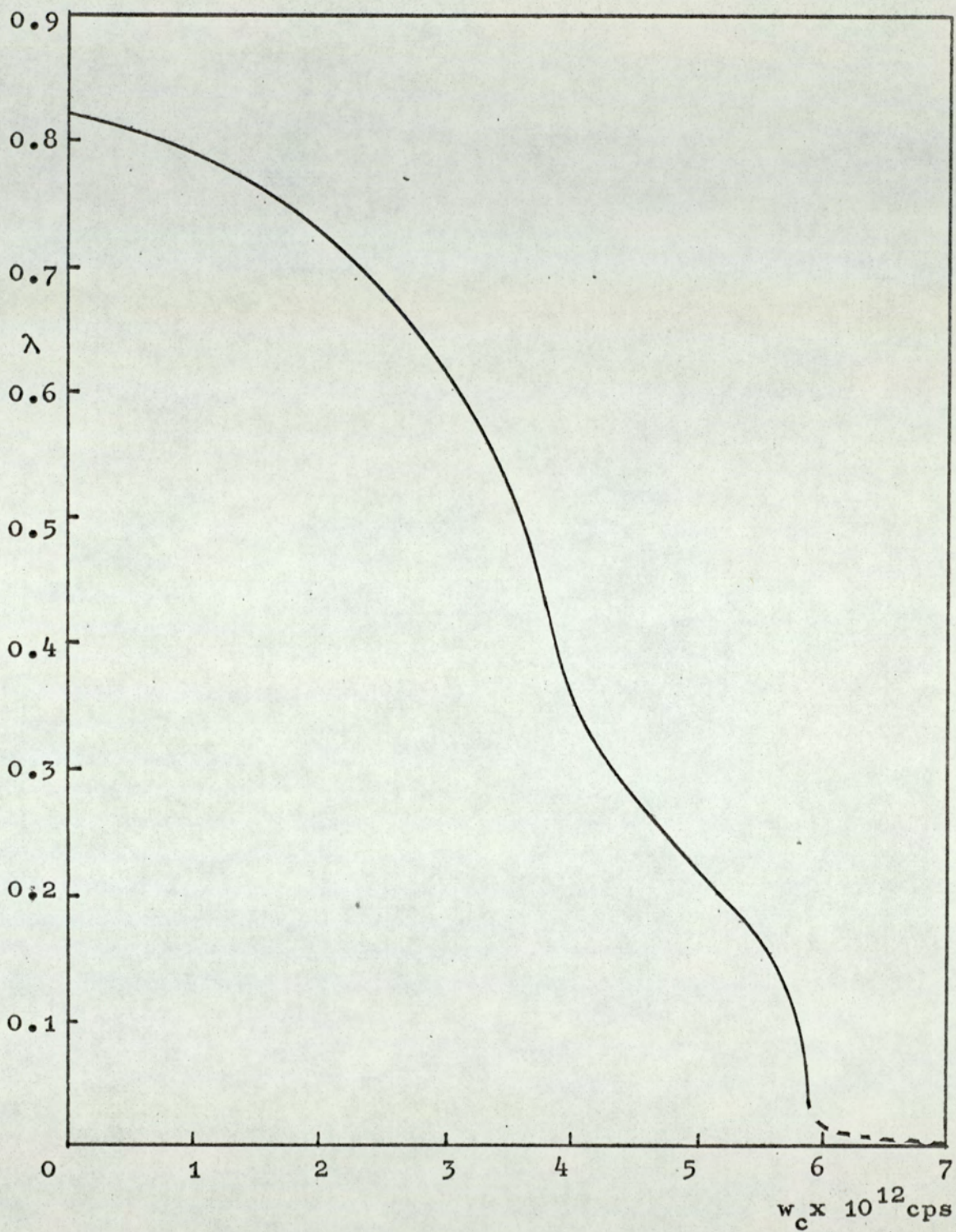
Figure 79. Dependence of phonon coupling on

cut-off frequency.
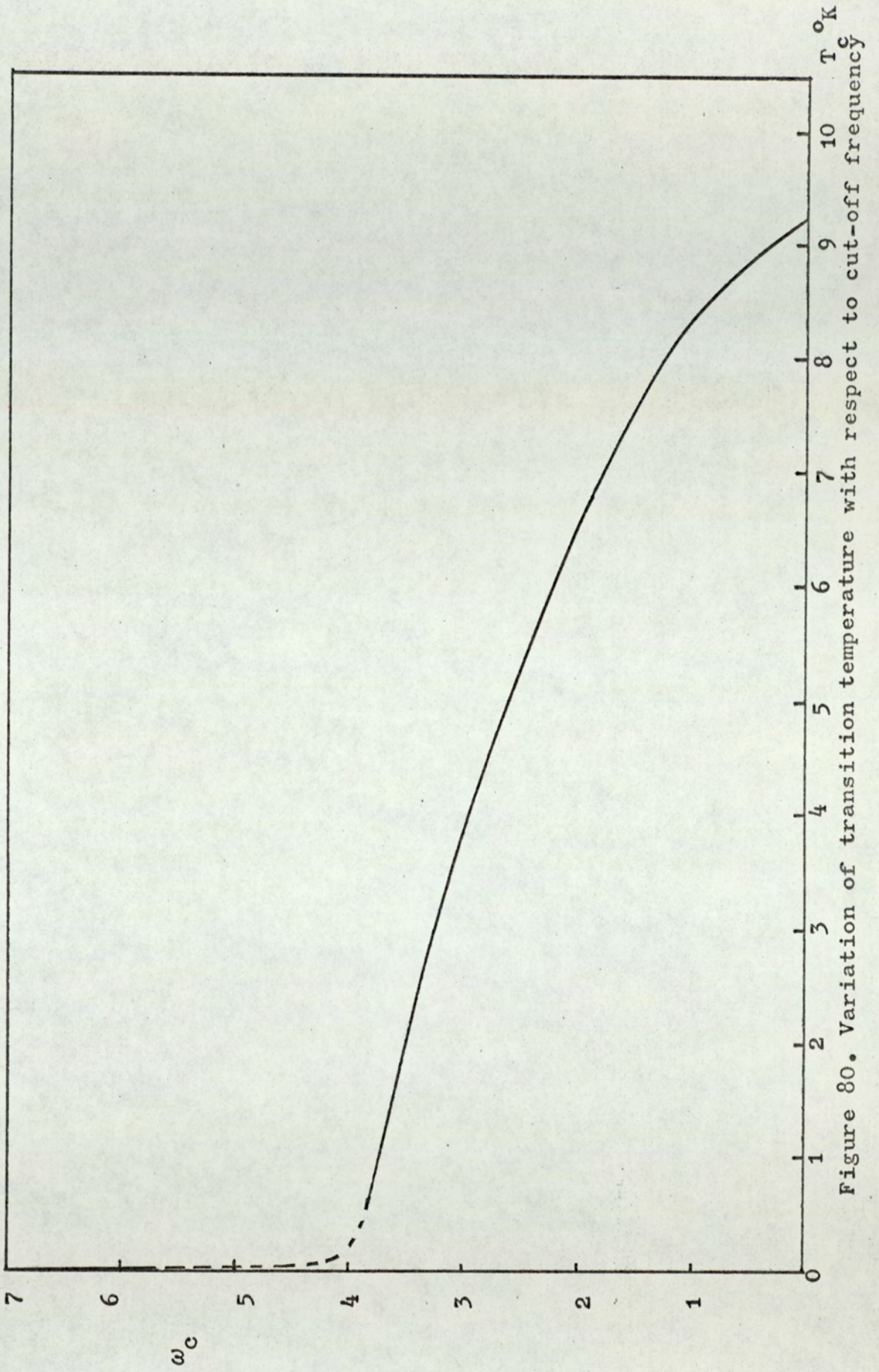
Figure 80. Variation of transition temperature with respect to cut-off frequency
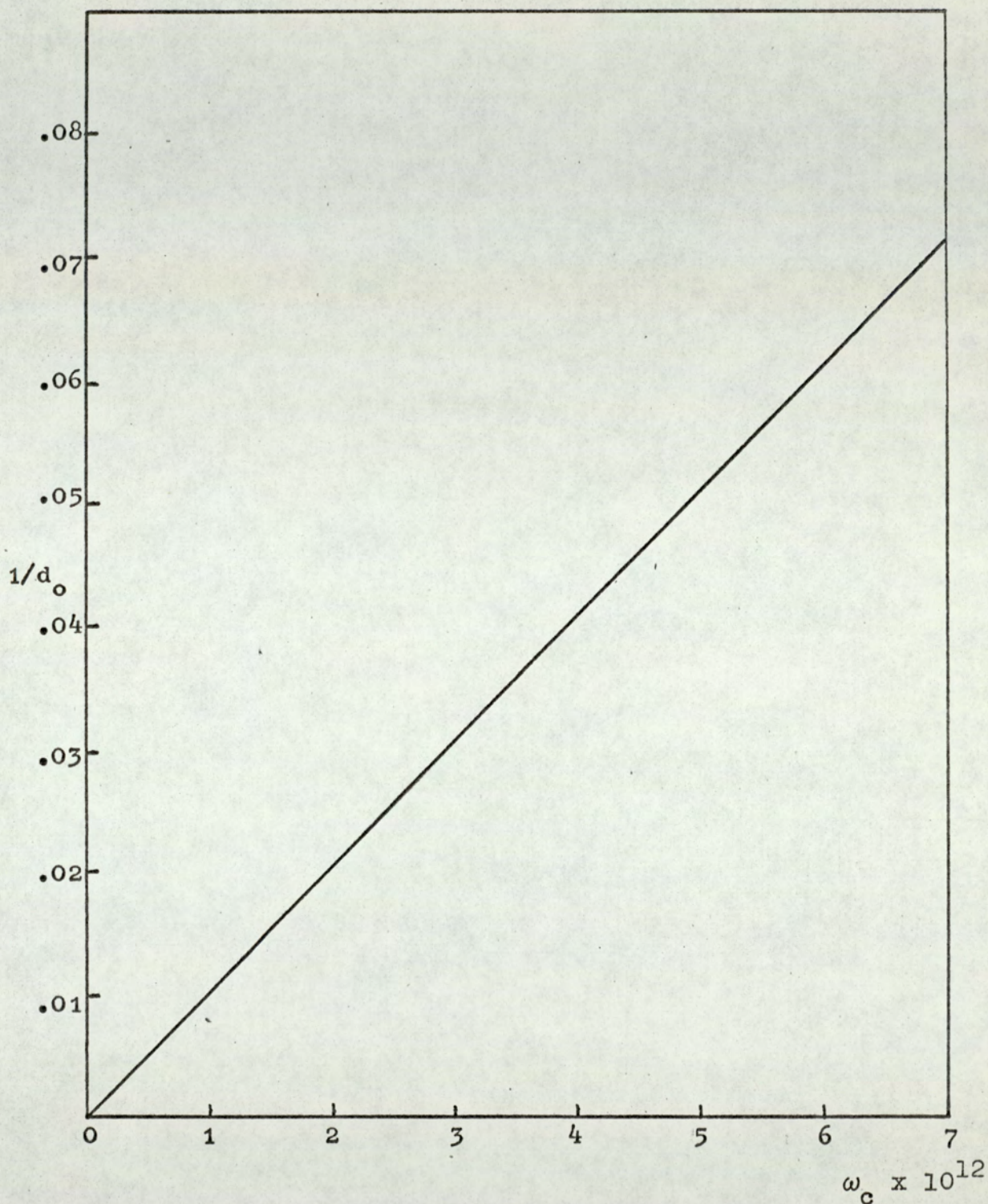
Figure 81. Dependence of cut-off frequency on

grain size as given by equation (5.5)
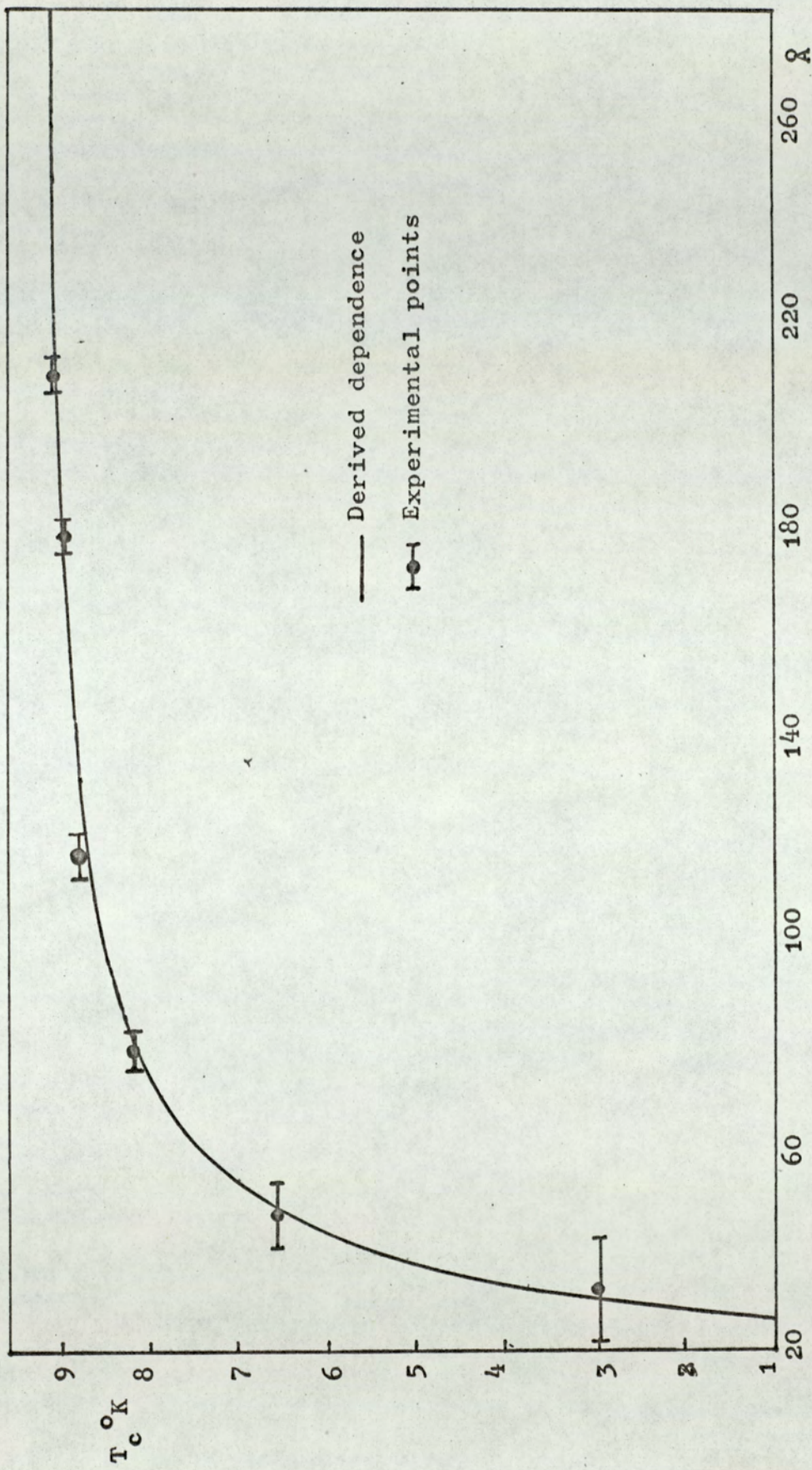
Figure 82. Derived dependence of transition temperature on grain size.

was obtained by combining McMillan's equation, as shown in Figure 76 with the variation of λ with respect to the critical frequency, as shown in Figure 79.

Bolef[92] determined the longitudinal velocity of sound in niobium as 5053 m sec^{-1} (for particle motion in the 110 direction) and the transverse velocities of sound as 1830 m sec^{-1} (particle motion in 100 direction) and 2556 m sec^{-1} (particle motion in $\overline{110}$ direction). The average value of c, 3146 m sec^{-1}, was substituted in equation (5.6) to yield the graph shown in Figure 81, the dependence of the cut-off frequency on grain size. A combination of equation (5.6), plotted in Figure 81, and the variation of transition temperature with respect to the cut-off frequency, Figure 80, yields the derived dependence of transition temperature on grain size, Figure 82. As can be seen, within experimental error, the experimental values of grain size measured by the X-ray line broadening technique described in section 4.6, are in good agreement with the derived curve.

5.9. Critical Currents in Superconducting Films

Two experimental difficulties exist in the measurement of the critical value of current density necessary to suppress super-conductivity in thin films. Flat rectangular, unshielded film geometries have a non-uniform distribution of current, the details of the current distribution need to be known to determine the critical current density. The warming of the film by Joule heating if small normal regions are present, for example at electrical contacts, can be an acute problem since current densities approach 10^6 A cm^{-2}.

The problem of Joule heating may be overcome by ensuring good

thermal contact between the film and the surrounding liquid helium, and by using current pulses rather than a steady current.

In this way Mydosh and Meissner[93] and Mercereau and Hunt[94] have observed a $(1 - T_R^2)^{3/2}$ dependence of critical current in tin films. London and Clarke observed a similar dependence in a 1050 Å niobium film.

Bardeen[58] had predicted that the current density should follow a $(1 - T_R^2)^{3/2}$ dependence, this was confirmed by Glover and Coffey for tin films, who assumed a current distribution in the film as given by Bowers[56]. From the experiments Glover and Coffey deduced that the measured critical current I_c could be determined as:

$$I_c \ (T_R) \ \alpha \ (1 - T_R^2)/(1 + T_R^2)^{\frac{1}{2}} \qquad (5.9)$$

The results from the present work, as shown in Figure 63, were replotted as critical current I_c versus $(1 - T_R^2)/(1 + T_R^2)^{\frac{1}{2}}$, Figure 85. As can be seen, the curves obtained may be divided into two sections. At low values of $(1 - T_R^2)/(1 + T_R^2)^{\frac{1}{2}}$ the slope of the curves varies from 0.8 for the 50 Å thick film to almost 1.0 for the 5440 Å thick film. As the temperature decreases and the values of the critical currents increase, the slope of the curves diminishes. The slopes vary from 0.32 for the 50 Å thick film to 0.5 for the 5440 Å thick film. The decrease in the value of the slope could be caused by Joule heating of the film at high critical current densities. (due to the experimental arrangement being required for other measurements apart from current densities) To check on this possibility two films, 1235 Å thick and 385 Å thick, were immersed directly in liquid helium and the critical current at 4.2°K was determined. A
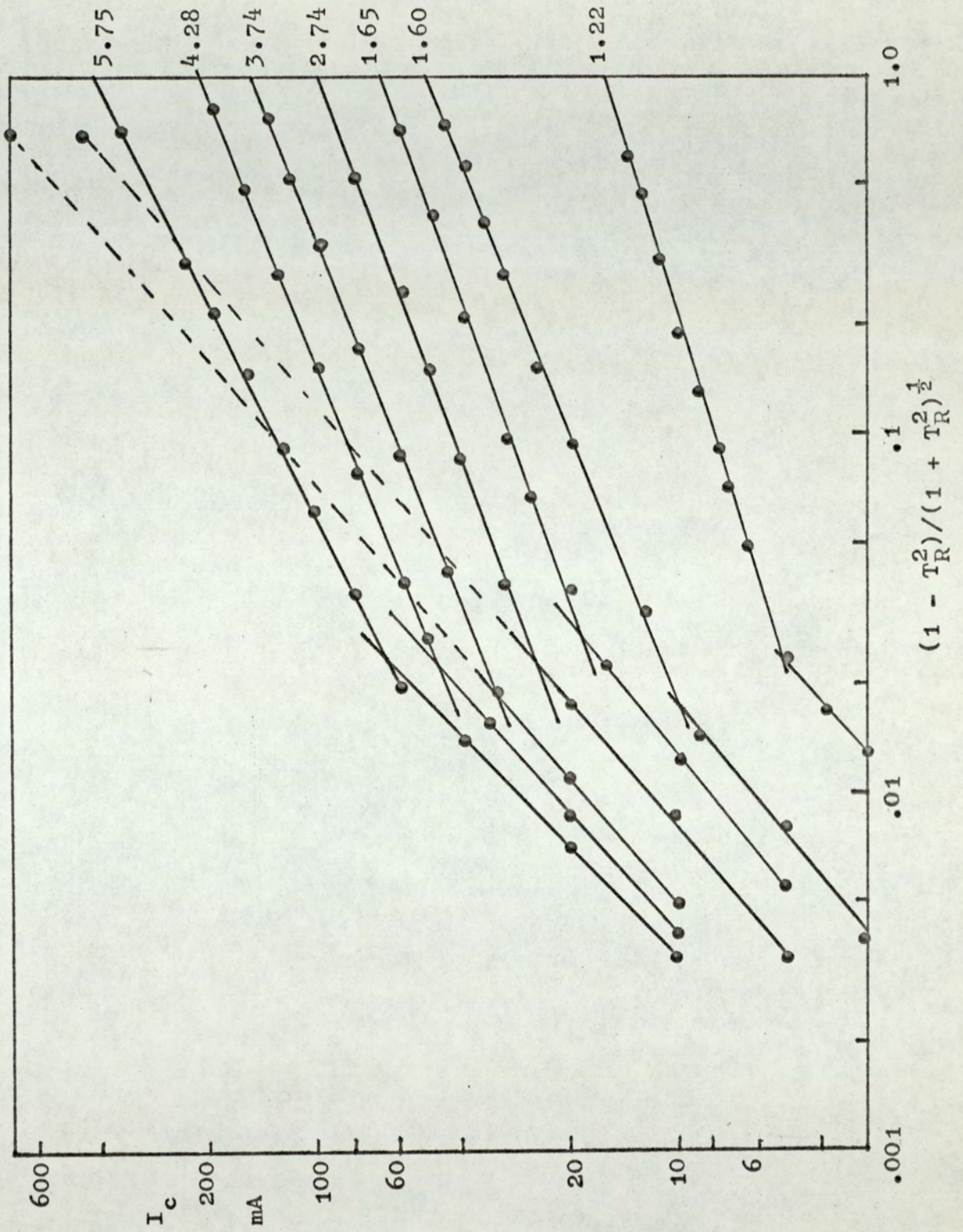
Figure 83. Critical current vs $(1 - T_R^2)/(1 + T_R^2)^{\frac{1}{2}}$
(after Glover and Coffey)[57]

Table 17. Critical currents and critical current densities at $0°K$. (assuming uniform distribution)

Thickness of film $\mathring{A}$	Critical current $I_c(0)$ mA	Critical current Density $J_c(0)$ A cm^{-2}
50	16.5	1.65×10^5
85	50	2.94×10^5
90	68	3.78×10^5
385	100	1.30×10^5
1235	155	6.3×10^4
2505	220	4.40×10^4
5440	430	3.95×10^4

Table 18. Comparison of critical current densities at $4.2°K$.

Source	Thickness $\mathring{A}$	$J_c(4.2)$ A cm^{-2}
Edgecumbe et al.[28] Sputtered.	1500	4×10^6
	500	1×10^6
Frerichs and Kircher.[25] Sputtered.	700 to 3100	1×10^4
Fowler.[16] Thermal Evaporation	800	1×10^6
Neugebauer and Ekvall.[17] Thermal Evaporation.	3000	3×10^6
	4500	1.4×10^6
Present work. Thermal Evaporation.	385	6.0×10^5
	1235	2.9×10^5

considerable increase of the critical current was observed. The
critical current for the 385 $\overset{\circ}{A}$ thick film was increased from 87 mA
to 460 mA, and for the 1235 $\overset{\circ}{A}$ thick film from 135 mA to 700 mA.
Plotting the increased currents on Figure 85 revealed that the initial
steeper slopes of the graphs could be extrapolated to pass through the
increased current values.

Assuming that similar increases will result for all films
immersed directly in liquid helium, then the 5440 $\overset{\circ}{A}$ thick film, with
an initial slope of almost unity will extrapolate to give a value of
critical current at $0^{\circ}K$ of 2.7 A. Substitution of this value of
$I_c(0)$ into equation (2.34) and assuming a value of $\lambda_E(0)$ of 1000 $\overset{\circ}{A}$[79],
results in a current density of the order of 4×10^7 A cm^{-2}.

Extrapolating the actual results obtained from the present work
to a temperature of $0^{\circ}K$ results in the critical currents listed in
Table 17. The corresponding values of critical current density are
also shown, assuming a uniform current density. It must be pointed
out that these values of current density are merely intended as a
guide to the order of magnitude of current density that is supported
by a niobium film deposited on a glass slide, where heat transfer is
limited by the thermal conductivity of the glass.

A comparison of critical current densities, at $4.2^{\circ}K$, obtained
from the present work and the results of previous workers is shown
in Table 18.

CHAPTER 6

Conclusions

6.1. General Remarks

The problems of the high temperatures involved for the thermal
evaporation of niobium and the susceptibility of niobium films to
gaseous contamination during deposition have been described in section
1.7.

An apparatus and a technique have been described for the
production of pure niobium films. The vacuum system should be
capable of maintaining a pressure of about 5×10^{-8} torr during the
evaporation. The deposition rate should be of the order of 250 $\overset{o}{A}$ min^{-1}
and the substrate maintained at a temperature of about 500°K. As
described in section 3.4.3, an extensive outgassing of the niobium
sample and evaporation prior to the actual deposition of a film is
required. This is to take advantage of the strong gettering action
of freshly deposited niobium for oxygen or oxygen-containing gases,
to reduce the partial pressure of these gases in the vacuum system.

The apparatus was designed so that the films could be deposited
and the electrical properties over the temperature range 2°K to 300°K
examined without exposing the films to an atmospheric environment.

A few films were examined in this way, unfortunately a leak then
developed in the cryostat close to the substrate mounting. This
resulted in gaseous contamination of the films even with high deposition
rates and high substrate temperatures.

Attempts to repair the leak were unsuccessful and the alternative
approach of depositing the films in one system and examining the
electrical properties in a separate cryostat had to be employed.

The transfer of the films from the deposition chamber to the
cryostat resulted in the growth of an oxide layer on the films. An
estimate of the oxide thickness could be made by comparing the
thickness of the film as determined by the interferometer with the
thickness determined electrically, as described in section 1.5. An
alternative approach was the actual measurement of oxide thickness by
means of an ellipsometrical technique described in section 2.5.

6.2. Normal Electrical Resistivity of Niobium Films

Films deposited at low deposition rates, 15 $\overset{\circ}{A}$ m^{-1} and at
pressures of the order of 1 x 10^{-6} torr, were found to have negative
temperature coefficients of resistivity, and resistivity ratios of
less than unity.

The resistivities and resistivity ratios of a series of pure
films deposited under similar conditions, of pressure, deposition rate
and substrate temperature, were found to vary with film thickness.

The resistivity increased from the bulk value of about 15 $\mu\Omega$-cm
to a value of 88 $\mu\Omega$-cm for a film 45 $\overset{\circ}{A}$ thick. The resistivity ratio
decreased from a value of 5.75 for a film 5440 $\overset{\circ}{A}$ thick to 1.16 for a
film 45 $\overset{\circ}{A}$ thick. A comparison of films of similar thickness showed
that the resistivity ratios of films prepared in the present work
were as good as or better than the resistivity ratios reported by
previous workers. Since the resistivity ratio may be taken as a
measure of the purity of the film, this would indicate that the present
method of preparation is as good as any previously reported for the
production of pure niobium films.

From the values of residual resistivity it was estimated that
in thick niobium films prepared in the present work, the electron mean

free path was 520 $\overset{o}{A}$ and that the fraction of electron suffering specular reflection from the film boundaries was 0.1.

6.3. Transition Temperature

The superconducting transition temperatures of the thick niobium films prepared were found to be close to the bulk value, measured as 9.22^{o}K. As the film thickness and the resistivity ratio decreased, then so did the transition temperature, a minimum value of 3.0^{o}K was observed for a film 45 $\overset{o}{A}$ thick.

The decrease in the transition temperature was attributed to the observed decrease in grain size as the film thickness decreased. By assuming that the decrease in grain size was responsible for the cutting off of some low frequency phonons, a modification to the phonon spectrum in these films was suggested. By applying the McMillan equation, with the suggested modifications to the phonon spectrum, to the films, values are derived for transition temperatures and grain sizes which are in good agreement with the experimental results obtained from the present work.

6.4. Critical Current Densities

Critical currents for films immersed directly in liquid helium were observed to be about a factor of five greater than the currents measured at 4.2^{o}K when the films were mounted in the cryostat assembly described in section 3.2.4. This was most probably due to Joule heating of the film either by the formation of normal regions in the film or resistive current contacts to the film. For thick films at low values of critical current when the film temperature was close to the transition temperature, the critical current was proportional to $(1 - T_R^2)/(1 + T_R^2)^{\frac{1}{2}}$, as predicted by Glover and Coffey. By extrapolation, the critical currents for some thick films (5440 $\overset{o}{A}$,

2505$\overset{\circ}{A}$ and 1230 $\overset{\circ}{A}$) were estimated at $0^{\circ}K$ and the corresponding critical current densities, according to the theory of Glover and Coffey, determined to give an average value of about 3.5×10^7 A cm^{-2}.

6.5. Determination of Oxide Thickness and Film Thickness

From observations using the ellipsometer the oxide thickness on these niobium films was determined to be 35 $\overset{\circ}{A}$ after five days exposure to the atmosphere.

In the first hour of exposure about 10 $\overset{\circ}{A}$ of oxide had formed on the film. After five days the rate of oxide formation had dropped to about 0.04 $\overset{\circ}{A}$ hour^{-1} ($\sim$1 $\overset{\circ}{A}$ per day). The oxide thickness on one film was determined as 45 $\overset{\circ}{A}$ nine weeks after the film was first exposed to the atmosphere.

The actual film thickness was determined by measuring the thickness on the interferometer and then subtracting the oxide thickness. When compared with the thickness determined electrically the agreement was found to be good even for very thin films.

The interferometer technique is very accurate, $\pm$ 20 $\overset{\circ}{A}$ or less, for films thicker than about 200 $\overset{\circ}{A}$; however, for very thin films the errors can be as large as $\pm$ 50%

The electrical determination of film thickness was accurate for thin films but was found to be very susceptible to small errors in the determination of $(dR/dT)^{-1}$ for thick films. However, providing some care was taken in the determination of $(dR/dT)^{-1}$ values, good agreement with the thickness measurement by interferometer was obtained.

6.6. Suggestions for Future Work

It has been assumed that the cutting off of the low frequency phonons in thin films of niobium would account for the observed decrease in the transition temperature. To test the validity of this assumption

a method is required to determine the phonon distribution in thin films of niobium. One method could be that used by Leger and Klein[85] for aluminium films.

Klein and Leger[95] have shown that the second derivative of the tunnelling current, d^2I/dV^2, through an aluminium-aluminium junction in the normal state reflects the phonon density spectrum. Using this method the phonon distribution functions were determined for granular aluminium films which showed enhanced transition temperatures. The appearance of a low frequency phonon tail in the phonon spectrum was observed. Similarly for niobium films it should be possible to observe if the low frequency phonons are cut off from the phonon spectrum.

An alternative method would be that of directly measuring λ, the electron-phonon interaction parameter. It has been suggested by Hopfield[96] that this could be accomplished by measurement of the infra-red (2 to 2 0μ) optical properties of the metal.

In transition metals the first band to band transitions are generally visible near 2μ, and at frequencies below this one expects a dielectric function

$$\epsilon = A + \frac{4\Pi B}{-\omega^2 + i\omega/\tau} \tag{6.1}$$

where A, B and τ are constants.

For a material in which this analysis describes the experimental data the parameter λ is given by

$$\lambda = \frac{\hbar}{2\Pi\tau}\left(\frac{1}{kT}\right) \tag{6.2}$$

where k is Boltzmann's constant and T the temperature at which

the experiment was carried out.

Equation (6.2) is correct only if the τ observed in optical experiments is due to phonon scattering. If in the optical experiments the lifetime is determined by impurity scattering or surface scattering the resistivity ρ and B can be used to determine λ from the relation.

$$\lambda = B \frac{\hbar}{2\Pi k} \cdot \frac{d\rho}{dT} \tag{6.3}$$

This expression is for the high temperature limit where $T > \theta_D$.

This technique requires only clean surfaces for examination and in this respect it is ideally suited to the study of thin films, particularly if the films can be examined before removal from the deposition chamber. The present ellipsometer could be modified for wavelengths of 1 to 2μ fairly easily without any major modifications to the system.

REFERENCES

1. P. Drude: Ann. Physic. $\underline{1}$, 556, (1900)

2. H. A. Lorentz: Amsterdam Proc. (1904 - 1905)

3. A. Sommerfield: Z. Physic. $\underline{47}$, 1, (1928)

4. K. Fuchs: Proc. Cambridge Phil. Soc. $\underline{34}$, 100, (1938)

5. H. Mayer: Structure and Properties of Thin Films,

    C. A. Neugebauer et al, Eds. New York, Wiley.

    Page 225 (1959)

6. H. K. Onnes: Commun. Phys. Lab. Univ. Leiden.

    No. 119b, 120b, 122b, 124c, (1911)

7. C. J. Gorter and H. B. G. Casimir: Physica. $\underline{1}$, 305,

    (1934)

8. F. London and H. London: Physica. $\underline{2}$, 341, (1935)

9. V. L. Ginzburg and L. V. Landeau: J.E.P.T. $\underline{20}$, 1064,

    (1950)

10. A. A. Abrikosov: J.E.P.T. $\underline{5}$, 1174, (1957)

11. A. B. Pippard: Proc. Roy. Soc. $\underline{A216}$, 547, (1953)

12. J. Bardeen, L. N. Cooper and J. R. Schrieffer:

    Phys. Rev. $\underline{108}$, 1175, (1957)

13. L. P. Gorkov: J.E.P.T. $\underline{36}$, 1918, (1959)

14. D. Saint-James and P. G. de Gennes: Phys. Letters.

    $\underline{7}$, 306, (1963)

15. H. London and G. R. Clarke: Rev. Mod. Phys. $\underline{36}$, 320,

    (1964)

16. P. Fowler: J. Appl. Phys. $\underline{34}$, 3538, (1963)

17.

17. C. A. Neugebauer and R. A. Ekvall: J. Appl. Phys. $\underline{35}$, 547, (1964)

18. C. A. Neugebauer and J. R. Rairden: Proc. IEEE, 1234 (1964)

19. Y. Asada and H. Nose: J. Phys. Soc. Japan. $\underline{26}$, 347, (1969)

20. T. E. Hutchinson: J. Appl. Phys. $\underline{36}$, 270, (1965)

21. T. E. Hutchinson and K. H. Olsen: J. Appl. Phys. $\underline{38}$, 4933, (1967)

22. M. Conella: Ph. D. Thesis 1969, Tulane Univ. Louisiana.

23. D. Gerstenberg and P. M. Hall: J. Electrochem. Soc. $\underline{111}$, 936, (1964)

24. R. Frerichs: J. Appl. Phys. $\underline{33}$, 1898, (1962)

25. R. Freeichs and C. J. Kircher: J. Appl. Phys. $\underline{34}$, 3541, (1963)

26. J. J. Hauser and H. C. Theuerer: J. Appl. Phys. $\underline{35}$, 554, (1964)

27. H. C. Theuerer and J. J. Hauser: Phys. Rev. $\underline{134}$, A198, (1964)

28. J. Edgecumbe, L. G. Rosner and D. E. Anderson: J. Appl. Phys. $\underline{35}$, 2198, (1964)

29. I. J. Sosniak and G. W. Hull: J. Appl. Phys. $\underline{38}$, 4390, (1967)

30. I. J. Sosniak: J. Appl. Phys. $\underline{39}$, 4157, (1968)

31. S. Ogawa, K. Takiguchi and T. Hasegawa: J. Vac. Sci. & Tech. $\underline{8}$, 192, (1971)

32. G. Brauer, H. Muller and G. Kuhner:

    J. Less - Common Metals, $\underline{4}$, 533, (1962)

33. W. DeSorbo: Phys. Rev. $\underline{132}$, 107, (1963)

34. N. Norman: Acta Cryst. $\underline{13}$, 1013, (1960)

35. N. Norman: J. Less - Common Metals. $\underline{4}$, 52, (1962)

36. N. Norman, P. Kofstad and O. J. Krudtaa:

    J. Less - Common Metals. $\underline{4}$, 124, (1962)

37. B. T. Matthias. 'Progress in Low Temperature Physics'

    C. J. Gorter Ed. Page 138, N. Y. (1957)

38. J. R. Schrieffer: 'Theory of Superconductivity'

    Benjamin, New York, (1964)

39. G. M. Eliashberg: J.E.P.T. $\underline{11}$, 696, (1960)

40. V. Ambegaokar and L. Tewordt: Phys. Rev. $\underline{134}$, A805,

    (1964)

41. D. J. Scalapino, Y. Wada and J. C. Swihart:

    Phys. Rev. Letters. $\underline{14}$, 102, (1965)

42. J. P. Carbotte and R. C. Dynes: Phys. Rev. $\underline{187}$, 525,

    (1969)

43. P. B. Allen and M. L. Cohen: Phys. Rev. $\underline{172}$, 476,

    (1968)

44. W. L. McMillan: Phys. Rev. $\underline{167}$, 331, (1968)

45. P. Morel and P. W. Anderson: Phys. Rev. $\underline{125}$, 1263,

    (1962)

46. T. T. Chen, J. T. Chen, J. R. Leslie and H. J. T. Smith:

    Phys. Rev. Letters. $\underline{22}$, 526, (1969)

47. M. Strongin, O. F. Kammerer, J. E. Crow, R. D. Parks,

   D. H. Douglas and M. A. Jenson: Phys. Rev. Letters.

    $\underline{21}$, 1320, (1968)

48. J. W. Garland, K. H. Benneman and F. M. Mueller:

    Phys. Rev. Letters. 21, 1315, (1968)

49. J. W. Garland and P. B. Allen: International

    Conference on the Science of Superconductivity,

    Stanford, (1969)

50. L. A. Feigin and A. I. Shal'nikov: Doklady, 1, 377,

    (1956)

51. N. I. Ginzburg and A. I. Shal'nikov: J.E.T.P. 8,

    243, (1962)

52. V. L. Newhouse, J. W. Bremer and H. H. Edwards:

    Proc. IRE 48, 1395, (1960)

53. H. H. Edwards and V. L. Newhouse: J. Appl. Phys.

    33, 868, (1962)

54. R. F. Broom and E. H. Rhoderick: Proc. Phys. Soc.

    79, 586, (1962)

55. E. H. Rhoderick and E. M. Wilson: Nature. 194, 1167,

    (1962)

56. Bowers: Unpublished, pertinent results quoted in

    references 55 and 57.

57. R. E. Glover and H. T. Coffey: Rev. Mod. Phys. 36,

    299, (1964)

58. J. Bardeen: Rev. Mod. Phys. 34, 667, (1962)

59. R. W. Ditchburn: J. Opt. Soc. Am. 45, 743, (1955)

60. W. E. J. Neal and R. W. Fane: Private Communication.

61. F. B Haller: Rev. Sci. Instr. 35, 1356, (1964)

62. J. Holden, L. Holland and L. Laurenson: J. Sci. Instr.

    36, 281, (1959)

63. R. J. Seward: Ph. D. Thesis, Univ. of Southampton (1967)

64. K. R. O'Shea: Ph. D. Thesis, Univ. of Aston (1971)

65. S. Tolansky: 'Multiple Beam Interferometry',

    Clarendon Press, (1949)

66. W. F. Koehler: J. Opt. Soc. Am. 43, 738, (1953)

67. L. G. Shultz: J. Opt. Soc. Am. 41, 261, (1951)

68. G. K. White and S. B. Woods: Can. J. Phys. 35, 892,

    (1957)

69. L. Young and F. G. R. Zobel: J. Electrochem. Soc.

    113, 277, (1966)

70. W. L. Bragg: The Crystalline State, Vol. 1 p:189,

    Bell, London, (1919)

71. P. Scherrer: Gotting. Nachr. 2, 98, (1918)

72. C. A. Neugebauer and M. B. Webb: J. Appl. Phys.

    33, 74 (1962)

73. A. A. Milgram and C. Lu: J. Appl. Phys. 37, 4773,

    (1966)

74. N. M. Bashara and L. A. Weitzenkamp: J. Appl. Phys.

    35, 1983, (1964)

75. B. Vodar: J. Phys. Radium. 17, 213, 298, (1956)

76. E. H. Sondheimer: Advan. Phys. 1, 1, (1952)

77. K. L. Chopra: 'Thin Film Phenomena' p.350, McGraw-Hill

    New York, (1969)

78. D. C. Larson and B. T. Boiko: Appl. Phys. Letters.

    5, 155, (1964)

79. R. V. Isaeva: J.E.T.P. 4, 209, (1966)

79a. T. F. Stronberg and C. A. Swenson: Phys. Rev. Letters.
    $\underline{9}$, 370, (1962)

80. A. I. Golovashkin, I. E. Leksina, G. P. Motulevich and
    A. A. Shubin: J.E.T.P. $\underline{29}$, 27, (1969)

81. M. Strongin, O. F. Kammerer, and A. Paskin: Phys. Rev.
    Letters. $\underline{14}$, 949, (1965)

82. W. Buckel and R. Hilsch: Z. Physic. $\underline{139}$, 109, (1954)

83. B. Abeles, R. W. Cohen and G. W. Cullen: Phys. Rev.
    Letters. $\underline{17}$, 632, (1966)

84. B. Abeles, R. W. Cohen and W. R. Stowell: Phys. Rev.
    Letters. $\underline{18}$, 902, (1967)

85. A. Leger and J. Klein: Phys. Letters. $\underline{28A}$, 751,
    (1969)

86. A. Rothwarf: Phys. Letters. $\underline{30A}$, 55, (1969)

87. R. C. Theil: Z. Physik. $\underline{200}$, 227, (1967)

88. S. W. Marshall and R. M. Wilenzick: Phys. Rev.
    Letters. $\underline{16}$, 219, (1966)

89. P. Debye: Ann. Physik. $\underline{39}$, 789, (1912)

90. A.E. H. Love: 'A Treatise on the Mathematical Theory
    of Elasticity', p.281, Cambridge Univ.
    Press (1920)

91. Y. Nakagawa and A. D. B. Woods: Phys. Rev. Letters.
    $\underline{11}$, 271, (1963)

92. D. I. Bolef: J. Appl. Phys. $\underline{32}$, 100, (1961)

93. J. A. Mydosh and H. Meissner: Phys. Rev. $\underline{140}$, A1568,
    (1965)

94. J. E. Mercereau and T. K. Hunt: Phys. Rev. Letters.
$\underline{8}$, 243, (1962)

95. J. Klein and A. Leger: Phys. Letters. $\underline{28A}$, 134,
(1968)

96. J. J. Hopfield: Comments on Solid State Physics.
$\underline{3}$, 48, (1970)

APPENDIX I

A typical set of results from the electrical
measurements on a niobium film.

Film Nb 56.

Deposition for 1 min 45 sec at a pressure of 4×10^{-8} torr
Substrate temperature 500 °K.

Thickness 420 Å (interferometer), deposition rate
240 Å min^{-1}. Thickness 385 Å (less oxide).

Critical current mA	Au-Fe/chromel thermocouple μV	Temperature °K
95	1091	3.10
85	1066	4.83
80	1055	5.59
68	1042	6.48
59	1034	7.04
49	1024	7.73
40	1020	8.00
30	1017	8.21
20	1016	8.28
10	1015	8.35
5	1014	8.41
2	1014	8.41
1	1013.5	8.445
.1	1013	8.48

continued.

Measuring current, 0.5 mA.

current +ve	current -ve	resistance ohms	Au-Fe chromel	copper const.	T^{o}K
6.390	6.370	12.760	1010		8.69
6.443	6.419	12.862	1006		8.97
6.454	6.435	12.889	991		10
6.481	6.455	12.936	919		15
6.516	6.494	13.010	847		20
6.538	6.584	13.122	775		25
6.724	6.703	13.427	652	588	30
6.860	6.831	13.691	577	542	35
6.996	6.971	13.967	513	496	40
7.848	7.820	15.668	255	256	60
8.629	8.611	17.240	+044	+049	80
9.400	9.595	18.995	354	407	100
10.388	10.370	20.758	685	818	120
11.32	11.31	22.63	1043	1279	140
12.17	12.17	24.34	1412	1789	160
13.02	13.04	26.06	1796	2346	180
13.82	13.85	27.67	2178	2946	200
14.65	14.65	29.30	2573	3590	220
15.41	15.43	30.84	2975	4264	240
16.17	16.20	32.37	3395	4997	260
16.92	16.93	33.85	3815	5757	280
17.61	17.65	35.26	4234	6552	300